Shear-deformable Hybrid Finite Element Method for Buckling Analysis of Composite Thin-walled Members

By

Vida Niki

Thesis submitted in fulfilment
of the full requirement for the degree of
Doctor of Philosophy

School of Civil and Environmental Engineering

Faculty of Engineering and Information Technology

University of Technology Sydney (UTS)

December 2018

Certificate of authorship and originality

I certify that the work in this thesis has not previously been submitted for a degree nor has it been submitted as part of requirements for a degree except as fully acknowledged within the text.

I also certify that the thesis has been written by me. Any help that I have received in my research work and the preparation of the thesis itself has been acknowledged. In addition, I certify that all information sources and literature used are indicated in the thesis.

This research is supported by the Australian Government Research Training Program.

Vida Niki

Production Note:
Signature removed
prior to publication.

To Ashkan

Acknowledgements

I would like to express my deepest appreciation to my supervisor Dr. R. Emre Erkmen for his continuous support and guidance throughout my studies. His immense knowledge, motivation and patience helped me bring this study into success. I could not have imagined having a better supervisor for my Ph.D study.

My sincere thanks also go to Professor Bijan Samali who provided me an opportunity to do my PhD in Australia. His kind and insightful advice helped me to overcome the obstacles I have been facing throughout my studies.

I would especially like to express my heartfelt gratefulness for having my beloved husband, Dr. Ashkan Afnani, by my side who always has been a source of motivation for me.

Words cannot express how grateful I am to my parents, Mohebatollah and Behrokh, for all of their sacrifices, encouragement and support without which doing my PhD would have been impossible.

Finally, I would like to thank my lovely sons, Ryan and Nickan, who could manage to be the source of distraction and inspiration at the same time for me throughout my studies.

Table of Contents

List of Symbols

$\phi(z)$	=	angle of rotation of the cross-section
Δ	=	lateral deflection of flanges
$\sigma(s)$	=	normal stress
$\tau(s)$	=	shear stress
P	=	normal force
M_x	=	bending moment about x axis
M_y	=	bending moment about y axis
B	=	bimoment
Q_y	=	shear force in y direction
Q_x	=	shear force in x direction
T_v	=	Saint Venant twist
T_ω	=	flexural twist
A	=	area of the cross-section
I_x	=	moment of inertia of the cross-section around the x axis
I_y	=	moment of inertia of the cross-section around the y axis

$\omega(s)$	=	sectorial coordinate of the cross-section
$S_{\omega}(s)$	=	sectorial moment of the cross-section
I_{ω}	=	sectorial moment of inertia of the cross-section
$S_{\omega}(s)$	=	sectorial moment of area
$x(s), y(s)$	=	coordinates of an arbitrary point P on the mid-surface
a_x, a_y	=	coordinates of a pole A on the cross-section
$u(s,z)$	=	horizontal displacement of point P
$v(s,z)$	=	vertical displacement of point P
$w(s,z)$	=	longitudinal displacement of point P
γ_{zt}	=	shear strain on the mid-surface
t	=	tangential component of displacement at the mid-surface
α	=	angel between the tangent at point P and the x axis
P_{cr}	=	critical buckling load
xyz	=	local coordinate at the pre-buckling state
$x'y'z'$	=	local coordinate at the buckled state
E	=	Modulus of Elasticity of the material
G	=	shear modulus

J	=	torsional constant of the cross-section
C_w	=	cross-sectional warping constant
M_{cr}	=	critical buckling moment
u_T	=	lateral displacement of the top flange
u_B	=	lateral displacement of the bottom flange
ϕ_T	=	rotation of the top flange
ϕ_B	=	rotation of the bottom flange
Φ_k	=	fibre orientation of k^{th} layer of composite laminate cross-section
σ_1, σ_2	=	Stresses in two directions for orthotropic material
$\varepsilon_1, \varepsilon_2$	=	Strains in two directions for orthotropic material
E_1, E_2	=	Young‗s moduli in two directions for orthotropic material
ν_{12}, ν_{21}	=	Poisson‗s ratios in two directions for orthotropic material
τ_{12}	=	shear stress
γ_{12}	=	shear strain
$\boldsymbol{\sigma}$	=	stress vector
$\boldsymbol{\varepsilon}$	=	strain vector

$\mathbf{Q}$	=	constitutive matrix for composite material
$\bar{\mathbf{Q}}$	=	Rotated constitutive matrix for composite material
$Q_{ij}, \bar{Q}_{ij}$	=	components of constitutive matrix for composite material
$\mathbf{T}$	=	Transformation matrix
θ	=	Angle between the fibre orientation and the axis of the beam
EI	=	bending stiffness of column
L	=	length of column
$\mathbf{u}$	=	displacement vector
Π_p	=	potential energy functional
$\mathbf{C}$	=	elastic stiffness matrix
$\bar{\mathbf{F}}$	=	prescribed body force
$\bar{\mathbf{T}}$	=	boundary traction vectors
$\bar{\mathbf{u}}$	=	prescribed boundary displacements
$\mathbf{S}$	=	compliance matrix
$w(x)$	=	axial displacement of any point on the cross-section
$u(x)$	=	lateral displacement of any point on the cross-section
$v(x)$	=	vertical displacement of any point on the cross-section

$\phi(x)$	=	angle of twist of the cross-section
ε_x	=	axial strain
γ_{xz}	=	shear strain
$\bar{Q}_{ij}^{*}$	=	components of constitutive matrix in plane stress condition
$\hat{\bar{Q}}_{11}^{(k)*}$	=	components of constitutive matrix for with $\tau_{xy}^{(k)} = 0$ assumption
$E_1^{(k)}, E_2^{(k)}$	=	Young's moduli of the k^{th} layer in two directions for orthotropic material
$\upsilon_{12}^{(k)}, \upsilon_{21}^{(k)}$	=	Poisson's ratios in two directions for orthotropic material
M	=	bending moment stress resultant
V	=	shear stress resultant
σ_x	=	normal stress
τ_{xz}	=	shear stress
J_{yy}	=	composite section constant
F_s	=	shear force
N^p	=	axial load at pre-buckling state
V^p	=	vertical load at pre-buckling state

M^p	=	bending moment at pre-buckling state
$\mathbf{\Pi}$	=	total potential energy
U	=	strain energy
W	=	work done by external forces
V_0	=	volume of the element
β_1, β_2	=	Lagrange Multipliers
U_d	=	internal strain energy density
Π_{III}	=	hybrid functional
$\mathbf{L}^{\mathrm{T}}$	=	linear interpolation vector
$\mathbf{N}^{\mathbf{T}}$	=	cubic interpolation vector
$\mathbf{K}_{bi}$	=	element stiffness matrix
$\mathbf{K}_{gi}$	=	element geometric stiffness matrix
P_e	=	Euler buckling load
$\hat{N}_{\mathrm{crz}}$	=	buckling load of the column
$\hat{N}_{\mathrm{crz}}^{\mathrm{B}}$	=	buckling load when the shear stiffness is infinite
$\hat{S}_{\mathrm{yy}}$	=	buckling load when the bending stiffness is infinite

$w(s,z)$	=	axial displacement of an arbitrary point $A(x,y)$
$u(s,z)$	=	lateral displacement of an arbitrary point $A(x,y)$
$v(s,z)$	=	vertical displacement of an arbitrary point $A(x,y)$
$W(z)$	=	axial displacement of pole $P(a_x, a_y)$
$U(z)$	=	lateral displacement of pole $P(a_x, a_y)$
$V(z)$	=	vertical displacement of pole $P(a_x, a_y)$
ω	=	sectorial area
$\boldsymbol{\sigma}$	=	stress vector
$\boldsymbol{\varepsilon}$	=	strain vector
N	=	axial load
V_y	=	shear force
V_x	=	shear force
T_{sv}	=	St. Venant torsion
T_{ω}	=	twisting moment
τ_{zx}	=	shear stress
W_{Wagner}	=	Wagner stress resultant

I_p	=	sectional property
I_{py}	=	sectional property
I_{px}	=	sectional property
$I_{p\omega}$	=	sectional property
J_d	=	torsional constant
w_{sh}	=	vertical displacement in the shell element
u_{sh}	=	displacement in x direction of the shell element
w_{sh}	=	displacement in y direction of the shell element
$\theta_{x,sh}$	=	bending rotation about x axis in the shell element
$\theta_{y,sh}$	=	bending rotation about y axis in the shell element
$\theta_{z,sh}$	=	bending rotation about z axis in the shell element

List of Figures

Figure 7.14: Cross-sectional dimensions of the channel-section

List of Tables

Abstract

Thin-walled members are widely used in mechanical and civil engineering applications. The use of thin-walled elements made of fibre-reinforced composite materials has increased significantly in the past decades due to the superior features of these materials. However, because of their slenderness, susceptibility of thin-walled composite members to buckling is the main concern in the structural design of these elements. For the buckling analysis of thin-walled members with any loading types and boundary conditions, one tends to use numerical methods rather than the closed-form solutions which are limited to simple loading and boundary conditions. Finite element methods (FEM) as the most commonly used numerical techniques can be categorised into two main groups: single-field FEM and multi-field or hybrid FEM. The first group is further categorised into two types: displacement-based elements and stress-based elements.

In buckling analysis of thin-walled members with fibre-reinforced laminated composite materials, shear deformations can have a significant effect. Single-field finite element methods adopt different approaches to include shear deformations. Displacement-based methods take account of the effects of shear deformations by modifying the kinematic assumptions of the thin-walled theory. On the other hand, in stress-based methods, the inter-element equilibrium conditions have to be satisfied a-priori, which further complicates the assemblage procedure.

A shear-deformable hybrid finite element method for the buckling analysis of composite thin-walled members is developed in this thesis by enforcing the strain-displacement relations to the potential energy functional. In the developed method, the resulting matrix equations are defined only in terms of the nodal displacement values as

unknowns which makes the assemblage procedure as simple as in a displacement-based finite element. The shear deformations are taken into account in the current hybrid finite element method by using the strain energy of the shear stress field which eliminates the mentioned difficulties in the other finite element methods.

Chapter 1: Introduction

1.1. Introduction

Thin-walled members are widely used in mechanical and civil engineering applications such as building construction, aerospace, aircraft, and ship-building because of their relatively low weight to strength ratio. Due to their complex behaviour, thin-walled members cannot be analysed by using classical beam theories, and therefore, theories that consider the special kinematics of open thin-walled elements are used instead.

Traditionally, thin-walled elements have been constructed from the metallic material such as steel or aluminium. However, the use of fibre-reinforced composite materials has been increasing significantly in the past decades as thin-walled members. The main reason for this increase is the superior features of composite materials such as high ratio of tensile strength and stiffness to weight, light weight, long-term durability, non-corrosive nature, electromagnetic neutrality, enhanced fatigue life, resistance to chemical attack, and low thermal expansion compared to other construction materials.

Due to their slenderness, susceptibility of thin-walled composite members to buckling is the main concern in the structural design of these elements. Therefore, it is crucial to predict the buckling loads accurately to have a reliable design.

There are different methods of analysis to assess the buckling behaviour of thin-walled members. Closed-form solutions were the first to be developed for such purposes. Although they lead to exact results for the buckling load, their use is limited to simple loading and boundary conditions because the differential equations can only be solved for such cases. Consequently, numerical methods have been developed for the analysis of structures with complicated geometry, loading and boundary conditions. Among the numerical methods, Finite Element Method (FEM) is the most commonly used technique.

Finite element methods can be categorised into two main groups: single-field FEM and multi-field or hybrid FEM. The first group, which is known as the *primal* finite element, is further categorised into two types based on its unknown field variables: displacement-based elements and stress-based elements. On the other hand, there are more than one unknown field variables in hybrid finite element methods.

In buckling analysis of thin-walled members with fibre-reinforced laminated composite materials, shear deformation effects can play an important role. Consequently, a large number of finite elements are developed to incorporate such effects. Displacement-based methods, which are developed based on the principle of total potential energy, consider the effects of shear deformations by modifying the kinematic assumptions of the thin-walled theory. On the other hand, stress-based methods are developed based on the principle of complementary energy. In these methods, although there is no need to modify the kinematic assumptions to include the shear deformations, the inter-element equilibrium conditions have to be satisfied a-priori, which further complicates the assemblage procedure.

The hybrid finite element methods have been developed for buckling analysis of thin-walled members to overcome the shortcomings of the single-field finite element methods discussed above and make use of their advantages. In hybrid methods, which are generally developed based on the Hellinger-Reissner variational principle, there are more than one field variables, and the displacements and transverse stresses are calculated independently. The hybrid functional can be obtained by enforcing the constraint conditions to the energy functional by using the Lagrange Multipliers Method.

Developing the hybrid finite element method for buckling analysis of thin-walled members made of isotropic materials has been the subject of studies recently. However, one cannot find many shear-deformable hybrid finite element methods in the literature developed for the buckling analysis of thin-walled elements made of fibre-reinforced laminate composite materials.

1.2. Objectives

The objective of the current study is

- developing a hybrid finite element method for the buckling analysis of composite thin-walled members and
- including shear deformation effects in the hybrid model

The method is obtained based on the potential energy functional by applying the strain-displacement relations through the Lagrange multipliers method. Although the multi-field Hellinger-Reissner functional is used in the formulation, the resulting matrix equations are defined only in terms of the nodal displacement values as unknowns.

Consequently, the assemblage procedure is as straightforward as in a displacement-based finite element. Also, in the current hybrid finite element method, the shear deformations are taken into account by using the strain energy of the shear stress field. Therefore, the kinematic assumptions of the classical thin-walled beam are not modified. The advantage of the current method over the stress-based method is that in the hybrid method the inter-element force equilibrium does not need to be satisfied a-priori.

The developed formulations are implemented in FORTRAN programming language, and the accuracy, efficiency and applicability of the method in addition to its capability in capturing the shear deformation effects are verified through a number of numerical examples. In addition to the FRP laminate composites, the buckling analysis of other elements with composite cross-sections such as the sandwich or built-up elements is performed by the current hybrid finite element formulation.

1.3. Contents of the thesis

The chapters of the present thesis are organised as follow:

Chapter 2 starts with the definition of thin-walled members followed by the introduction of Vlasov theory, its assumptions and the additional stress resultants in thin-walled elements. Then the instability of thin-walled elements is discussed in this chapter and different types of buckling modes are introduced.

Chapter 3 includes a comprehensive introduction of the fibre-reinforced composite materials. The advantages and disadvantages of these materials are discussed at the beginning of the chapter. The stacking sequence of the laminate layers and their denotation, the manufacturing procedure of laminate composite profiles and mechanics of composite laminates are explained. Finally, a comprehensive review of the literature on the buckling analysis of thin-walled laminated composites beams is presented in this chapter.

Chapter 4 is dedicated to the introduction of the hybrid finite element method developed in the current thesis. It starts with presenting the literature review of the analytical solutions and numerical methods as different kinds of techniques for buckling analysis of thin-walled members. Then, different types of finite element method are described along with a short discussion on the advantages and disadvantages of each method. A literature review of hybrid methods is presented, and the hybrid finite element model developed in this study for the buckling analysis of composite thin-walled members is introduced in more details.

In chapter 5, the flexural buckling behaviour of fibre-reinforced laminated composite thin-walled columns subjected to axial concentrated compressive load is performed by the developed hybrid finite element method. The chapter starts with an extensive literature review of previous research works relevant to the flexural buckling behaviour of thin-walled fibre reinforced composite elements. Then, the kinematic relations to describe the column behaviour are developed based on the kinematics of general open thin-walled elements and the constitutive relations for fibre-reinforced composite laminates are applied. Consequently, the stress and stress resultants equations are obtained. The hybrid formulation for the flexural buckling analysis is developed and the discretised form of the hybrid functional is obtained after the interpolation of stress resultants and lateral displacements. Finally, the efficiency and accuracy of the developed hybrid finite element model are validated through numerical examples. In addition, columns with various boundary conditions are studied and the effect of fibre orientation and the column slenderness on the flexural buckling load are discussed.

A number of applications of the developed finite element formulation are presented in Chapter 6, starting with comparisons with two well-known solutions in the literature to include shear deformation effects in buckling analysis of columns. Then, the significance of considering shear deformation effects in buckling analysis of short columns is discussed through a few examples. Next, the use of the developed hybrid model for the analysis of sandwich columns is studied, followed by the application for laced built-up columns.

A hybrid finite element formulation is developed in Chapter 7 for lateral-torsional buckling analysis of thin-walled beams. The chapter starts with a comprehensive literature review of the previous research. The beam kinematic relations and the relevant constitutive equations are developed next, followed by obtaining the expressions of stress and stress resultants. The hybrid formulation is then developed by relaxing the strain-displacement equations through the Lagrange Multipliers Method. Then, interpolations functions are used for stress resultants and displacement components to formulate the finite element. Finally, the accuracy and efficiency of the method are verified through numerical examples and comparison with results from the literature.

In Chapter 8, the main findings of the thesis are summarised, and recommendations are made for further research in the subject.

Chapter 2: Review of Buckling Analysis of Thin-walled Members

2.1. Introduction

Thin-walled beams are defined as members in which the thickness is about 1/10th of the other dimensions of the cross-section. Because of the relatively low weight to strength ratio, these elements are widely used in numerous mechanical and civil engineering applications such as aerospace, building, aircraft and ship-building. Due to their slenderness, thin-walled beams are susceptible to various modes of instability depending on the loading type and boundary condition. Therefore, obtaining the buckling load values is crucial in accurately predicting the response of a thin-walled structure.

Due to the complex behaviour of thin-walled beams and additional modes of deformation, classical beam theories are not applicable for these types of elements. For the first time, Vlasov (1961) developed a theory that considered the special kinematics of beams with open thin-walled cross-sections. This theory is introduced in more details in the following section.

2.2. Vlasov theory for thin-walled beams

A beam is described as being in the state of uniform torsion if it is subjected to equal and opposite torques at each end, and is free to warp. In order to accommodate this torsion, the beam undergoes in-plane shear strains and associated shear stresses.

Saint Venant (1883) formulated the first theory for beams under uniform torsion. He assumed that such a loading would produce shear stresses in the member while normal stresses remained zero.

However, the warping effect arising in a thin-walled beam subjected to a twisting moment cannot be ignored. If the beam is longitudinally restrained, the tendency towards warping would result in significant additional normal and shear stresses in the section. Consequently, Saint Venant theory is not valid for the analysis of thin-walled structure.

In 1961, Vlasov (1961) developed a formulation for the analysis of open thin-walled sections under non-uniform torsion. The main assumptions of the theory of Vlasov are:

1. The cross-section is assumed to be rigid during the deformations, which means that deformations in the plane of the cross-section are negligible. However, the out of plane warping is allowed in the kinematics of Vlasov theory.
2. The shear strains on the mid-surface of each of the thin plates are considered to be negligible.
3. The normal stresses perpendicular to the centreline of the section are assumed to be negligible.

It should be noted that the classical beam theory assumption that ―the plane sections remain planar during the deformation” is not adopted in the Vlasov beam theory. Consequently, the warping deformations are considered in the kinematical formulation of the beam.

Vlasov introduced two new types of resultant forces called ―Flexural Twist” and ―Bimoment” and an additional cross-sectional property called ―sectorial moments of area” in order to explain the warping phenomenon.

A thin-walled beam subjected to a twisting moment will distort as shown in Figure 2.1. The distortion is composed of the rotation ϕ of web and flanges with respect to their centre of gravity, and the lateral deflection Δ of flanges. The first part of the deformation, i.e. corresponding to ϕ, is conjugate with Saint Venant twist T_{sv}, while the second portion is caused by the stress resultant T_{ω}, called the ―flexural twist”.

$$T = T_{sv} + T_{\omega} \tag{2.1}$$

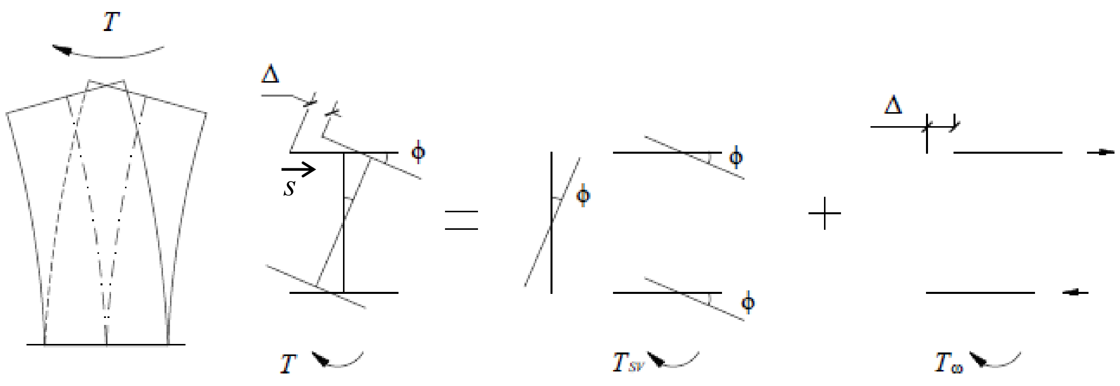

Figure 2.1: Thin-walled beam subjected to a twisting moment

In addition, the "bimoment" is a mathematical function defined by Vlasov as a pair of equal and opposite bending moments acting in two parallel planes and is responsible for warping displacements in thin-walled beams (Figure 2.2).

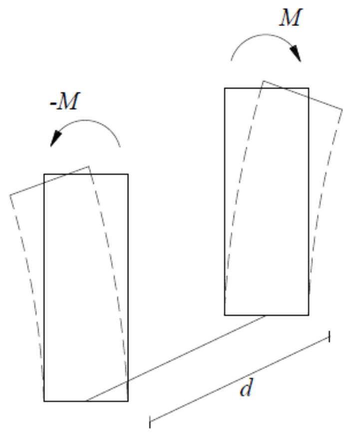

Figure 2.2: Thin-walled beam subjected to a twisting moment

Therefore, in thin-walled beams, the warping longitudinal stresses and warping shear stresses due to bimoment and flexural twist are added to the classical normal and shear stresses, resulting in the following definition of stresses:

$$\sigma(s) = \frac{P}{A} + M_x \frac{y(s)}{I_x} + M_y \frac{x(s)}{I_y} + B \frac{\omega(s)}{I_\omega} \tag{2.2}$$

$$\tau(s) = Q_y \frac{S_x(s)}{t_s I_x} + Q_x \frac{S_y(s)}{t_s I_y} + T_v \frac{t(s)}{I_s} + T_\omega \frac{S_\omega(s)}{t_s I_\omega} \tag{2.3}$$

in which $\omega(s)$, $S_\omega(s)$ and I_ω are sectorial coordinate, sectorial moment and sectorial moment of inertia of the cross-section, respectively.

Coordinate s, which is measured from the sectorial origin S_0, identifies the coordinates of an arbitrary point $A(x(s), y(s))$ on the mid-surface. (Figure 2.3)

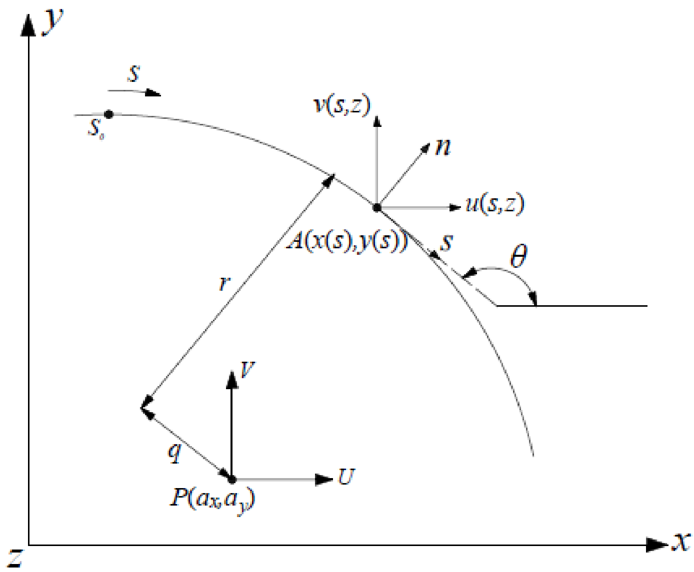

Figure 2.3: Coordinates and displacements of a mid-surface

Based on the first assumption of Vlasov theory, the displacement in the plane of the cross-section can be described as rigid body motion; hence the horizontal and vertical displacements of point *A* could be defined from the horizontal and vertical displacements of a pole $P(a_x, a_y)$ and the angle of rotation $\phi(z)$ of the cross-section as follows:

$$u(s,z) = U(\mathrm{z}) - \left[y(s) - a_y \right] \phi(z) \tag{2.4}$$

$$v(s,z) = V(\mathrm{z}) + \left[x(s) - a_x \right] \phi(z) \tag{2.5}$$

According to the second assumption of Vlasov theory, the shear strain on the mid-surface of the thin-walled element is negligible:

$$\gamma_{zt} = \frac{\partial w}{\partial s} + \frac{\partial t}{\partial z} = 0 \tag{2.6}$$

where *t* is the tangential component of displacement at the mid-surface and is obtained as

$$t(s,z) = u(s,z)\cos\theta(s) + \mathrm{v}(s,z)\sin\theta(s) \tag{2.7}$$

where θ is the angle between the tangent at point A and the x axis. From Eqs. (2.6) and (2.7) we have:

$$w(s,z) = \int\Big([U(\mathrm{z}) - (y(s) - a_y)\phi'(z)]\cos\theta(s) + [V(\mathrm{z}) + (x(s) - a_x)\phi'(z)]\sin\theta(s)\Big)\mathrm{d}s \tag{2.8}$$

By considering $h(s) = (x(s) - a_x)\sin\theta(s) - (y(s) - a_y)\cos\theta(s)$, $dx = ds\cos\theta(s)$ and $dy = ds\sin\theta(s)$, and applying the integration, the longitudinal displacement of point A can be written as:

$$w(s,z) = W(z) - x(s)U'(z) - y(s)V'(z) - \omega(s)\phi'(z) \tag{2.9}$$

As one can see, the last term in Eq. (2.9) is the longitudinal displacement due to warping, and constitutes the difference between the kinematics of the classical beam theory and the theory of thin-walled beams.

2.3. Instabilities of Thin-walled members

2.3.1. Introduction

Failure of structures may occur as a result of either fracture of the material or undesirable large deflections. Buckling, which belongs to the latter, can be defined as the loss of the stability in equilibrium configuration without any fracture or separation of material.

During buckling in thin-walled elements, internal membrane strain energy is converted to bending strain energy through changes in the deformed configuration of the structure without any changes in the applied load. As the membrane stiffness is significantly greater than bending stiffness in thin plates, large bending deformations occur during the buckling in order to absorb an equivalent level of internal energy to the pre-buckling configuration. In other words, the pre-buckling configuration – large membrane stiffness with small membrane deformations – changes to the post-buckling configuration, which can be described with small bending stiffness along with large bending deformations.

The buckling phenomenon can be schematically described by the load-deflection diagram of Figure 2.4. In classical linear buckling theory, when the load increases from zero, the out-of-plane displacement remains zero (Path I) until P_{cr} is reached. For a perfect element which is loaded perfectly at the mid-plane, the load can be increased until compression fracture occurs (Path II). It should be noted that Path II corresponds to an unstable state of equilibrium, which means that a slight imperfection in geometry or material leads to the buckling of the member. The point at which the member moves from a state of stable equilibrium to unstable is called the bifurcation point. After this point, an alternative configuration to the unstable equilibrium state exists which corresponds to the buckled configuration (Path III). In nonlinear theory, the load-carrying capacity of the structure may still increase from the bifurcation point and the load-deflection curve follows Path IV.

All the paths discussed so far correspond to ideal geometry, material and loading conditions. In real life structures, out-of-plane deflections will occur from the beginning of the loading regime due to inevitable member imperfections and load eccentricities (Path V).

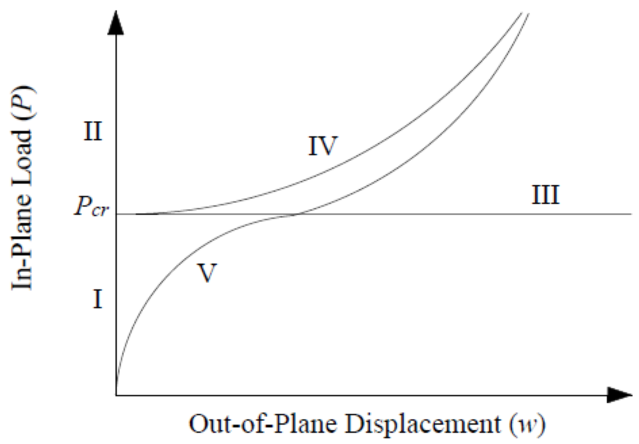

Figure 2.4: Load-deflection representation of buckling phenomenon

Buckling phenomenon can be categorized into global buckling (which is also called lateral buckling or flexural-torsional buckling), local buckling and distortional buckling. Global buckling is the rotation and lateral translation of the whole body whereas local buckling is the instability of a part of the cross-section such as the column flange. Distortional buckling is the combination of global and local buckling.

2.3.2. Global buckling

Global buckling refers to buckling modes that involve a significant portion of the domain of the member, and constitute lateral or twist deformations of the beam without distortions in the cross-section. The half-wavelength of global buckling is the distance between the lateral supports of the member. Examples of this type of buckling are lateral or twisting buckling of columns, and lateral-torsional buckling of beams.

Lateral-torsional buckling includes lateral movement of the member along with the twist of cross-section around the shear centre, and can only occur in flexural members loaded along their strong axis (Nethercot and Trahair 1976).

Closed-form solutions of lateral-torsional buckling for uniform bending and simple boundary conditions were developed more than half a century ago based on the Vlasov theory for thin-walled beams (Chajes and Winter 1965, Timoshenko and Gere 1961). The kinematics of the problem are shown in Figure 2.5.

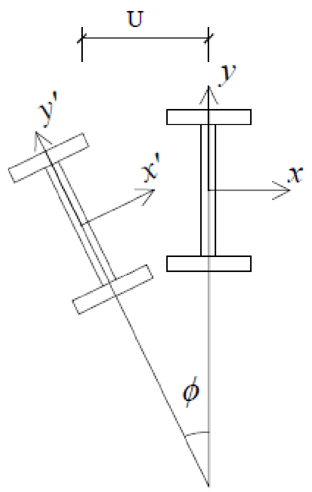

Figure 2.5: Coordinate system for the analysis of lateral-torsional buckling

The local coordinate system xyz corresponds to the pre-buckling state of the beam while $x'y'z'$ system is used to illustrate the buckled shape of the cross-section. The buckling movement can be described in terms of horizontal and vertical displacements of the cross-sectional centreline (i.e. along x and y axes) and rotation ϕ around z axis. The external load is the moment about x axis (i.e. M_x).

It is assumed in the formulation that the twisting of the member is prevented at the end supports but the cross-section warping is free. The equilibrium equation in terms of the cross-sectional twist can be written as (Timoshenko and Gere 1961, Trahair 1993a)

$$\frac{d^4\phi}{dz^4}-\frac{GJ}{EC_w}\frac{d^2\phi}{dz^2}-\frac{M_x^2}{E^2I_yC_w}\phi=0 \tag{2.10}$$

where ϕ is the cross-sectional twist, E is the Modulus of Elasticity of the material, G is the shear modulus, J is the torsional constant of the cross-section, C_w is the cross-sectional warping constant, and I_y is the moment of inertia of the cross-section around the weak axis. Eq. (2.10) is solved analytically for a simply-supported beam subjected to a uniform bending moment to obtain the critical load (Timoshenko and Gere 1961)

$$M_{cr}=\frac{\pi}{L}\sqrt{EI_yGJ\left(1+\frac{EC_w}{GJ}\frac{\pi^2}{L^2}\right)} \tag{2.11}$$

However, such solutions are practically impossible for more complicated beams. Alternatively, numerical solutions can be employed for accurate lateral-torsional buckling analysis of beams. Due to the complexity involved in such analyses, they are not commonly used by practicing engineers for the design of beams. In practice, the buckling load resulting from other loading and boundary conditions are calculated by the use of a correction factor that is multiplied to the results from a beam with uniform bending moment (Lim *et al.* 2003, Wong and Driver 2010).

2.3.3. Local Buckling

On the other hand, Local Buckling is defined as the buckling of web and flanges comprising the cross-section without lateral and/or torsional movement of the whole cross-section. Local buckling typically has a half-wavelength of approximately an order of magnitude smaller than the global buckling.

The effect of local buckling on the overall integrity of the structure can be significantly different from the global buckling. In other words, while the global buckling of a beam or column results in catastrophic collapse of the structure, higher load levels can normally be achieved after the initial local buckling of the plate elements. In this case, the additional strength is referred to as post-buckling strength, which is taken into account in most of the design standards through different means.

2.3.3.1. The Effective Width Method

The most commonly used method to consider the effect of local buckling in the design of thin-walled members is the Effective Width Method (von Karman *et al.* 1932). In this method, the effective cross-sectional properties (e.g. cross-sectional area and second moment of inertia) are calculated by neglecting the portions of the plate elements in the section that are considered to undergo local buckling. These areas are calculated based on the dimensions of each plate segment spanning between the points of support, and the number of segment edges that are supported. The global buckling load values are then calculated based on these reduced cross-sectional properties.

Although this method is theoretically straightforward, the following conceptual deficiencies can be identified:

1. The effective width of each of the plate segments are solely calculated based on the geometry and boundary conditions of the segment. Consequently, equilibrium and compatibility conditions are not satisfied between the adjacent elements.
2. The effective plate width values are calculated by assuming uniform normal stresses at plate segments and therefore the gradient of stresses are ignored, which effects the accuracy of the method (Schafer 2008).

2.3.3.2. The Direct Strength Method

Direct Strength Method (DSM) is an alternative design procedure for thin-walled members. In this method, the local, distortional, and global buckling loads of the member are separately calculated. The anticipated buckling load of the member is then calculated by considering a combination of the above buckling loads and the yield limit of the material.

The Direct Strength Method has been largely developed by comparing the test results of thin-walled members with calculated buckling loads (Hancock *et al.* 1994, Schafer and Pekoz 1998). The main advantage of the Direct Strength Method over the Effective Width Method is that the interaction between plate segments is considered in the analysis, which means that equilibrium and compatibility are satisfied between adjacent elements (e.g. web and flanges). Additionally, calculations of the buckling loads using

DSM do not require lengthy calculations and iterative process of the Effective Width Method.

However, experimental work by Rusch and Lindner (2001) concluded that the use of the Direct Strength Method for cold-formed I-shaped members can result in overestimation of the buckling load, and that the Effective Width Method results in more accurate prediction of the buckling load.

2.3.4. Distortional Buckling

Distortional buckling can be described as an interaction between the global and local buckling modes (Bradford 1985). In other words, this mode of buckling involves buckling of individual plate elements of the cross-section along with the buckling movement of the whole section. The half-wavelength of distortional buckling is in-between the local and global buckling. The deformations corresponding to each of the mentioned buckling modes is described diagrammatically in Figure 2.6**.**

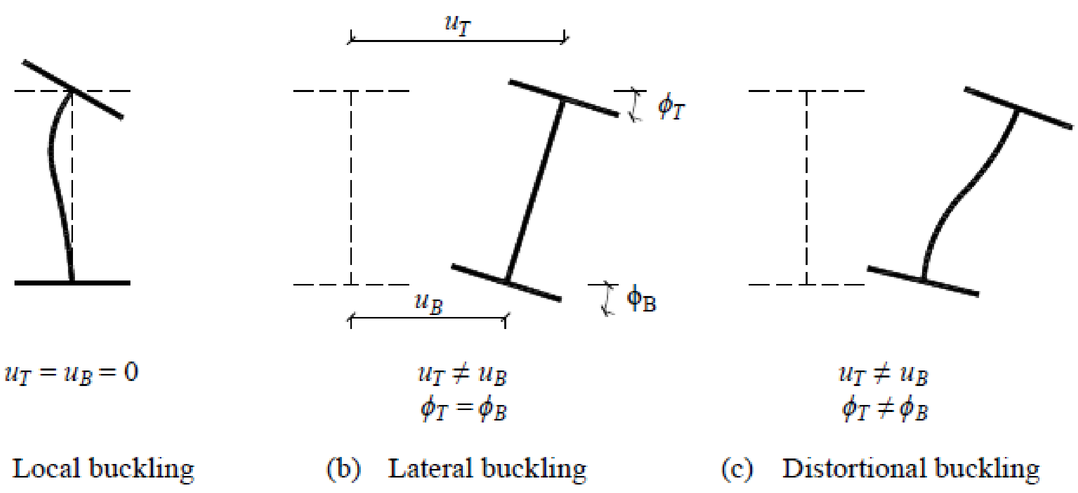

Figure 2.6: Buckling modes of thin-walled beams

One of the earliest studies on the distortional buckling of beams is performed by Hancock *et al.* (1980), who presented a closed-form solution for beam buckling load by considering web distortions on lateral-torsional buckling of doubly-symmetric simply-supported I-sections. They concluded that beams with high flange to web thickness ratio are susceptible to buckling in lower loads compared to the expected classical lateral buckling load. Jönsson (1999) developed a thin-walled distortional beam theory by modifying the kinematic assumptions of Vlasov thin-walled theory through including distortional displacement fields.

However, due to the complexity of the problem, the application of closed-form solutions for the assessment of distortional buckling is limited to simply geometry, loading and boundary conditions. Alternatively, finite element models of distortional buckling can be used for more accurate results. Bradford and Trahair (1981) presented one of the first finite element models for distortional buckling of thin-walled beams. Their model captured the distortional displacement field using six nodal displacements at every cross-section. The displacements included the translation and rotation of the top and bottom of the web and the rotations of the top and bottom flanges. The above nodal values were used to determine the deformed shape of the web while flanges were considered as rigid in the formulation. Bradford and Ronagh (1997) enhanced the finite element of Bradford and Trahair (1981) by including the derivatives of the flange rotations in the nodal displacement vector resulting in a model with 8 nodal displacements per cross-section.

Roberts and Jhita (1983) studied buckling modes of symmetric I-beams through energy methods. They studied beams with various ratios of flange width to web height, and observed that distortional buckling can be the critical buckling case for slender beams and can cause a drop in the buckling load.

Bradford and Waters (1988) studied distortional buckling in mono-symmetric I-sections. They observed that when the smaller flange in a mono-symmetric beam is in compression, the decrease in buckling moment due to distortional buckling becomes more significant as the degree of mono-symmetry increase (i.e. the difference between the sizes of the flanges increases). The opposite was seen to be true in cases when the larger flange is in compression. It was observed that the distortional buckling becomes more significant for more slender webs.

Bradford (1994) studied the buckling of post-tensioned composite beams, and concluded that the distortional buckling is the critical mode of instability in beams with continuous lateral support at the top flange, and can cause significant reduction in the ultimate strength of the beam. Bradford (2000) proposed a special-purpose inelastic finite element for buckling analysis of beams with continuous and complete tension flange restraint. Vrcelj and Bradford (2009) produced a spline finite strip method to study the inelastic buckling behaviour of composite beams. Chen and Wang (2012) performed a comprehensive finite element study of composite beams and concluded that the use of web stiffeners to prevent distortional buckling would considerably increase the buckling load.

Zhou *et al.* (2016) studied distortional buckling behaviour of composite concrete-steel structures. They developed empirical relations that incorporated the effect of distortional buckling in negative moment areas by using a modified elastic foundation beam method.

2.4. Summary

Thin-walled members are introduced in this chapter, and the classical theory of thin-walled beams is discussed in more detail. This discussion shows that due to the inherent geometry of these members, instabilities can have a significant effect in decreasing the load-carrying capacity of thin-walled members and hence, buckling analysis should be an integral part of the design. Three main categories of instabilities in thin-walled members, namely, global, local and distortional buckling are discussed, and the corresponding literature is presented.

Chapter 3: Composite Elements

3.1. Introduction

In this chapter, an extensive introduction of the fibre-reinforced composite materials including their characteristics, manufacturing process and mechanics is presented.

The advantages and disadvantages of these materials are discussed in Section 3.2. The stacking sequence of the laminate layers and their denotation is described in Section 3.3 followed by the manufacturing procedure of laminate composite profiles in Section 3.4. The mechanics of composite laminates is discussed in Section 3.5 while the final section is dedicated to a comprehensive review of the literature on the buckling analysis of thin-walled laminated composite beams.

3.2. Advantages and disadvantages

Composite materials are made by assembling two or more components synthetically to obtain desired properties and characteristics. A composite element mainly consists of two components: a reinforcing component and a compatible matrix binder. Fibre-reinforced composite-laminated materials are the most commonly used types of composite materials. In these types of materials, the fibres provide the strength and stiffness, and the matrix is responsible for binding the fibres together, keeping them in place, transferring and distributing the load between them, providing the inter-laminar shear strength of the composite, protecting the element from high temperature and corrosion, and resisting crack propagation and damage.

Fibre-reinforced composite materials have been increasingly used in the past decades in a variety of structures such as aerospace structures, automobile industry, naval and civil engineering fields. The main reason for this increase is the superior features of these types of materials which can be summarized as:

- High ratio of tensile strength and stiffness to weight,
- Light weight,
- Long term durability,
- Non-corrosive nature,
- Electromagnetic neutrality,
- Enhanced fatigue life,
- Resistance to chemical attack,
- Low thermal expansion compared to other construction materials.

Figure 3.1: Some prototypes made up of Fibre-reinforced composite materials

Because of their high ratios of strength to weight the slender FRP shapes such as thin-walled open sections have been extensively used in the construction industry. Due to their slenderness their susceptibility to buckling is the main concern in the structural design of these elements. Therefore, it is important to predict the buckling loads accurately to have a reliable design.

3.3. Stacking sequence

Fibre-reinforced composite materials are made in the shape of a thin layer called “lamina”. The composite structural elements are created by stacking the fibre-reinforced layers together in variable angles. By choosing the orientation of fibres in each lamina and stacking sequences of layers in the element the desirable properties for the structural element are obtained. A brief explanation about the stacking sequence notations is presented in the following.

The fibre orientation of each layer with respect to the global coordination is determined by angle Φ_k about the x axis which in here is the angle between the fibre direction in each layer and the longitudinal axis of the element (z axis) (Figure 3.2).

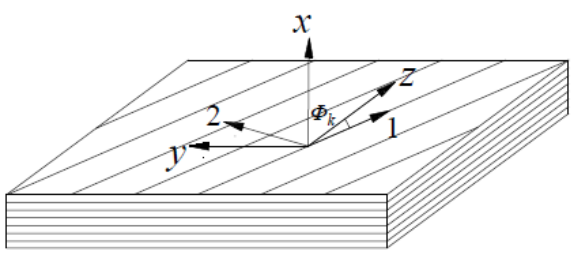

Figure 3.2: Fibre Orientation of Layers with Respect to the Global Orientation

To denote the stacking sequence of laminates, the angles of composite laminate layers are written in brackets or parentheses from the top outermost ply to the bottom ply. If the fibre orientations of layers are symmetric with respect to the mid-plane of the element the laminate configuration is called “symmetric” angle-ply stacking sequence. In this case, we can simply write the angles of the layers in the top half of the cross-section and print a subscript of “s” for the bracket to denote “symmetric”. In addition, in the case that a stacking sequence is repeated in a group of layers we can write them once and write the number of the repetition as a subscript for that group. A number of different stacking sequences and their denotations are presented in Figure 3.3.

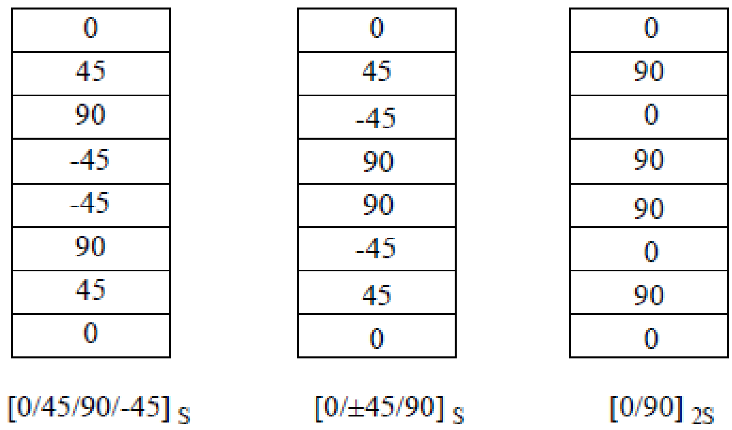

Figure 3.3: Some Examples of Stacking sequence of Laminates with their Denotations

This study is limited to composite laminates with symmetric angle-ply stacking sequence.

3.4. Production

The most commonly used method of manufacturing of composite laminate profiles is called ―Pultrusion”, which is a portmanteau word combining ―Pull” and ―Extrusion”.

Both the Extrusion and Pultrusion methods are used to manufacture profiles of constant cross-section. The Extrusion process, which is used for steel, aluminium and wood-based composites, consists of pushing of the material through a die of a certain shape to produce the desired section. However, the pultrusion method is used for the production of fibre-reinforced composite profiles, and is achieved by pulling the material through a heated die. A schematic of the pultrusion process is shown in Figure 3.4.

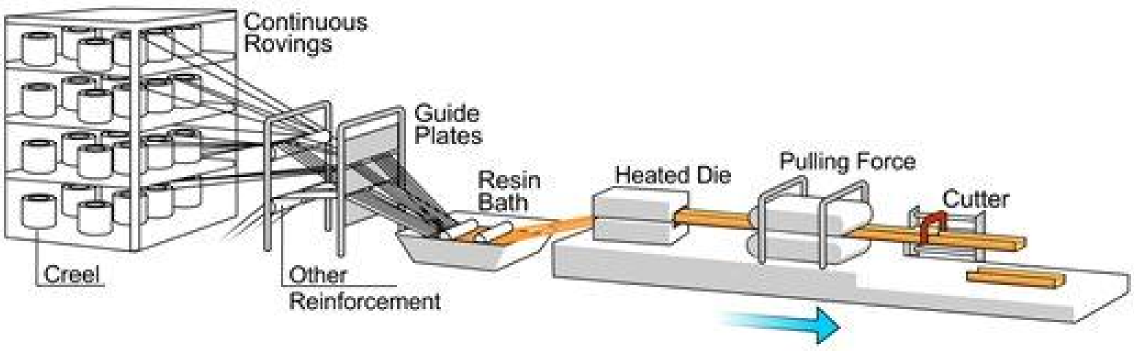

Figure 3.4: Pultrusion Process (Courtesy of Allnex Industries)

In this method, the reinforcing fibres are pulled through a guide that precisely places the fibres in the required location with respect to the final section. The fibres are then impregnated with the binding matrix, which is normally resin. The combination of the fibres and the matrix material is then pulled through a heated die where the cross-section is shaped into its desired profile. Pultrusion allows for continuous production of composite profiles of complex shapes at a high manufacturing rate.

3.5. Mechanics of Composite laminates

The relationship between the stress and strain in an isotropic material is independent of the direction of the applied force, and can be described in terms of the constants Young‘s modulus and the Poisson‘s ratio for linear elastic materials. However, a fibre-reinforced plate has different elastic properties in the longitudinal direction of the fibres and in the transverse direction, i.e. it is orthotropic. Subscripts 1 and 2 are used for the longitudinal and transverse directions, respectively from hereafter. The stiffness of fibre-reinforced plates are significantly larger in the 1-direction than in the 2-direction.

The stress-strain relationships for the two directions of an orthotropic plate subjected to uniaxial loading can be written as

$$\sigma_1 = E_1 \varepsilon_1 \tag{3.1}$$

$$\sigma_2 = E_2 \varepsilon_2 \tag{3.2}$$

In a more general case, stresses are applied at more than one direction of the plate, in which case the strain in 1 and 2 directions can be written as

$$\varepsilon_1 = \frac{\sigma_1}{E_1} - \nu_{21} \varepsilon_2 \tag{3.3}$$

$$\varepsilon_2 = \frac{\sigma_2}{E_2} - \nu_{12} \varepsilon_1 \tag{3.4}$$

where the Poisson‘s ratio ν_{12} can be defined as the ratio of strain in the transverse direction over the strain in the longitudinal direction as a result of loading along the fibres, i.e.

$$\nu_{12} = \frac{\varepsilon_2}{\varepsilon_1}, \text{ for loading in 1-direction} \tag{3.5}$$

If shear stresses are present, the relationship between the shear stress and strain can be written as

$$\tau_{12} = \gamma_{12} G_{12} \tag{3.6}$$

The above equations can be written in matrix form as

$$\begin{Bmatrix} \sigma_1 \\ \sigma_2 \\ \tau_{12} \end{Bmatrix} = \begin{bmatrix} Q_{11} & Q_{12} & 0 \\ Q_{12} & Q_{22} & 0 \\ 0 & 0 & Q_{66} \end{bmatrix} \begin{Bmatrix} \varepsilon_1 \\ \varepsilon_2 \\ \gamma_{12} \end{Bmatrix} \tag{3.7}$$

or in a more condensed form as

$$[\boldsymbol{\sigma}] = [\mathbf{Q}][\boldsymbol{\varepsilon}] \tag{3.8}$$

where

$$Q_{11} = \frac{E_1}{1 - \nu_{12}\nu_{21}} \tag{3.9}$$

$$Q_{22} = \frac{E_2}{1 - \nu_{12}\nu_{21}} \tag{3.10}$$

$$Q_{12} = \frac{\nu_{12} E_2}{1 - \nu_{12}\nu_{21}} = \frac{\nu_{21} E_1}{1 - \nu_{12}\nu_{21}} \tag{3.11}$$

$$Q_{66} = G_{12} \tag{3.12}$$

Note that Eq. (3.7) is only valid if the load is only applied along the fibres or perpendicular to them. The orthotropic plate in this condition is called ―specially orthotropic".

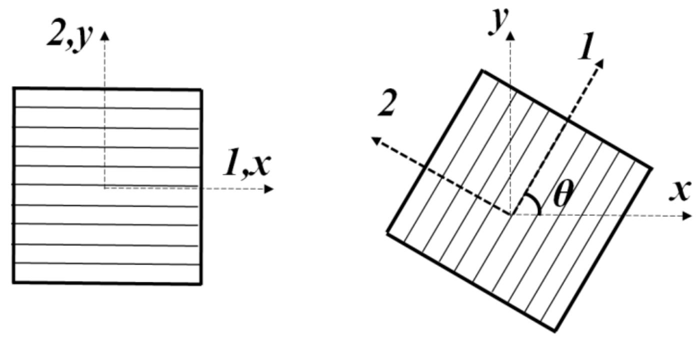

(a) specially-orthotropic plate (b) generally-orthotropic plate

Figure 3.5: Orthotropic Plate (1-2 fibre alignment, *x-y* load direction)

In ―generally orthotropic" plates, namely, in cases where the applied load is at an angle other than 0 or 90 degrees, a transformation matrix **T** is used to obtain the rotated relationship, i.e.,

$$[\boldsymbol{\sigma}] = [\mathbf{T}]^{-1}[\mathbf{Q}][\mathbf{T}][\boldsymbol{\varepsilon}] \tag{3.13}$$

where T is the transformation matrix and can be written in terms of the rotation angle as

$$\mathbf{T} = \begin{bmatrix} \cos^2\theta & \sin^2\theta & 2\sin\theta\cos\theta \\ \sin^2\theta & \cos^2\theta & -2\sin\theta\cos\theta \\ -\sin\theta\cos\theta & \sin\theta\cos\theta & \cos^2\theta - \sin^2\theta \end{bmatrix} \tag{3.14}$$

in which θ is the angle between the fibre orientation and the axis of the beam, as shown in Figure 3.5.

The rotated **Q** matrix can be defined as $\bar{\mathbf{Q}}$ such that

$$\bar{\mathbf{Q}} = [\mathbf{T}]^{-1}[\mathbf{Q}][\mathbf{T}] \tag{3.15}$$

$$\bar{\mathbf{Q}} = \begin{bmatrix} \bar{Q}_{11} & \bar{Q}_{12} & \bar{Q}_{16} \\ \bar{Q}_{12} & \bar{Q}_{22} & \bar{Q}_{26} \\ \bar{Q}_{16} & \bar{Q}_{26} & \bar{Q}_{66} \end{bmatrix} \tag{3.16}$$

Based on this definition, the constitutive relationship of a generally orthotropic plate can be written as

$$[\boldsymbol{\sigma}] = \left[\bar{\mathbf{Q}}\right][\boldsymbol{\varepsilon}] \tag{3.17}$$

The components of matrix $\bar{\mathbf{Q}}$ can be written explicitly as

$$\bar{Q}_{11} = Q_{11}\cos^4\theta + 2\left(Q_{12} + 2Q_{66}\right)\sin^2\theta\cos^2\theta + Q_{22}\sin^4\theta, \tag{3.18}$$

$$\bar{Q}_{12} = \left(Q_{11} + Q_{22} - 4Q_{66}\right)\sin^2\theta\cos^2\theta + Q_{12}\left(\sin^4\theta + \cos^4\theta\right), \tag{3.19}$$

$$\bar{Q}_{22} = Q_{11}\sin^4\theta + 2\left(Q_{12} + 2Q_{66}\right)\sin^2\theta\cos^2\theta + Q_{22}\cos^4\theta, \tag{3.20}$$

$$\bar{Q}_{16} = \left(Q_{11} - Q_{22} - 2Q_{66}\right)\sin\theta\cos^3\theta + \left(Q_{12} - Q_{22} + 2Q_{66}\right)\sin^3\theta\cos\theta, \tag{3.21}$$

$$\bar{Q}_{26} = \left(Q_{11} - Q_{22} - 2Q_{66}\right)\sin^3\theta\cos\theta + \left(Q_{12} - Q_{22} + 2Q_{66}\right)\sin\theta\cos^3\theta, \tag{3.22}$$

$$\bar{Q}_{66} = \left(Q_{11} + Q_{22} - 2Q_{12} - 2Q_{66}\right)\sin^2\theta\cos^2\theta + Q_{66}\left(\sin^4\theta + \cos^4\theta\right). \tag{3.23}$$

It can be observed from the above equations that for θ values other than 0 and 90 degrees, $\bar{Q}_{16}$ and $\bar{Q}_{26}$ are nonzero. Consequently, normal strains produce shear stresses and vice versa. This phenomenon is called extension-shear coupling.

3.6. Literature review

In this section a comprehensive literature review of the previous studies and research works about the buckling analysis of laminated fibre-reinforced composite material is presented.

For the first time, Bauld and Tzeng (1984) performed a study for buckling analysis of thin-walled beams with laminated fibre-reinforced composite material by extending the Vlasov's thin-walled beam theory for isotropic material. In their study, the shear deformation effects were neglected.

The lateral-torsional buckling of FRP beams were experimentally tested by Mottram (1992) and the results showed the importance of shear deformation effects in buckling analysis of laminated fibre-reinforced composite material. Barbero and Tomblin (1993) performed an experimental study for determining the Euler buckling load of various FRP I-shaped columns.

By using the Galerkin method for solving the equilibrium differential equation, an analytical study for optimal fibre orientation for lateral buckling strength of thin-walled composite members was presented by Pandey *et al.* (1995b). Lin *et al.* (1996) performed a parametric study for optimum fibre direction in the lateral buckling behaviour of FRP I-shaped beams. Murakami and Yamakawa (1996) presented an analytical solution of anisotropic cantilever beams by using the Airy's stress function and two beam theories. Davalos and Qiao (1997) performed a combined analytical and experimental study of flexural-torsional and lateral-distorsional buckling of fibre-reinforced plastic (FRP) composite wide-flange (WF) beams. However, the closed-form solutions are limited to certain loading types and boundary conditions. On the other hand, the numerical techniques such as finite element method can be used for obtaining the approximate solutions that are applicable to general cases with various types of loading and boundary conditions.

The shear deformation effects play an important role in the linear stability analysis of beams with built-up or composite sections and in elements made of fibre-reinforced composite-laminated materials with relatively low shear modulus.

Libove (1988) considering the bending shear deformability, developed a theory for calculating shear-flows and normal stresses applied to thin-walled beams of closed section. An analytical study of the transverse shear strain effect on the lateral buckling of thin-walled open-section fibrous composite beams was developed by Sherbourne and Kabir (1995). However, they did not consider the shear flexibility due to warping. Omidvar (1998) investigated the transverse shear deformation effect in the analysis of orthotropic laminated composite thin-walled beams and presented a new formulae for shear coefficients.

Maddur and Chaturvedi (2000) developed a finite element solution for buckling analysis of laminated fibre-reinforced composite I-shaped beams based on first-order shear deformation theory. A displacement-based one-dimensional finite element model applicable to various types of buckling of an axially loaded composite I-section was developed by Lee and Kim (2001). Kollár (2001) developed a closed form solution for the buckling analysis of axially loaded thin-walled open section columns made of orthotropic composite material including the shear deformation effects. By extending Kollar‘s work, Sapkas and Kollar (2002) derived an explicit expression for the lateral-torsional buckling load of thin-walled open-section orthotropic composite beams considering both the transvers shear and the restrained warping induced shear deformations. Qin and Librescu (2002) presented a shear-deformable analytical model for anisotropic thin-walled beams based on the Extended Galerkin‘s Method. Roberts (2002) presented theoretical studies of the influence of shear deformation on the flexural, torsional, and lateral buckling of pultruded FRP I-profiles by applying a reduction factor. Roberts and Masri (2003) developed closed-form solutions for the influence of shear deformation on global flexural, torsional, and lateral buckling of pultruded FRP profiles. Qiao *et al.* (2003) performed a combined analytical and experimental study for flexural-torsional buckling of fibre-reinforced I-shaped cantilever beams. Based on the shear-deformable beam theory, Lee (2005) developed a one-dimensional finite element model for the flexural analysis of I-shaped laminated composite beams. Machado and Cortínez (2005) derived closed-form solutions for the lateral stability analysis of cross-ply laminated thin-walled beams subjected to combined axial and bending loads. Lee (2006) studied lateral buckling of thin-walled composite beams with mono-symmetric cross-sections. By using systematic variational formulation based on the classical lamination theory, a geometrically nonlinear model was given in his model, and a displacement-based one-dimensional finite element model was developed to formulate the problem. Piovan and Cortínez (2007) developed a theoretical model for the generalized linear analysis of composite thin-walled beams with open or closed cross-sections which incorporates, in a full form, the shear deformability. A shear-flexible finite element model for buckling analysis of thin-walled composite I-beams was developed by Back and Will (2008). They derived the governing equations based on the principle of minimum total potential energy.

Kim *et al.* (2008) presented the element stiffness matrix for the buckling analysis of a thin-walled composite beam subjected to an axial load. By extending the nonlinear anisotropic thin-walled beam theory developed by Bauld and Tzeng (1984), they proposed a theory for buckling analysis of a thin-walled composite beam subjected to an axial compressive force.

Kim and Lee (2013) performed shear-deformable lateral buckling analysis of laminate composite mono-symmetric I-sections by defining the displacement fields based on the first-order shear deformable beam theory. Nguyen *et al.* (2015) developed a formulation for optimum design of thin-walled composite members to maximize the critical flexural-torsional buckling load of axially loaded columns. This buckling load is calculated by a displacement-based one-dimensional finite element model.

As will be discussed in more details in the following chapters, a hybrid finite element formulation is developed in this study for the flexural and lateral-torsional buckling analysis of thin-walled composite laminates. The hybrid functional is developed based on the total potential energy using the Lagrange Multipliers Method. The shear deformation effects are considered in this method without modifying the kinematic assumptions.

Chapter 4: Shear Deformable Hybrid Finite-element Method

4.1. Introduction

Different methods of analysis have been developed to assess the buckling behaviour of thin-walled members. Closed-form solutions were the first to be developed for such purposes. Although they lead to exact results for the buckling load, their use is limited to simple loading and boundary conditions because the differential equations can only be solved for such cases. Consequently, numerical methods have been developed for the analysis of structures with complicated geometry, loading and boundary conditions. Among the numerical methods, Finite Element Method (FEM) is the most commonly used numerical technique which can be categorized in two main groups: single-field FEM and multi-field FEM.

In this chapter, a brief literature review of the closed-form solutions for buckling analysis of thin-walled members is presented in section 4.2. A summary of the available numerical methods with an emphasis on the finite element method is described in section 4.3. Then, different types of finite element method are described in Section 4.4 along with a short discussion on the advantages and disadvantages of each method. In section 4.5 a literature review of hybrid methods is presented, and in section 4.6 the hybrid finite element model developed in this study for the buckling analysis of composite thin-walled members and used in the following chapters of this thesis is introduced in more details.

4.2. Closed-form solutions

Development of the closed-form solutions for the buckling analysis of thin-walled members have been started from the late nineteen century (Michell 1899, Prandtl L 1899, Reissner 1904, Wagner 1936). In these methods, the differential equations are developed and solved for the exact design conditions of the element which leads to the exact values for the buckling loads. However, the analytical solutions can be developed only for simple structures with simple loading and boundary conditions since obtaining the exact solution of the differential equations for the more general cases is not straightforward.

As an example, Euler (1757) formulated the differential equation for the flexural buckling analysis of a column subjected to a compressive axial load at the centroid of the cross-section as

$$EIv'' + Pv = 0 \quad \rightarrow \quad v'' + \frac{P}{EI}v = 0 \tag{4.1}$$

He developed the solution of the above differential equation for the case of the simply-supported column $\left(v(0) = v(l) = 0\right)$ as

$$v = A\sin \beta x \tag{4.2}$$

in which $\beta L = \pi$ is defined. The Euler buckling load obtained from the differential equation is given as

$$P = \frac{\pi^2 EI}{L^2} \tag{4.3}$$

This equation does not provide an exact solution for columns with other loading and boundary conditions.

Due to the mentioned limitations of the analytical solutions, they are not suitable options for the practical problems with complicated loading types and boundary conditions. Therefore, one tends to use the numerical methods for the buckling analysis of thin-walled members. Although the numerical solutions provide approximate results for buckling analysis, they can be used for complicated problems with any configurations, types of loading and boundary conditions.

4.3. Numerical methods

The numerical methods can be categorized in different groups such as finite difference methods, finite integral method, finite strip method and finite element method.

Among these numerical methods, the finite element method is the most widely used method for the buckling analysis of complex structures with various loading and boundary conditions. In the finite element method, the whole element is discretised into small segments, and by summing the variational formulation for each segment, the variational functional for the entire element is obtained. The displacements, stresses and strains of the element are expressed in terms of internal parameters that are independent from one segment to the other. The independent inter-boundary displacements are compatible along the inter-element boundary automatically.

The element type and element mesh in a finite element model can be chosen based on the conditions of the structure. The larger the number of elements, the more accurate is the finite element solution but also the more time and computer memory is needed.

Finite element methods can be categorized in two main groups: single-field finite elements and multi-field or hybrid finite elements. The first group, which is known as the *primal* finite element, is further categorized in two types based on its unknown field variables: displacement-based elements and stress-based elements. It means that, in the displacement-based methods the displacements and in the stress-based methods the stresses are the only field variables. On the other hand, there are more than one unknown field variables present in Hybrid finite element methods.

In the following sections, each method is explained in more details and previous works in the literature are introduced.

4.4. Displacement-based and Stress-based FEM

There are two types of primal finite element methods in structural and solid mechanics. The first one is the displacement-based method, in which the displacements are the only field variables. In this method, assumed displacements are compatible both within each element and along the inter-element boundary. The other primal finite element method is the stress-based method in which the stresses are the only field variables. In the stress-based method, the stresses are equilibrating within each element and the tractions are reciprocating along the inter-element boundary (Pian 1995).

The majority of finite elements used in the analysis of composite laminates are developed based on the displacement-based method as a result of its straightforward procedure. In these types of finite element methods, the Principle of Stationary Potential Energy is used to develop the formulation. On the other hand, the Principle of Stationary Complementary Energy is used for developing stress-based finite element methods.

Krajcinovic (1969) obtained a displacement-based finite element model for the buckling analysis of thin-walled open sections. His model had two nodes with 4 degrees of freedom for each node. Using Vlasov theory, Barsoum and Gallagher (1970) developed displacement-based finite element formulations for flexural and lateral-torsional buckling analysis of thin-walled beams. Their finite element model was formulated based on the principle of stationary of virtual work. Attard (1986) presented a finite element formulation for the lateral buckling analysis of thin-walled beams by using the second variation of the total potential energy. Yang and McGuire (1986) developed a formulation of thin-walled beams based on the principle of virtual displacements.

In composite laminates, shear deformation effects can be significant due to a relatively small shear rigidity of fibre-reinforced laminates. Consequently, a large number of finite elements are developed to incorporate such effects in the buckling analysis of composite thin-walled members.

Lin *et al.* (1996) presented a finite element model to study the buckling behaviour of thin-walled glass FRP members. Lee *et al.* (2002) and Lee and Kim (2002) developed a displacement-based one-dimensional finite element model based on Vlasov's thin-walled beam theory to obtain critical loads for thin-walled composite beams with various boundary conditions. By using systematic variational formulation based on the classical lamination theory, Lee (2006) developed a geometrically nonlinear model, and a displacement-based one-dimensional finite element to formulate the problem. Kim *et al.* (2007) proposed a numerical method for buckling analysis of thin-walled composite beams subjected to end moments. In their study, the bifurcation type buckling theory of thin-walled composite beams subjected to pure bending is developed based on the energy functional. Back and Will (2008) developed a shear-flexible finite element for buckling analysis of thin-walled composite members based on the principle of minimum total potential energy. Kim and Lee (2013) performed shear-deformable lateral buckling analysis of laminate composite elements. In their method, the displacement fields were defined using the first-order shear deformable beam theory, and the second order torque terms were introduced from the geometric nonlinearity. Erkmen and Attard (2011) included the shear deformations effects in the buckling analysis of thin-walled members by modifying the kinematic assumptions of the Vlasov Theory. Erkmen and Mohareb (2008) developed a shear deformable stress-based finite element formulation by using the complementary energy functional. The advantage of their method over the displacement-based formulations is that the shear deformations effects can be included without the need for modifying the Vlasov kinematic assumptions. However, the assemblage procedure is more complicated in their method as the inter-element equilibrium conditions have to satisfied a-priori.

One disadvantage of displacement-based finite element methods in buckling analysis of thin-walled members is related to the inclusion of shear deformation effects. In these types of methods, the kinematic assumptions have to be modified in order to include the shear deformations.

The other deficiency of the displacement-based finite element method for the analysis of composite laminates is that the transverse stresses obtained are not continuous across the layers. The reason is that in these methods, the displacement values are the primary variables and are used to calculate the strains, from which the stresses are obtained. Therefore, because of the discontinuity in the stress-strain relationship at the interface of the laminates (e.g. due to change in fibre orientations), there would be a jump in the resulting stress values.

On the other hand, as discussed above, the stress-based finite element formulations require the inter-element equilibrium condition to be satisfied a-priori, which further complicates the assemblage procedure.

To overcome the shortcomings of the displacement- and stress-based method, the hybrid finite element method has been developed for the buckling analysis of composite thin-walled members. In the following section, a brief literature review of the development of the hybrid finite element is presented, followed by a more detailed discussion of the specific procedure used in this study.

4.5. Hybrid Finite Element Method

Hybrid Finite element formulations are generally based on the Hellinger-Reissner functional, in which the displacement and stress fields are assumed independently. For the first time, a multi-field finite element was developed based on the compatible displacements along the element boundary and the assumed equilibrating stresses within the element, and the term “hybrid” element was invented (Pian (1964), Pian and Tong (1968)). Since then, many researchers have developed different versions of multi-field finite element formulation. In one of the methods for classifying the finite element method, the term “mixed” is used for the finite element method in which the element is based on a multi-field variational functional and the term “hybrid” is used for the finite element method which is obtained by enforcing the constraint conditions through Lagrange multipliers (Pian 1978). As in this method of classification, the two elements are not mutually exclusive, the term “hybrid/mixed” was proposed by Pian (1985) for naming all non-primal finite element methods. On the other hand, R.H. Gallagher suggested another method of classification in which the two elements are mutually exclusive (Pian 1994). Based on his classification, both methods are defined as the ones that are developed by multi-field variational functional. However, the “mixed” finite element method refers to formulations in which all the field variables appear explicitly during the assemblage procedure, whereas in the “hybrid” method, stress field variables are eliminated at the element level and only displacement field appears explicitly during assemblage. The hybrid functional can be obtained from both the potential energy functional and the complementary energy functional by enforcing the constraint conditions using the Lagrange Multipliers Method.

Tang *et al.* (1981) formulated a quasi-conforming or string-net element by using the three-field Hu-Washizu variational functional. Lee and Rhiu (1986) presented a mixed finite element formulation based on the Hellinger-Reissner principle with independent strain.

A number of elements have been developed for geometric and material nonlinearity using this method. Spacone *et al.* (1996) proposed a mixed finite element formulation for nonlinear analysis of beams. Petrangeli and Ciampi (1997) concluded that equilibrium-based approaches result in more accurate and robust finite elements that the traditional compatibility-based approach.

Taylor *et al.* (2003) developed a finite element formulation using a three-field variational formula based on an extension of the Hu-Washizu principle. Their element is capable of capturing shear-deformable effects. It was shown that the mixed method results in more accurate results, especially for very coarse mesh discretization. Nukala and White (2004) formulated a geometric and material nonlinear beam finite element based on the Hellinger-Reissner stress variational principle. They adopted the two-field form of the variational principle by using displacement and generalised stresses. Alemdar and White (2005) presented several displacement-based, stress-based, and mixed beam finite elements for nonlinear analysis of frame structures based on Euler-Bernoulli kinematics. They concluded that among the above, the mixed element yields the most accurate results as the use of independent force fields in the element formulation results in more accurate modelling of element curvature fields. Wackerfuß and Gruttmann (2009) developed a mixed hybrid formulation for the nonlinear analysis of beams with rectangular cross-sections. The developed variational formulation adopted displacements, rotations, stress resultants and beam strains as the independent variables. It was demonstrated that the developed formulations allow for nonlinear analyses with very large load steps due to the robustness of the formulation. Alsafadie *et al.* (2010) adopted a corotational technique to develop a mixed finite element formulation based on the incremental form of the Hellinger-Reissner variational principle to capture elasto-plastic material response. Their method is capable of capturing both the Saint-Venant and warping torsion. Santos *et al.* (2010) developed geometrically exact hybrid formulations for three-dimensional analysis of beams using complementary energy-based formulation. Erkmen (2014) formulated a shear-deformable hybrid finite element based on the principle of the complementary energy. In his model, the element equilibrium and force boundary conditions are imposed as auxiliary constraints where conjugate displacement terms can be identified as Lagrange multipliers.

In this study, the hybrid finite element is developed by using the potential energy functional as the starting point and applying the strain-displacement relations through the Lagrange multipliers method.

As discussed in the previous section, the introduction of shear deformation effects in single-field finite elements presents the following difficulties:

- In the displacement-based method, the shear deformation effects should be applied by modifying the kinematic assumptions of the Vlasov thin-walled theory.
- In the stress-based method, the inter-element force equilibrium needs to be satisfied a-priori, which complicates the assemblage procedure of the analysis.

By using the hybrid finite element method, the final equations are defined in terms of the nodal displacement components as unknowns. Consequently, the assemblage procedure would be as straightforward as a displacement-based finite element. It should be noted that these displacement unknowns are obtained by using a multivariable Hellinger-Reissner functional, in which the shear deformation effects are taken into account by using the strain energy of the shear stress field. As a result, the shear deformation effects are considered without any alterations to the classical thin-walled beam kinematics. In addition, in the current hybrid method there is no need to satisfy the inter-element force equilibrium a-priori.

4.6. Development of the hybrid functional from the potential energy functional

The finite element developed in this study is based on the stationary condition of the potential energy functional.

$$\Pi_p = \int_V \left[\frac{1}{2} \boldsymbol{\varepsilon}^{\mathbf{T}} \mathbf{C} \boldsymbol{\varepsilon} - \bar{\mathbf{F}} \mathbf{u} \right] \mathrm{d}V - \int_S \bar{\mathbf{T}}^{\mathbf{T}} \mathbf{u} \mathrm{d}S = \text{stationary} \tag{4.4}$$

By using the strain-displacement relations, $\boldsymbol{\varepsilon}=\mathbf{Du}$, the variational principle that includes displacements as the only variable can be given as

$$\Pi_p(\mathbf{u}) = \int_V \left[\frac{1}{2} (\mathbf{Du})^{\mathbf{T}} \mathbf{C} (\mathbf{Du}) - \bar{\mathbf{F}} \mathbf{u} \right] \mathrm{d}V - \int_S \bar{\mathbf{T}}^{\mathbf{T}} \mathbf{u} \mathrm{d}S = \text{stationary} \tag{4.5}$$

in which $\mathbf{C}$ is the elastic stiffness matrix, $\bar{\mathbf{F}}$ is the prescribed body force and $\bar{\mathbf{T}}$ is the boundary traction vectors.

One of the methods for developing the multi-field variational principle is imposing the constraint conditions through the Lagrange multipliers (Washizu 1982).

The Hu-Washizu variational principle is obtained by relaxing the strain-displacement relation through the Lagrange multipliers which are the stresses. Therefore, this functional contains three field variables: displacements $\mathbf{u}$, strains ε and stresses σ.

$$\Pi_{HW}\left(\mathbf{u},\boldsymbol{\varepsilon},\boldsymbol{\sigma}\right)=\int_V\left[\frac{1}{2}\boldsymbol{\varepsilon}^{\mathrm{T}}\mathbf{C}\boldsymbol{\varepsilon}-\boldsymbol{\sigma}^{\mathrm{T}}\left(\boldsymbol{\varepsilon}-\mathbf{D}\mathbf{u}\right)-\bar{\mathbf{F}}\mathbf{u}\right]\mathrm{d}V-\int_{S_\sigma}\bar{\mathbf{T}}^{\mathrm{T}}\mathbf{u}\mathrm{d}S-\int_{S_w}\bar{\mathbf{T}}^{\mathrm{T}}\left(\mathbf{u}-\bar{\mathbf{u}}\right)\mathrm{d}S=\text{stationary}\qquad(4.6)$$

where $\bar{\mathbf{u}}$ is the prescribed boundary displacements.

By substituting the constitutive relations, one can eliminate either the strain variable or the stress variable, and a functional with two field variables is obtained:

$$\Pi_{HW}\left(\mathbf{u},\boldsymbol{\sigma}\right)=\int_V\left[-\frac{1}{2}\boldsymbol{\sigma}^{\mathrm{T}}\mathbf{S}\boldsymbol{\sigma}-\boldsymbol{\sigma}^{\mathrm{T}}\left(\mathbf{D}\mathbf{u}\right)-\bar{\mathbf{F}}^{\mathrm{T}}\mathbf{u}\right]\mathrm{d}V-\int_{S_\sigma}\bar{\mathbf{T}}^{\mathrm{T}}\mathbf{u}\mathrm{d}S-\int_{S_w}\bar{\mathbf{T}}^{\mathrm{T}}\left(\mathbf{u}-\bar{\mathbf{u}}\right)\mathrm{d}S=\text{stationary}\qquad(4.7)$$

$$\Pi_{HW}\left(\mathbf{u},\boldsymbol{\varepsilon}\right)=\int_V\left[-\frac{1}{2}\boldsymbol{\varepsilon}^{\mathrm{T}}\mathbf{C}\boldsymbol{\varepsilon}-\left(\mathbf{C}\boldsymbol{\varepsilon}\right)^{\mathrm{T}}\left(\mathbf{D}\mathbf{u}\right)-\bar{\mathbf{F}}^{\mathrm{T}}\mathbf{u}\right]\mathrm{d}V-\int_{S_\sigma}\bar{\mathbf{T}}^{\mathrm{T}}\mathbf{u}\mathrm{d}S-\int_{S_w}\bar{\mathbf{T}}^{\mathrm{T}}\left(\mathbf{u}-\bar{\mathbf{u}}\right)\mathrm{d}S=\text{stationary}\qquad(4.8)$$

where $\mathbf{S}$ is the compliance matrix.

Eq.(4.7) is the original Hellinger-Reissner principle which can be written in the following form after applying the divergence theorem:

$$\Pi_{HW}=\int_V\left[-\frac{1}{2}\boldsymbol{\sigma}^{\mathrm{T}}\mathbf{S}\boldsymbol{\sigma}-\left(\mathbf{D}^{\mathrm{T}}\boldsymbol{\sigma}\right)^{\mathrm{T}}\mathbf{u}-\bar{\mathbf{F}}^{\mathrm{T}}\mathbf{u}\right]\mathrm{d}V-\int_{S_\sigma}\left(\mathbf{T}-\bar{\mathbf{T}}\right)^{\mathrm{T}}\mathbf{u}\mathrm{d}S-\int_{S_w}\bar{\mathbf{T}}^{\mathrm{T}}\bar{\mathbf{u}}\mathrm{d}S=\text{stationary}\qquad(4.9)$$

By satisfying the equilibrating stress and prescribed tractions along the boundary, Hellinger-Reissner principle is reduced to the principle of stationary complementary energy with the stresses as the only field variables.

$$\Pi_C = \int_V \frac{1}{2}\boldsymbol{\sigma}^{\mathrm{T}}\mathbf{S}\boldsymbol{\sigma}\mathrm{d}V - \int_{S_w} \overline{\mathbf{T}}^{\mathrm{T}}\overline{\mathbf{u}}\mathrm{d}S = \text{stationary} \tag{4.10}$$

As it will be shown explicitly in the Chapters 5 and 7, Eq. (4.9) can be expressed in terms of the independent field variables of displacement components and stress resultants. Depending on the mode of buckling (e.g. flexural, lateral-torsional), different field variables are considered in the formulations.

It should be noted that in Eq. (4.9), the effect of shear deformations is taken into account by including the strain energy resulting from shear stress, embedded in the stress matrix. As a result, the kinematics of the formulations is the same as the classic thin-walled theory. This is shown explicitly in the following chapters of this thesis.

The method is developed for the buckling analysis of fibre-reinforced composite laminates by substituting the constitutive relations of laminate elements, as discussed in Chapter 3.

Chapter 5: Shear Deformable Hybrid Finite Element Formulation for Flexural Buckling Analysis of Thin-walled Composite Columns

5.1. Introduction

In this chapter, the flexural buckling behaviour of fibre-reinforced laminated composite thin-walled columns subjected to axial concentrated compressive load is studied.

The chapter starts with a comprehensive literature review of previous research works relevant to the flexural buckling behaviour of thin-walled fibre reinforced composite elements (section (5.2)). After discussing the problem statement in section (5.3), the kinematic relations to describe the column behaviour are developed based on the kinematics of general open thin-walled elements in section (5.4). Then, in section (5.5) the constitutive relations for the thin-walled column with a laminate composite cross-section subjected to an axial load are obtained. Using the developed kinematic relations and the constitutive equations, the stress and stress resultants equations are obtained in section (5.6). In section (5.7), the hybrid formulation is developed from the potential energy functional by relaxing the strain-displacement equations as auxiliary conditions through the Lagrange Multipliers method. The discretised form of the hybrid functional for buckling analysis is obtained after the interpolation of stress resultants and lateral displacements in section (5.8). Numerical results are presented in section (5.9) to validate the efficiency and accuracy of the developed hybrid finite element model in flexural buckling analysis of thin-walled columns with fibre-reinforced laminate composite cross-sections. Columns with various boundary conditions are studied and the effect of fibre orientation and the column slenderness on the flexural buckling load are presented.

5.2. Literature review

In this section a literature review of the previous studies and research works about the flexural buckling of thin-walled composite columns is presented.

For an isotropic long column subjected to a compressive load at the centroid of the cross-section, the column formula developed by Euler (1757) can be used to determine the buckling load. In Euler theory it is assumed that the column has no imperfections or load eccentricity.

The buckling behaviour of axially loaded columns with composite materials has been the subject of many studies. In the following, a literature review of the works done in the past including the experimental studies, analytical solutions and finite element models is presented.

A buckling solution for uniaxially-loaded composite open-section elements was developed by Rehfield and Atilgan (1989). Barbero and Raftoyiannis (1990) presented an analytical model to predict the buckling behaviour of pultruded composite columns. Barbero and Tomblin (1993) performed an experimental study for determining the flexural buckling load of various fibre-reinforced composite I-shaped columns. An analytical study for optimal fibre orientation for lateral buckling strength of thin-walled composite members was presented by Pandey *et al.* (1995b). In their study, the beam stiffness coefficients are obtained based on the Vlasov-type linear hypothesis and columns with various types of loading are considered.

Kollár (2001) derived a closed form solution for the buckling analysis of axially loaded thin-walled open section columns made of orthotropic composite materials. The shear deformation effects are included in his model by modifying the Vlasov's theory. A general analytical model applicable to various modes of buckling of an axially loaded composite I-section was developed by Lee and Kim (2001). By using the principle of the stationary value of total potential energy they obtained a displacement-based one-dimensional finite element model. Hassan and Mosallam (2004) presented the results of an experimental study on the buckling behaviour of axially loaded thin-walled pultruded fibre-reinforced polymer composite columns.

Back and Will (2008) developed a shear-flexible finite element model for buckling analysis of thin-walled composite I-beams. The governing equations in their model are derived based on the principle of minimum total potential energy. In addition, they obtained the geometric stiffness for the buckling analysis of axially loaded, thin-walled composite beams.

Kim *et al.* (2008) presented the element stiffness matrix for the buckling analysis of a thin-walled composite beam subjected to an axial load. By extending the nonlinear anisotropic thin-walled beam theory developed by Bauld and Tzeng (1984), they proposed a theory for buckling analysis of a thin-walled composite beam subjected to an axial compressive force. Kim and Lee (2014) developed a numerical algorithm to calculate the exact buckling load of the thin-walled laminated composite column subjected to variable axial force. A formulation for optimum design of thin-walled composite beams was developed by Nguyen *et al.* (2015). The objective of their optimization problem is to maximize the critical flexural-torsional buckling load of an axially loaded column. This buckling load is calculated by a displacement-based one-dimensional finite element model.

In this study, a hybrid finite element formulation for flexural buckling analysis of an axially-loaded thin-walled composite column is developed. In this method, the shear deformation effects are included in the formulation by using the strain energy of the equilibrating shear stress field without modifying the basic kinematic assumptions of the beam theory (unlike in the displacement-based finite element methods). In addition, the non-collinear elements can be connected very easily in this method without the need to satisfy the inter-element equilibrium (unlike in the complementary energy based methods).

5.3. Problem statement

Figure 5.1 shows a column that is subjected to a concentrated compressive force P applied at the centroid of the cross-section at the end of the column. By increasing the applied load, the column will behave differently depending on its slenderness. In short columns, the element will fail when the stress exceeds the compressive yield strength of the material. However, columns with high slenderness ratio will buckle before the yield strength of the material is reached.

The internal axial force, shear force and bending moment are shown in the free-body diagram of a small segment of the member at the buckled state in Figure 5.1.

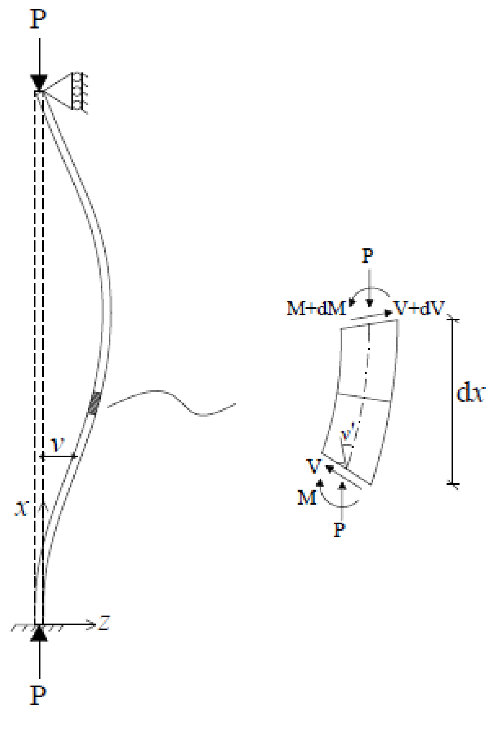

Figure 5.1: An Axially Loaded Column and the Free-body Diagram of a Small Segment

5.4. Kinematics

In order to develop the theoretical model the following assumptions are adopted in this study:

1. The thin-walled member is assumed to be prismatic and straight.
2. Cross-sections remain plane during deformation in accordance with the first assumption of Thin-walled Beam Theory of Vlasov.
3. Strains are small.
4. Material is linearly elastic and obeys Hooke's law.
5. Inextensional buckling assumption is adopted, which means that the shortening of the column during the buckling behaviour is ignored.
6. Pre-buckling deformation effects are neglected.

The coordinate system that is adopted here is the Orthogonal Cartesian Coordinate System (x,y,z) in which the x axis is along the longitudinal axis of the column, and y and z axes lie on the plane of the cross-section and are parallel to the weak and strong axes of the cross-section, respectively. (Figure 5.2)

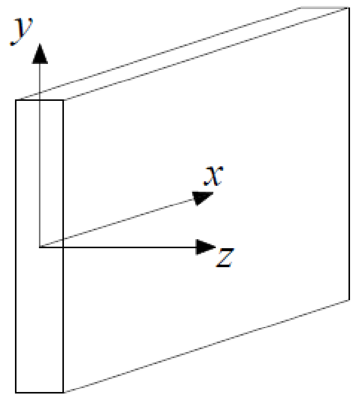

Figure 5.2: The orthogonal Cartesian system

The longitudinal displacement of any point on the cross section of the column can be expressed in terms of the displacements of the centroid of the cross-section as:

$$w = \bar{w}(x) - u'(x)y - v'(x)z - \phi'(x)\omega \tag{5.1}$$

in which $u(x)$ and $v(x)$ are lateral displacements in y and z respectively and $\phi(x)$ is the angle of twist of the cross-section. All primes denote differentiation with respect to longitudinal coordinate x.

As shown in Figure 5.1, in flexural buckling of the column, the vertical displacement $u(x)$ and the angle of twist of the cross-section $\phi(x)$ are equal to zero. Therefore, Eq. (5.1) will reduce to

$$w = \bar{w}(x) - v'(x)z \tag{5.2}$$

In addition, in agreement with the inextensional buckling assumption, the shortening of the column is assumed to be negligible during buckling (so that the axial force and bending moment remain unchanged). As a result, the displacement along the x axis can be given as

$$w = -v'(x)z \tag{5.3}$$

Consequently, the longitudinal normal strain induced by the flexural buckling deformations can be expressed as

$$\varepsilon_x = -v''(x)z \tag{5.4}$$

Based on the second assumption of the Vlasov theory:

$$\gamma_{xz} = 0 \tag{5.5}$$

Thus, Euler-Bernoulli beam kinematics is adopted for the analysis.

5.5. Constitutive relation

Consider a laminate composed of n orthotropic layers in which the fibre orientation of each layer with respect to the global coordination is determined by angle Φ_k about the z axis (Figure 5.3). Assuming that perfect inter-laminar bond exists between the layers, the stress-strain relationship for the k^{th} layer is given as:

$$\boldsymbol{\sigma}^{(k)} = \bar{\mathbf{Q}}^{(k)}\boldsymbol{\varepsilon} \Rightarrow \begin{Bmatrix} \sigma_x^{(k)} \\ \sigma_y^{(k)} \\ \tau_{xz}^{(k)} \\ \tau_{xy}^{(k)} \end{Bmatrix} = \begin{bmatrix} \bar{Q}_{11}^{(k)} & \bar{Q}_{12}^{(k)} & 0 & \bar{Q}_{16}^{(k)} \\ \bar{Q}_{12}^{(k)} & \bar{Q}_{22}^{(k)} & 0 & \bar{Q}_{26}^{(k)} \\ 0 & 0 & Q_{44}^{(k)} & 0 \\ \bar{Q}_{16}^{(k)} & \bar{Q}_{26}^{(k)} & 0 & \bar{Q}_{66}^{(k)} \end{bmatrix} \begin{bmatrix} \varepsilon_x \\ \varepsilon_y \\ \gamma_{xz} \\ \gamma_{xy} \end{bmatrix} \tag{5.6}$$

In here, subscripts 1 to 6 are consistent with the convention adopted for laminated composites (Wang 1997). In Eq. (5.6)

$$\bar{Q}_{11}^{(k)} = Q_{11}^{(k)} \cos^4 \Phi_k + 2\left(Q_{12}^{(k)} + 2Q_{66}^{(k)}\right)\sin^2 \Phi_k \cos^2 \Phi_k + Q_{22}^{(k)} \sin^4 \Phi_k \tag{5.7}$$

$$\bar{Q}_{12}^{(k)} = \left(Q_{11}^{(k)} + Q_{22}^{(k)} - 4Q_{66}^{(k)}\right)\sin^2 \Phi_k \cos^2 \Phi_k + Q_{12}^{(k)}\left(\sin^4 \Phi_k + \cos^4 \Phi_k\right) \tag{5.8}$$

$$\bar{Q}_{22}^{(k)} = Q_{11}^{(k)} \sin^4 \Phi_k + 2\left(Q_{12}^{(k)} + 2Q_{66}^{(k)}\right)\sin^2 \Phi_k \cos^2 \Phi_k + Q_{22}^{(k)} \cos^4 \Phi_k \tag{5.9}$$

$$\bar{Q}_{26}^{(k)} = \left(Q_{11}^{(k)} - Q_{22}^{(k)} - 2Q_{66}^{(k)}\right)\sin^3 \Phi_k \cos \Phi_k + \left(Q_{12}^{(k)} - Q_{22}^{(k)} + 2Q_{66}^{(k)}\right)\sin \Phi_k \cos^3 \Phi_k \tag{5.10}$$

$$\bar{Q}_{16}^{(k)} = \left(Q_{11}^{(k)} - Q_{12}^{(k)} - 2Q_{66}^{(k)}\right)\sin \Phi_k \cos^3 \Phi_k + \left(Q_{12}^{(k)} - Q_{22}^{(k)} + 2Q_{66}^{(k)}\right)\sin^3 \Phi_k \cos \Phi_k \tag{5.11}$$

$$\bar{Q}_{66}^{(k)} = \left(Q_{11}^{(k)} + Q_{22}^{(k)} - 2Q_{12}^{(k)} - 2Q_{66}^{(k)}\right)\sin^2\Phi_k\cos^2\Phi_k + Q_{66}^{(k)}\left(\sin^4\Phi_k + \cos^4\Phi_k\right) \tag{5.12}$$

$$Q_{44}^{(k)} = G_{13}^{(k)} \tag{5.13}$$

where

$$Q_{11}^{(k)} = \frac{E_1^{(k)}}{1 - \upsilon_{12}^{(k)}\upsilon_{21}^{(k)}} \tag{5.14}$$

$$Q_{12}^{(k)} = \frac{\upsilon_{12}^{(k)}E_1^{(k)}}{1 - \upsilon_{12}^{(k)}\upsilon_{21}^{(k)}} \tag{5.15}$$

$$Q_{22}^{(k)} = \frac{E_2^{(k)}}{1 - \upsilon_{12}^{(k)}\upsilon_{21}^{(k)}} \tag{5.16}$$

$$Q_{66}^{(k)} = G_{12}^{(k)} \tag{5.17}$$

where $E_1^{(k)}$ and $E_2^{(k)}$ are Young's moduli of the k^{th} layer in the local $\bar{x}_k$ and $\bar{y}_k$ directions, respectively, $G_{12}^{(k)}$ is the shear modulus in $\bar{x}_k\bar{y}_k$ plane of the k^{th} layer, $G_{13}^{(k)}$ is the shear modulus in $\bar{x}_k\bar{z}_k$ plane, $\upsilon_{12}^{(k)}$ is the Poisson's ratio defined as the ratio of the transverse strain in the $\bar{y}_k$ direction to the axial strain in $\bar{x}_k$ direction due to the normal stress in $\bar{x}_k$ direction, and $\upsilon_{21}^{(k)}$ is the Poisson's ratio defined as the ratio of the transverse strain in the $\bar{x}_k$ direction to the axial strain in $\bar{y}_k$ direction due to the normal stress in $\bar{y}_k$ direction (Omidvar and Ghorbanpoor 1996, Reddy 2003). In this study laminate configuration is limited to symmetric angle-ply stacking sequence with respect to mid-plane.

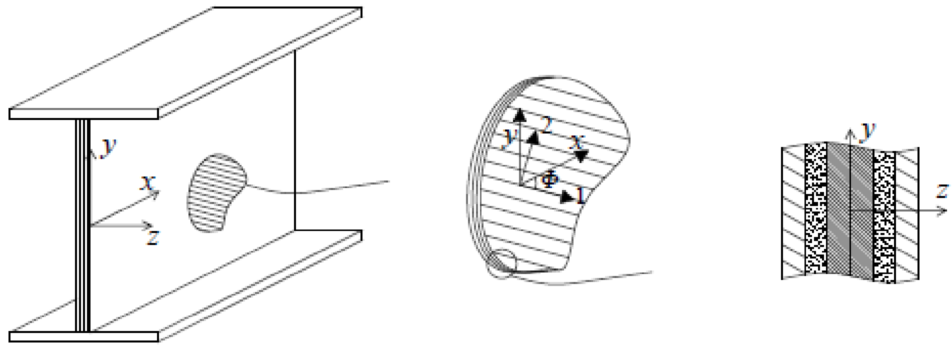

(a) Thin-walled column (b) Fibre orientations c) Laminates across the thickness

Figure 5.3: Thin-walled Column Composed of Fibre-reinforced Laminates

As one can see in Figure 5.3, the y direction is assumed to be perpendicular to the element thickness so in the web the coordinate system rotates 90 degrees around the x axis. Adopting the assumption of free stress in y direction $\sigma_y = 0$, Eq. (5.6) will be reduced to

$$\begin{Bmatrix} \sigma_x{}^{(k)} \\ \tau_{xz}{}^{(k)} \\ \tau_{xy}{}^{(k)} \end{Bmatrix} = \begin{bmatrix} \bar{Q}_{11}^{(k)*} & 0 & \bar{Q}_{16}^{(k)*} \\ 0 & Q_{44}^{(k)} & 0 \\ \bar{Q}_{16}^{(k)*} & 0 & \bar{Q}_{66}^{(k)*} \end{bmatrix} \begin{bmatrix} \varepsilon_x \\ \gamma_{xz} \\ \gamma_{xy} \end{bmatrix} \tag{5.18}$$

in which

$$\bar{Q}_{11}^{(k)*} = \bar{Q}_{11}^{(k)} - \frac{\bar{Q}_{12}^{(k)2}}{\bar{Q}_{22}^{(k)}} \tag{5.19}$$

$$\bar{Q}_{16}^{(k)*} = \bar{Q}_{16}^{(k)} - \frac{\bar{Q}_{12}^{(k)}\bar{Q}_{26}^{(k)}}{\bar{Q}_{22}^{(k)}} \tag{5.20}$$

$$\bar{Q}_{66}^{(k)*} = \bar{Q}_{66}^{(k)} - \frac{\bar{Q}_{26}^{(k)2}}{\bar{Q}_{22}^{(k)}} \tag{5.21}$$

In addition, considering that it is an in-plane analysis, shear stress along the strong axis is assumed to be equal to zero (${\tau_{xy}}^{(k)} = 0$). Thus the final form of constitutive relations can be given as

$$\begin{Bmatrix} {\sigma_x}^{(k)} \\ {\tau_{xz}}^{(k)} \end{Bmatrix} = \begin{bmatrix} \hat{\bar{Q}}_{11}^{(k)*} & 0 \\ 0 & Q_{44}^{(k)} \end{bmatrix} \begin{bmatrix} \varepsilon_x \\ \gamma_{xz} \end{bmatrix} \tag{5.22}$$

in which

$$\hat{\bar{Q}}_{11}^{(k)*} = \bar{Q}_{11}^{(k)*} - \frac{\bar{Q}_{16}^{(k)*2}}{\bar{Q}_{66}^{(k)*}} \tag{5.23}$$

5.6. Stresses and stress resultants

This section aims at obtaining the stress expressions ${\sigma_x}^{(k)}$ and ${\tau_{xz}}^{(k)}$ in terms of stress resultants M and V .

From the first row of the constitutive relations matrix (Eq. (5.22)) the normal stress can be obtained in terms of strains as below

$${\sigma_x}^{(k)} = \hat{\bar{Q}}_{11}^{(k)*} \varepsilon_x \tag{5.24}$$

By substituting the expression of the longitudinal strains developed in the previous section (Eq. (5.4)) in Eq. (5.24), the longitudinal stress is obtained as

$${\sigma_x}^{(k)} = -\hat{\bar{Q}}_{11}^{(k)*} v''(x) z \tag{5.25}$$

Considering the definitions of stress resultant functions, bending moment is expressed as

$$M = -\int_A \sigma_x z \mathrm{d}A \tag{5.26}$$

Substituting Eq. (5.24) in Eq. (5.26), bending moment can be obtained in terms of the displacement derivatives as

$$M = J_{yy} v''(x) \tag{5.27}$$

in which, $J_{yy} = \int_A \hat{\bar{Q}}_{11}^{(k)*} z^2 \mathrm{d}A$ is defined.

Using Eqs. (5.25) and (5.27), the expression for the normal stress in terms of stress resultant function is obtained, i.e.

$$\sigma_x^{(k)} = -\hat{\bar{Q}}_{11}^{(k)*} M \frac{z}{J_{yy}} \tag{5.28}$$

The shear stress $\tau_{xz}^{(k)}$ which is due to the shear force can be obtained as follows.

The shear force F_s can be obtained from the longitudinal equilibrium of the free-body diagram of a piece cut from the member (Figure 5.4).

$$\mathrm{d}F_s + \int_{A'} (\sigma_x + \mathrm{d}\sigma_x) \mathrm{d}A - \int_{A'} \sigma_x \mathrm{d}A = 0 \tag{5.29}$$

in which A' is the cross-sectional area of the piece cut from the segment $\mathrm{d}x$. Substituting Eq. (5.29) in relation $\tau_{xz} = F_s / \mathrm{d}x$, the shear stress is calculated as

$$\tau_{xz} = \int_{A'} \frac{-\mathrm{d}\sigma_x}{\mathrm{d}x} \mathrm{d}A = -\int_{A'} \sigma'_x \mathrm{d}A \tag{5.30}$$

The longitudinal stress obtained in Eq. (5.25) is substituted into the above expressions and the shear stress expression in terms of displacements is obtained.

$$\tau_{xz} = \int_{A'} \hat{\bar{Q}}_{11}^{(k)*} z v''' \mathrm{d}A \tag{5.31}$$

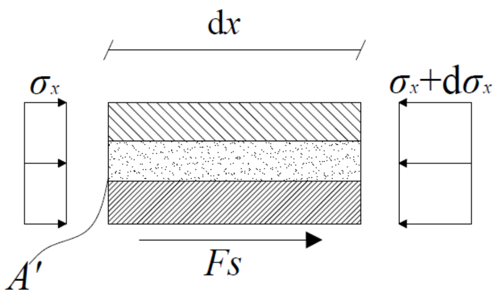

Figure 5.4: Free-body Diagram of a Piece Cut from the Column

On the other hand, the shear stress resultant is given as,

$$V = M' = J_{yy} v''' \tag{5.32}$$

Substituting Eq. (5.32) in Eq. (5.31), the shear stress is expressed in terms of shear stress resultant.

$$\tau_{xz}{}^{(k)} = \frac{\bar{S}_y}{J_{yy}} V \tag{5.33}$$

in which $\bar{S}_y = \int_{A'} \hat{\bar{Q}}_{11}^{(k)*} z \mathrm{d}A$ is defined.

The column is subjected to axial compressive load N^p, which does not cause any pre-buckling shear forces V^p and associated bending moments M^p (superscript p will relate to the pre-buckling state). Additionally, the increment of axial force vanishes ($\Delta N = 0$) throughout the buckling, in accordance with the inextensional buckling assumption.

5.7. Variational formulation

As discussed in chapter 4, the current hybrid formulation is developed from the potential energy functional by relaxing the strain-displacement equations as auxiliary conditions through the Lagrange Multipliers method.

The total potential energy of the buckled configuration of a system is expressed as the sum of strain energy U and work done by external forces W ,

$$\Pi = U + W \tag{5.34}$$

The strain energy of the column at the buckled configuration is given by

$$U = \frac{1}{2}\int_{V_0} \left(\sigma_x \varepsilon_x + \tau_{xz}\gamma_{xz}\right) \mathrm{d}V \tag{5.35}$$

where V_0 = Volume of the column.

The work done by the external forces can be written as

$$W = -\frac{1}{2}\int_L N^p v'^2 \mathrm{d}x \tag{5.36}$$

where L is the Length of the column and N^p is the initial axial compressive load.

In here, the auxillary conditions are the conditions of compatibility (the strain-displacement equations), which can be written as follows

$$\varepsilon_x + v''(x)z = 0 \tag{5.37}$$

$$\gamma_{xz} = 0 \tag{5.38}$$

These conditions are introduced to the total potential energy expression through the Lagrange Multipliers method.

$$\Pi_{\mathrm{II}} = U + W - \int_{V_0} \beta_1(\varepsilon_x + zv'')\mathrm{d}V - \int_{V_0} \beta_2(\gamma_{xz})\mathrm{d}V \tag{5.39}$$

in which β_1 and β_2 are the Lagrange Multipliers.

From the variations of the functional Π_{II} with respect to the strains one obtains

$$\frac{\partial U_d}{\partial \varepsilon_x} - \beta_1 = 0 \tag{5.40}$$

$$\frac{\partial U_d}{\partial \gamma_{xz}} - \beta_2 = 0 \tag{5.41}$$

where U_d is the internal strain energy density and is defined as $U = \int_{V_0} U_d \mathrm{d}V$. Eqs. (5.40) and (5.41) show that β_1 and β_2 are the energy conjugate of the strains ε_x and γ_{xz}, respectively. Therefore, they can be replaced with stresses σ_x and τ_{xz} in Eq. (5.39), i.e.

$$\Pi_{II} = U + W - \int_{V_0} \sigma_x(\varepsilon_x + zv'')\mathrm{d}V - \int_{V_0} \tau_{xz}(\gamma_{xz})\mathrm{d}V \tag{5.42}$$

By substituting Eqs. (5.35) and (5.36), Eq. (5.42) can be written as

$$\Pi_{II} = -\frac{1}{2}\int_{V_0}\left(\sigma_x\varepsilon_x + \tau_{xz}\gamma_{xz}\right)\mathrm{d}V - \int_{V_0} \sigma_x(zv'')\mathrm{d}V - \frac{1}{2}\int_L N^p v'^2 \mathrm{d}x \tag{5.43}$$

Substituting the inverse of the constitutive relations for composite laminates and using Eq. (5.26), the hybrid functional Π_{III} can be expressed as

$$\Pi_{III} = -\frac{1}{2}\int_{V_0}\begin{bmatrix}\sigma_x^{(k)} & \tau_{xz}^{(k)}\end{bmatrix}\begin{bmatrix}\hat{\bar{Q}}_{11}^{(k)*} & 0 \\ 0 & Q_{44}^{(k)}\end{bmatrix}^{-1}\begin{bmatrix}\sigma_x^{(k)} \\ \tau_{xz}^{(k)}\end{bmatrix}\mathrm{d}V + \int_L Mv''\mathrm{d}x - \frac{1}{2}\int_L \lambda N^p v'^2 \mathrm{d}x \tag{5.44}$$

By substituting Eqs. (5.28) and (5.33) into Eq. (5.44), the final form of hybrid formulation, Π_{III}, in the buckled state is obtained

$$\Pi_{III} = \int_L \left[\frac{-1}{2}\left(\frac{M^2}{J_{yy}} + \frac{V^2}{\Lambda_{yy}} \right) + Mv'' - \frac{1}{2}\lambda N^p v'^2 \right] \mathrm{d}x \tag{5.45}$$

where $\Lambda_{yy}^{-1} = \int_A \frac{1}{Q_{44}^{(k)}} \frac{\bar{S}_y^{\,2}}{J_{yy}^{\,2}} \mathrm{d}A$.

5.8. Finite element formulation

5.8.1. Interpolation of the stress resultant and displacement fields for buckling analysis

In this section the assumed interpolation for the variables in the hybrid functional (stress resultants M and V and the lateral displacement v) is introduced.

For an element i with a span of L, the buckling internal bending moment is assumed as linear, i.e.

$$M = \mathbf{L}^T \mathbf{M}_i \tag{5.46}$$

Therefore, the shear force is given as

$$V = \mathbf{L}'^{\mathrm{T}} \mathbf{M}_i \tag{5.47}$$

in which, $\mathbf{L}^{\mathrm{T}} = \langle (1 - x/L) \quad x/L \rangle$ and $\mathbf{M}_i^{\mathrm{T}} = \langle M(0) \quad M(L) \rangle$.

For lateral displacement two different interpolations are assumed.

$$v_i = \mathbf{N}^{\mathbf{T}} \mathbf{v}_i \tag{5.48}$$

First set of interpolation functions are based on cubic interpolation where the vector **N** can be written as

$\mathbf{N}^{\mathrm{T}} = \left\langle \left(1-3x^2/L^2+2x^3/L^3\right) \quad \left(x-2x^2/L+x^3/L^2\right) \quad \left(3x^2/L^2-2x^3/L^3\right) \quad \left(-x^2/L+x^3/L^2\right) \right\rangle$,

$\mathbf{v}_i^{\mathbf{T}} = \left\langle v_i(0) \quad v_i'(0) \quad v_i(L) \quad v_i'(L) \right\rangle$ are defined.

Second set of interpolation functions are based on trigonometric functions and in this case vector **N** can be written as $\mathbf{N}^{\mathrm{T}} = \left\langle N_1 \quad N_2 \quad N_3 \quad N_4 \right\rangle$ where $N_1 = 0.5\left[\cos\left(\pi x/L\right)+1\right]$, $N_2 = 0.25\left[L\cos\left(\pi x/L\right)+\left(2L/\pi\right)\sin\left(\pi x/L\right)+2x-L\right]$ $N_3 = 0.5\left[1-\cos\left(\pi x/L\right)\right]$ and $N_4 = 0.25\left[L\cos\left(\pi x/L\right)-\left(2L/\pi\right)\sin\left(\pi x/L\right)+2x-L\right]$.

5.8.2. Discretised form of the hybrid functional for buckling analysis

By substituting Eqs. (5.46) to (5.48) into Eq. (5.45), the discretised form of the hybrid functional for buckling analysis can be written as

$$\Pi_{III} = \sum_{i=1}^{N} \int_L \left(\begin{array}{l} \mathbf{M}_i^{\mathbf{T}} \mathbf{L} \mathbf{N}''^{\mathbf{T}} \mathbf{v}_i - \dfrac{1}{2} \lambda N^p \mathbf{v}_i^{\mathbf{T}} \mathbf{N}' \mathbf{N}'^{\mathbf{T}} \mathbf{v}_i \\ -\dfrac{1}{2J_{yy}} \mathbf{M}_i^{\mathbf{T}} \mathbf{L} \mathbf{L}^{\mathbf{T}} \mathbf{M}_i - \dfrac{1}{2\Lambda_{yy}} \mathbf{M}_i^{\mathbf{T}} \mathbf{L}' \mathbf{L}'^{\mathrm{T}} \mathbf{M}_i \end{array} \right) \tag{5.49}$$

This functional depends on the unknown $\mathbf{M}_i$. From the partial stationary condition with respect to $\mathbf{M}_i$ i.e. $\partial \delta^2 \Pi_{III} / \partial \mathbf{M}_i = 0$, one obtains

$$\mathbf{M}_i = \mathbf{H}_b \mathbf{G}_b \mathbf{v}_i \tag{5.50}$$

where

$$\mathbf{H}_b = \left\{ \int_L \frac{1}{J_{yy}} \mathbf{L}\mathbf{L}^{\mathbf{T}} + \frac{1}{\Lambda_{yy}} \mathbf{L}'\mathbf{L}'^{\mathrm{T}} \mathrm{d}x \right\}^{-1} \tag{5.51}$$

and

$$\mathbf{G}_b = \int_L \mathbf{L}\mathbf{N}''^{\mathbf{T}} \mathrm{d}x \tag{5.52}$$

It should be noted that the stationary condition with respect to the stress resultant parameters can be written at the element level. This is due to the relaxation of inter-element equilibrium as a result of which the nodal stress resultant parameters are not coupled between the elements. Using Eq. (5.50), the functional in Eq. (5.49) becomes

$$\Pi_{\mathrm{III}} = \frac{1}{2}\sum_{i=1}^{N} \int_L \left(\mathbf{v}_i^{\mathbf{T}} \mathbf{G}_b^{\mathbf{T}} \mathbf{H}_b \mathbf{G}_b \mathbf{v}_i \right) \mathrm{d}x - \frac{1}{2}\lambda \sum_{i=1}^{N} \int_L \mathbf{v}_i^{\mathbf{T}} N^p \mathbf{N}'\mathbf{N}'^{\mathbf{T}} \mathbf{v}_i \mathrm{d}x \tag{5.53}$$

From the stationary condition with respect to $\mathbf{v}_i$, i.e. $\partial \delta^2 \Pi_{III} / \partial \mathbf{v}_i = 0$, the discretised equilibrium equations of the system can be obtained as

$$\sum_{i=1}^{N} \left[\mathbf{K}_{bi} - \lambda \mathbf{K}_{gi} \right] \mathbf{v}_i = 0 \tag{5.54}$$

in which $\mathbf{K}_{bi}$ is the element stiffness matrix for buckling analysis and $\mathbf{K}_{gi}$ is the element geometric stiffness matrix.

5.9. Numerical examples

In this section, numerical comparisons with other finite element methods and closed-form solutions are presented in order to verify the capability and accuracy of the current hybrid finite element method. In addition, some parametric studies are presented to show the effect of different factors such as fibre orientation and element slenderness on the flexural buckling load. In example (5.9.1), the accuracy and efficiency of the current model is validated through the analysis of an axially-loaded simply-supported column with isotropic material. The results for both the cubic and trigonometric interpolation of the lateral displacement are presented in this example. Then, examples (5.9.2) and (5.9.3) are presented to verify the capability of the current hybrid model in capturing the behaviour of composite elements with different lay-ups for doubly-symmetric and mono-symmetric cross-sections, respectively. In addition, the effect of fibre orientation on the flexural buckling load of columns is illustrated in these examples. Lastly, in example (5.9.4) the buckling analysis of an axially loaded composite cantilever column with various stacking sequences is presented. In that example, the effect of element slenderness on the flexural buckling load of the column is presented as well.

5.9.1. Simply supported column with isotropic cross section

A simply supported column with a span of 2000 mm is analysed in this example. The dimensions of the cross-section which is a symmetric I-section are illustrated in Figure 5.5. The material is steel and the material properties are as follows:

$$E = 2\times10^5 MPa, \quad G = 77\times10^3 MPa, \quad \upsilon = 0.3$$

The column is subjected to an axial load P applied at the centroid C of the cross-section. The flexural buckling happens around the weak axis of the column which is the y axis.

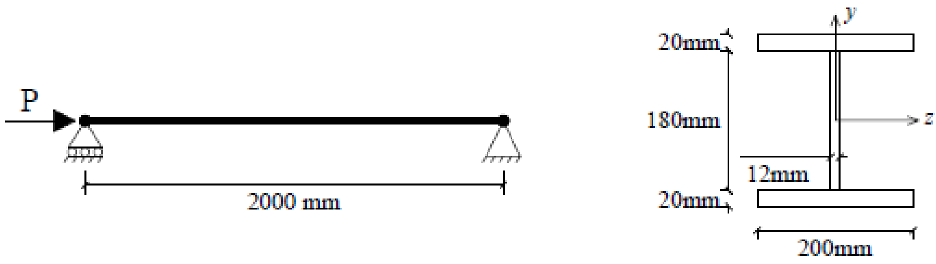

Figure 5.5: Simply Supported column with Symmetric Cross-section

In this example, in addition to the shear flexible model, the column is also analysed without considering the shear deformation effects for comparison reasons. In order to exclude the effect of shear deformations, Λ_{yy}^{-1} is set to zero in the developed finite element formulation. The flexural buckling loads predicted by the current method are compared with the following three models:

1. The closed form solution (The Euler buckling load): $P_e = \pi^2 EI/L^2$,
2. ABAQUS FEA shell element model,
3. The closed form solution suggested by Kollár (2001) for flexural-torsional buckling load of composite columns.

Results with both cubic interpolation and trigonometric interpolation for the lateral displacement are presented here. In order to show the efficiency of the current hybrid model the analyses are done for different numbers of elements.

5.9.1.1. Results and discussions

The predicted buckling loads obtained from the current non-shear deformable model are compared with the Euler buckling load $P_e = \pi^2 EI/L^2$ in Table 5.1.

Table 5.1: Buckling Loads of columns (in Newtons)

Element type	Number of Elements	Pcr (cubic)	Pcr (trigonometric)
Current study without shear deformation effects ($\Lambda_{yy}^{-1} = 0$)	2	13271.1	12208.3
	4	13178.9	12863.3
	8	13172.7	13089.6
	16	13172.3	13151.2
	32	13172.3	13167.0
	64	13172.3	13171.0
	128	13172.3	13172.0
$P_e = \pi^2 EI/L^2$	-	13172.3	

The values of flexural buckling load obtained by the hybrid shear deformable analysis are compared with the result from the shell element model. In the ABAQUS FEA model the four-noded shell element (S4R) is used. The finite element mesh in this model is illustrated in Figure 5.6, in which the values indicate the number of finite elements used in each direction.

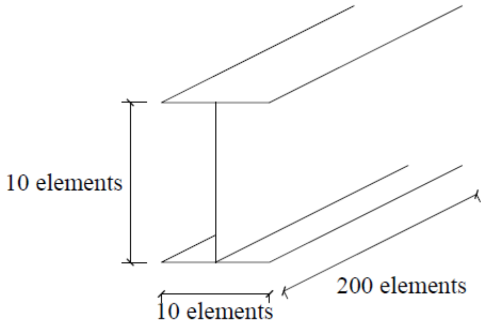

Figure 5.6: The finite element mesh used in ABAQUS

Table 5.2 shows the comparison between the results from the current hybrid model and the buckling load obtained by the described shell element model.

Table 5.2: Buckling Loads of columns (in Newtons)

Element type	Number of Elements	P_{cr} (cubic)	P_{cr} (trigonometric)
Current study with shear	2	12968.6	11971.7
	4	12857.3	12562.7
	8	12844.4	12766.9
	16	12842.3	12822.5
	32	12841.8	12836.7
	64	12841.8	12840.3
	128	12841.7	12841.2
ABAQUS	6000	12822	

Additionally, in this example the buckling load obtained from the current model is compared with the buckling load calculated using the closed-form solution suggested by Kollár (2001) for flexural-torsional buckling load of composite columns. The kinematic assumptions of the Kollar formulation is based on the fact that the axis of the deformed beam does not rotate with the same amount of that of the cross-section as in the Timoshenko beam kinematics. The closed form solution proposed by Kollar is given as

$$\frac{1}{\hat{N}_{\mathrm{crz}}} = \frac{1}{\hat{N}^{\mathrm{B}}_{\mathrm{crz}}} + \frac{1}{\hat{S}_{\mathrm{yy}}} \tag{5.55}$$

where $\hat{N}_{\mathrm{crz}}$, $\hat{N}^{\mathrm{B}}_{\mathrm{crz}}$ and $\hat{S}_{\mathrm{yy}}$ are defined as

$\hat{N}_{\mathrm{crz}}$: The buckling load of the column

$\hat{N}^{\mathrm{B}}_{\mathrm{crz}}$: The buckling load when the shear stiffness is infinite (the Euler buckling load)

$\hat{S}_{\mathrm{yy}}$: The buckling load when the bending stiffness is infinite.

In the current model, the value of $\hat{N}^{\mathrm{B}}_{\mathrm{crz}}$ is the buckling load obtained in the analysis without the shear deformation effect and the value of $\hat{S}_{yy}$ is equivalent to Λ_{yy} . These values are obtained as: $\hat{N}^{\mathrm{B}}_{\mathrm{crz}} = 13172.3N$ and $\Lambda_{yy} = 514000N$. Therefore, using Eq. (5.55) the buckling load is calculated. The values of buckling load obtained by the hybrid method and the Kollar solution are compared in Table 5.3.

Table 5.3: Buckling Loads of columns (in Newtons)

Element type	P_{cr} (cubic)	P_{cr} (trigonometric)
Current study with shear	12841.7	12841.2
Kollár (2001)	12843.2	

The following conclusions can be made from the analysis results:

1. From Table 5.2, it is verified that the buckling loads obtained from the analysis without shear deformation effects are equal to the buckling load obtained by the closed-form solution (0% difference).

2. From Table 5.2, one can see that the predicted values of the buckling load by the current shear deformable hybrid model is in an acceptable agreement with the results of the ABAQUS model (0.15% difference).
3. One can observe that the small number of elements is enough for relatively accurate results for buckling load. This verifies the efficiency of the current hybrid finite element model.
4. By comparing the predicted buckling loads from the shear deformable and non-shear deformable analyses, it can be observed that by considering the shear deformation effects, the magnitude of the buckling load decreases due to additional flexibility of the column. Therefore, ignoring shear deformation effects can lead to wrong assessment of column buckling load.
5. It is interesting to note that while cubic interpolation leads to upper bound convergence, trigonometric functions lead to lower bound convergence property. For more detailed analysis on the convergence property in buckling formulations where both force and displacement fields are interpolated one may refer to Erkmen *et al.* (2009). For the rest of the examples, only cubic interpolation of the displacement is used for the analysis.
6. Comparing the buckling load predicted by the shear deformable hybrid model with the buckling load calculated by the Kollar solution verifies the accuracy of the current model.

5.9.2. Column with Doubly symmetric laminate composite cross-section and various boundary conditions

In this example, a thin-walled composite column with doubly symmetric cross-section and various stacking sequences is studied in order to verify the capability of the current hybrid model in capturing the behaviour of composite elements with different lay-ups.

The element is assumed to be made of glass-epoxy with the following material properties:

$$E_1 = 53.78MPa, \quad E_2 = 17.93MPa$$
$$G_{12} = G_{13} = 8.96MPa$$
$$\upsilon_{12} = 0.25$$

The subscript 1 corresponds to the direction parallel to fibre orientation and subscripts 2 and 3 are related to the directions perpendicular to it.

The column has a doubly symmetric cross-section with dimensions demonstrated in Figure 5.7.

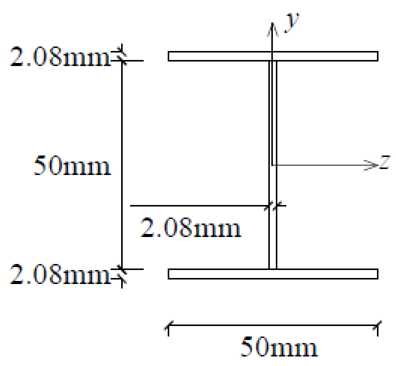

Figure 5.7: Cross-sectional Dimensions

The web and flanges are laminated symmetrically with respect to the mid-plane and consist of 16 layers with equal thickness of 0.13 mm.

A schematic configuration of symmetric angle-ply stacking sequence of $\left[\phi^o / \text{-}\phi^o\right]_{2s}$ with respect to mid-plane (8 layers) in a segment of the cross-section is illustrated in Figure 5.8. As described in previous parts, ϕ is the angle between fibre orientation and x axis.

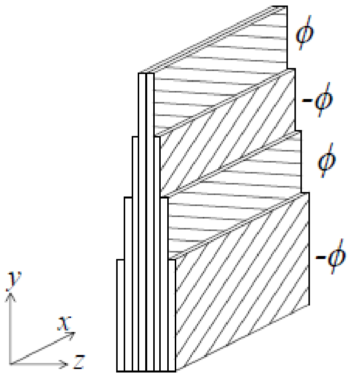

Figure 5.8: Schematic configuration of symmetric angle-ply stacking sequence $\left[\phi^o / \text{-}\phi^o\right]_{2s}$

The column is subjected to an axial load P which is applied at the centroid C of the cross-section. The flexural buckling happens around the weak axis of the column which is the y axis. The analyses are done for two different boundary conditions: simply supported (S-S) and clamped-free (C-F) boundary conditions. The length of the column is assumed to be equal to 4 m for S-S case and 1 m for C-F case.

The values of the buckling loads obtained by the current model for various lay-ups are compared with the following two models:

1. The formulation developed by Nguyen *et al.* (2015) based on a displacement-based one-dimensional finite element method.
2. The closed form solution suggested by Kollár (2001) for flexural-torsional buckling of composite columns

5.9.2.1. Results and discussion

The column is modelled efficiently by using four elements for S-S boundary conditions and eight elements for C-F boundary conditions. The predicted buckling loads from the hybrid method are presented and compared with the results from Nguyen *et al.* (2015) along with the percentage difference between them in Table 5.4 and Table 5.5 for S-S and C-F boundary conditions, respectively. The buckling load based on the model by Nguyen *et al.* (2015) is calculated by a displacement-based one-dimensional finite element model. In that method, geometric parameters and fibre orientation of composite elements are employed simultaneously as design variables to maximize the flexural-torsional critical buckling loads of axially loaded columns.

Table 5.4: Buckling Loads of columns (in Newtons) with S-S boundary condition

Lay-up	This study	(Nguyen *et al.* 2015)	Differences (%)
$\left[0^o\right]_{16}$	1502.6	1438.8	4.25
$\left[15^o / \text{-}15^o\right]_{4s}$	1207.7	1300	7.10
$\left[30^o / \text{-}30^o\right]_{4s}$	820.4	965.2	15.0
$\left[45^o / \text{-}45^o\right]_{4s}$	615	668.2	7.96
$\left[60^o / \text{-}60^o\right]_{4s}$	530.2	528.7	0.28
$\left[75^o / \text{-}75^o\right]_{4s}$	504.2	487.1	3.39
$\left[0^o / 90^o\right]_{4s}$	1001.8	959.3	4.24
$\left[0^o / -45^o / 90^o / 45^o\right]_{2s}$	808.5	813.8	0.65

Table 5.5: Buckling Loads of columns (in Newtons) with C-F boundary condition

Lay-up	This study	(Nguyen *et al.* 2015)	Differences (%)
$\left[0^o\right]_{16}$	6008.4	5755.2	4.21
$\left[15^o/\text{-}15^o\right]_{4s}$	4829.6	5199.7	7.12
$\left[30^o/\text{-}30^o\right]_{4s}$	3280.8	3861	15.03
$\left[45^o/\text{-}45^o\right]_{4s}$	2459.8	2672.7	7.97
$\left[60^o/\text{-}60^o\right]_{4s}$	2120.6	2114.8	0.27
$\left[75^o/\text{-}75^o\right]_{4s}$	2016.6	1948.3	3.39
$\left[0^o/90^o\right]_{4s}$	4006	3837.3	4.21
$\left[0^o/-45^o/90^o/45^o\right]_{2s}$	3233.3	3255.3	0.68

In addition, the buckling loads obtained from the current method are compared with the loads calculated by the closed-form solution proposed by Kollár (2001) for flexural-torsional buckling of composite columns (Eq. (5.55)) in Table 5.6. As mentioned in the first example, the value of $\hat{N}^{\mathrm{B}}_{\mathrm{crz}}$ is the buckling load when the shear stiffness is infinite (the Euler buckling load $= \pi^2 EI / (kL)^2$) and the value of $\hat{S}_{yy}$ is equivalent to Λ_{yy} in the current model.

Table 5.6: Buckling Loads of columns (in Newtons)

Lay-up	This study		Kollár (2001)		Differences (%)	
	SS	CF	SS	CF	SS	CF
$\left[0^o\right]_{16}$	1502.6	6008.4	1499.8	5981.8	0.19	0.44
$\left[15^o\,/\,\text{-}15^o\right]_{4s}$	1207.7	4829.6	1205.6	4811.3	0.17	0.38
$\left[30^o\,/\,\text{-}30^o\right]_{4s}$	820.4	3280.8	819.2	3271.4	0.14	0.29
$\left[45^o\,/\,\text{-}45^o\right]_{4s}$	615	2459.8	614.5	2455.0	0.09	0.20
$\left[60^o\,/\,\text{-}60^o\right]_{4s}$	530.2	2120.6	530.0	2117.9	0.04	0.13
$\left[75^o\,/\,\text{-}75^o\right]_{4s}$	504.2	2016.6	504.3	2015.1	0.02	0.07
$\left[0^o\,/\,90^o\right]_{4s}$	1001.8	4006	1000.0	3990.5	0.18	0.39
$\left[0^o\,/-45^o\,/\,90^o\,/\,45^o\right]_{2s}$	808.5	3233.3	807.3	3222.8	0.15	0.32

The following conclusions can be made from the analysis results:

1. From Table 5.4 and Table 5.5, it can be found that the results from the current study for both boundary conditions are in a good agreement with results from the other analysis.
2. From Table 5.6 one can observe that the results obtained from the current model for both boundary conditions are in an excellent agreement with the solution suggested by Kollár (2001).
3. In order to see the effect of fibre orientation on the flexural buckling load the values of obtained buckling load for each stacking sequence are plotted for both simply-supported and cantilever boundary conditions in the following figure (Figure 5.9).

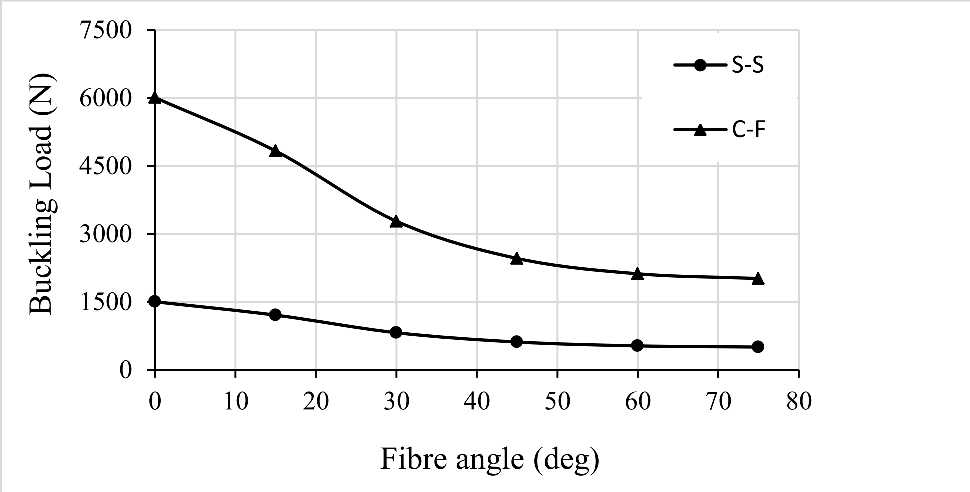

Figure 5.9: The buckling load for various fibre angles

5.9.3. Column with mono-symmetric laminate composite cross-section and various boundary conditions

In this example, a thin-walled composite column with mono-symmetric cross section and various stacking sequences is studied in order to show that the current hybrid formulation is able to capture the buckling behaviour of laminate composite cross-sections with mono-symmetric shapes.

The element is assumed to be made of glass-epoxy with the following material properties:

$$E_1 = 53.78MPa, \quad E_2 = 17.93MPa$$
$$G_{12} = G_{13} = 8.96MPa$$
$$\upsilon_{12} = 0.25$$

The subscript 1 corresponds to the direction parallel to fibre orientation and subscripts 2 and 3 are related to the directions perpendicular to it.

The column has a mono-symmetric cross-section with dimensions illustrated in Figure 5.10.

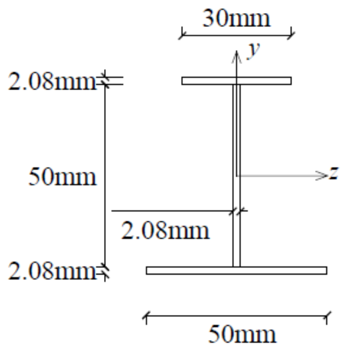

Figure 5.10: Cross-sectional Dimensions

The web and flanges are laminated symmetrically with respect to the mid-plane and consist of 16 layers with equal thickness of 0.13 mm.

The column is subjected to an axial load P which is applied at the centroid *C* of the cross-section.

The analyses are performed for simply supported (S-S) and clamped-free (C-F) boundary conditions. The length of the column is assumed to be equal to 4 m for both boundary conditions.

The values of the buckling loads obtained by the current model for various lay-ups are compared with a geometrically nonlinear model developed by Vo and Lee (2010). Their model is based on the classical lamination theory for general thin-walled open-section composite beams and is derived from the principle of the stationary value of total potential energy.

5.9.3.1. Results and discussions

The column is modelled efficiently by using four elements for both boundary conditions. The predicted buckling loads by the hybrid method are presented and compared with the results from the solution by Vo and Lee (2010) along with the percentage difference between them in Table 5.7 and Table 5.8 for S-S and C-F boundary conditions, respectively.

Table 5.7: Buckling Loads of columns (in Newtons) with S-S boundary conditions

Lay-up	This study	Vo and Lee (2010)	Differences (%)
$\left[0^o\right]_{16}$	914.5	841.0	7.7
$\left[15^o / \text{-}15^o\right]_{4s}$	735.1	767.0	4.8
$\left[30^o / \text{-}30^o\right]_{4s}$	499.3	576.0	13.7
$\left[45^o / \text{-}45^o\right]_{4s}$	374.3	401.0	7.0
$\left[60^o / \text{-}60^o\right]_{4s}$	322.7	318.0	1.3
$\left[75^o / \text{-}75^o\right]_{4s}$	306.9	292.0	4.6
$\left[90^o / -90^o\right]_{4s}$	304.4	288.0	5.5
$\left[0^o / 90^o\right]_{4s}$	609.8	568.0	6.7

Table 5.8: Buckling Loads of columns (in Newtons) with C-F boundary conditions

Lay-up	This study	Vo and Lee (2010)	Differences (%)
$\left[0^o\right]_{16}$	228.5	216.5	5.3
$\left[15^o / \text{-}15^o\right]_{4s}$	183.7	196.0	6.5
$\left[30^o / \text{-}30^o\right]_{4s}$	124.8	146.0	14.7
$\left[45^o / \text{-}45^o\right]_{4s}$	93.5	101.3	7.7
$\left[60^o / \text{-}60^o\right]_{4s}$	80.6	80.0	0.5
$\left[75^o / \text{-}75^o\right]_{4s}$	76.7	73.8	3.8
$\left[90^o / -90^o\right]_{4s}$	76.1	72.5	4.6
$\left[0^o / 90^o\right]_{4s}$	152.4	144.8	5.0

The following conclusions can be made from the analysis results:

1. From Table 5.7 and Table 5.8 we can see that the predicted buckling load in this study is in a good agreement with the buckling load obtained from the solution of Vo and Lee (2010). Therefore, it can be verified that the current hybrid formulation is well capable of capturing the buckling behaviour of laminate composite columns with mono-symmetric cross-sections.
2. In order to see the effect of fibre orientation on the flexural buckling load, values of obtained buckling load for each stacking sequence are plotted for both simply-supported and cantilever boundary conditions in the following figure. (Figure 5.11)

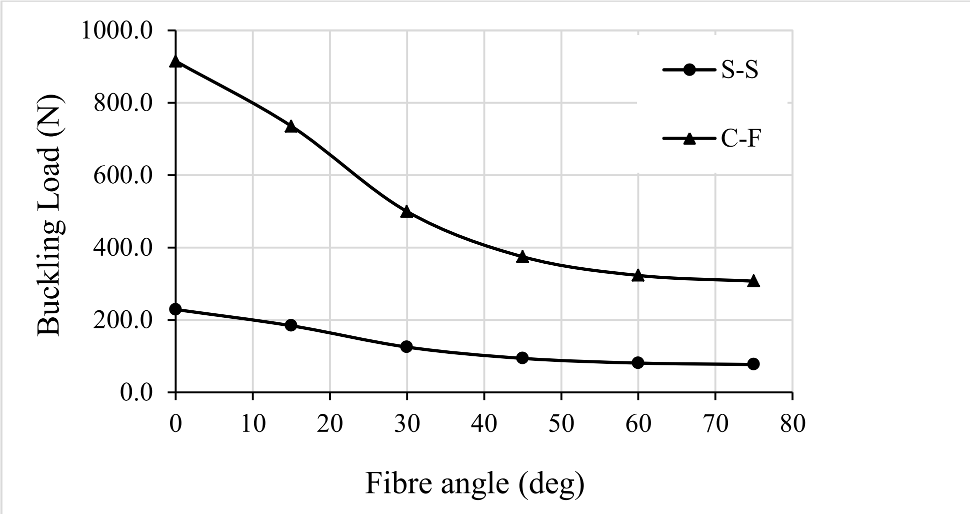

Figure 5.11: The buckling load for various fibre angles

5.9.4. Cantilever column with laminate composite cross-section

In this example, a cantilever column with laminated composite cross-section is studied. The element is assumed to be made of graphite-epoxy (AS4/3501) with the following material properties:

$$E_1 = 144MPa, \quad E_2 = 9.65MPa$$
$$G_{12} = 4.14MPa$$
$$\upsilon_{12} = 0.3$$

The subscript 1 corresponds to the direction parallel to fibre orientation and subscripts 2 and 3 are related to the directions perpendicular to it.

The column has a doubly symmetric cross-section. The length of the column and the cross-sectional dimensions are shown in Figure 5.12.

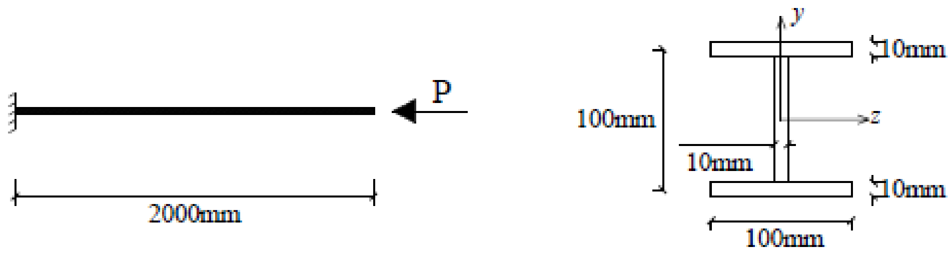

Figure 5.12: Cantilever column with Symmetric Cross-section

The web and flanges are assumed to be laminated symmetrically with respect to the mid-plane and consist of 4 layers with equal thickness of 2.5 mm. In this example three stacking sequences are considered: $\left[0^o\right]_4, \left[0^o/90^o\right]_s, \left[45^o/\text{-}45^o\right]_s$.

The column is subjected to an axial load P which is applied at the centroid C of the cross-section and the flexural buckling happens around the weak axis of the column which is the y axis.

The values of the buckling loads obtained by the current model for the various lay-ups are compared with the buckling loads calculated by a theoretical model developed by Cortínez and Piovan (2006) for the stability analysis of composite thin-walled beams. The Cortinez model which is developed and solved by finite element method, incorporates the shear flexibility by using the linearized formulation based on the Hellinger-Reissner principle.

In addition, the effect of column slenderness on the flexural buckling load of the column is depicted in this example.

5.9.4.1. Results and discussions

The column is modelled by only 2 elements in the current hybrid model. The predicted buckling loads by the current model along with the calculated buckling load by Cortinez solution are presented in Table 5.9.

Table 5.9: Buckling Loads of columns (in Newtons)

Stacking sequences	Current study	Cortínez and Piovan (2006)
$\left[0^o\right]_4$	162.3	148.7
$\left[0^o/90^o\right]_s$	86.9	80
$\left[45^o/-45^o\right]_s$	12.2	15.5

In addition, Figure 5.13 shows the values of buckling load for various values of h/L of the column for each stacking sequence. In the case of rectangular cross-section with isotropic materials h can be used as the slenderness ratio of the column ($\mathrm{r}=\sqrt{I/A}$). However, in the case of I sections with composite materials they are not the same.

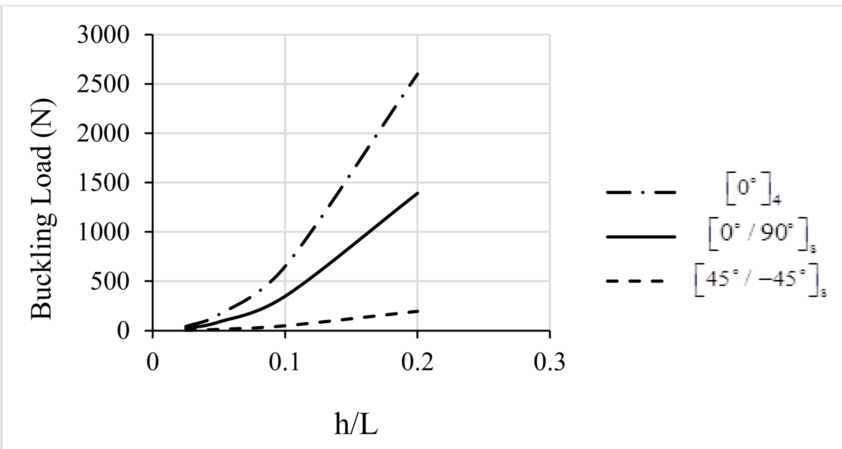

Figure 5.13: Buckling load for various values of h/L of column

The following conclusions can be made from the analysis results:

1. From Table 5.9 it can be seen that the results calculated by the current method are in an acceptable agreement with the results from other finite element model (about 8% differences).
2. It should be noted that, the considerable difference between the values of buckling load for the first case (stacking sequence of $\left[0^o\right]_4$) is due to the different assumptions taken by Cortinez for values of cross section stiffness. In the current study, the value of modulus of elasticity is set to be $\hat{\bar{Q}}_{11}^{(k)*}$ which is calculated for composite laminated cross-sections based on Eqs. (5.6) to (5.23), whereas in Cotinez's paper for this special stacking sequence the modulus of elasticity is assumed to be equal to E_1. If in the current hybrid model, $\hat{\bar{Q}}_{11}^{(k)*}$ is replaced by E_1 the same results as in Cotinez's paper will be obtained. However, in the author's opinion and based on the constitutive relations for composite materials (Eqs. (5.6) to (5.23)), the behaviour of the element with laminate composite cross-section in one direction will be affected by the material properties in the other direction ($E_2, \upsilon_{12}, \upsilon_{21}, G_{12}$) and the fibre orientation (Φ_k). Therefore, using only E_1 as the modulus of elasticity does not reflect the correct behaviour of the composite materials.
3. As one can see in Figure 5.13, the buckling load increases as the value of h/L column increases (the length of the column decreases). It means that the susceptibility to buckling will increase as the length of the column increases.

5.10. Summary and Conclusions

A shear-deformable hybrid finite element formulation has been developed for the flexural buckling analysis of axially loaded columns with fibre-reinforced laminate composite cross-sections. The hybrid functional has been obtained from the potential energy functional by relaxing the strain-displacement equations as auxiliary conditions through the Lagrange Multipliers method. The shear deformation effects are taken into account by using the strain energy of the equilibrating shear stress field without modifying the basic kinematic assumptions of the beam theory.

Numerical comparisons against other finite element methods and closed form solutions have been presented to show the validity and efficiency of the current method in capturing the flexural buckling behaviour of axially loaded columns with fibre reinforced laminate composite cross-sections. It has been illustrated that the flexural buckling loads obtained by the current method for the composite columns with various boundary conditions are in a very good agreement with the results calculated by the closed-form solutions and finite element models in the literature. The validity of the hybrid method for mono-symmetric cross-sections in addition to the doubly-symmetric cross-sections is shown. Additionally, the effects of fibre orientation and slenderness of the column on the value of flexural buckling load are studied.

Chapter 6: Applications of Shear Deformable Hybrid Finite Element Formulation for Flexural Buckling Analysis

6.1. Introduction

The shear-deformable hybrid finite element model was developed and verified for the flexural buckling analysis of columns with fibre-reinforced composite materials in Chapter 5. In this chapter, the application of the developed method for columns with various types of cross-sections is discussed, and the main advantages of the developed hybrid model over the alternative finite element methods are illustrated through numerical examples. These advantages include:

- Considering the shear deformation effects without modifying the kinematic assumptions; and
- Straightforward connection of non-collinear elements without the need to satisfy the inter-element equilibrium.

In section (6.2), two well-known solutions in the literature that included the shear deformation effects in flexural buckling analysis of axially loaded columns proposed by

Engesser and Haringx along with their differences and applications are presented. Then the agreement of the current hybrid method with the Engesser solution is proven by obtaining the buckling load for two special cases of pure bending and pure shear which are the upper limits for very large shear rigidity cases and very large flexural rigidity cases, respectively. Finally, a numerical example is presented to verify the agreement of the hybrid model with the Engesser solution.

In section (6.3), the importance of shear deformation effects in the flexural buckling analysis of short columns with laminate composite cross-section is presented and the capability of the current hybrid method for capturing these effects is discussed. The column is checked for local buckling as it can potentially be the governing type of buckling for short columns.

In section (6.4), the flexural buckling analysis of a sandwich column is performed by the developed hybrid model in this study and the accuracy and efficiency of the model is verified by comparing the results with the other solutions available in the literature.

In section (6.5), the buckling behaviour of a laced built-up column is studied. One of the important features of the current hybrid finite element method is that the non-collinear elements can be connected in a straightforward fashion in this method without the need to satisfy the inter-element equilibrium (Unlike in the complementary energy-based methods). In order to illustrate this capability, a laced built-up column is analysed in this section, and the obtained buckling load is compared with the Euler buckling load of the column.

6.2. Agreement with Engesser’s buckling load

6.2.1. Literature review

The influence of shear on the flexural buckling loads of straight bars was considered for the first time by Engesser (1891). He introduced a correction in Euler‘s differential equation and consequently, the Euler‘s buckling load. For the buckling analysis of helical springs, Haringx (1948-1949) developed an alternative approach. Since then, the accuracy and applicability of these two methods in structural engineering has been the subject of study by many researchers. Timoshenko and Gere (1961) discussed these approaches by referring to Engesser‘s method as –standard” and Haringx‘ as –modified”. They concluded that the standard method is on the safe side in most cases while the modified method is more accurate for the elements in which the effect of shear is extremely large.

By using a more fundamental one-dimensional approach Ziegler (1982) proved that the Engesser‘s method is correct for bars, whereas for helical springs Haringx‘ approach gives accurate results. In addition, he showed the reason that the Haringx‘s approach is correct for springs.

Blaauwendraad (2010) confirmed that although the Haringx‘ theory is correct for helical springs and elastomeric bearings, it is not recommended to be used in buildings and civil engineering. He proved that in structural members, both theories predict the correct buckling load for shear-rigid members. However, for shear-weak members the Engesser‘s method correctly reaches the limit value of the Timoshenko beam-column, whereas the Haringx‘ method is on the unsafe side.

The main difference between these two approaches is due to the different assumptions for the normal load orientation at the deformed state of the member. In the following, the assumptions and the final formulas for buckling load suggested by each method are discussed (Ziegler 1982).

6.2.2. Engesser's approach

Figure 6.1 shows an axially-loaded simply-supported column at the buckled state. The lateral displacement v and the shear angle ψ are depicted in Figure 6.1 as well.

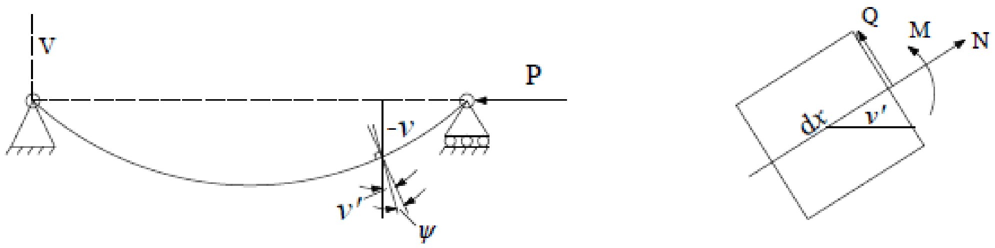

Figure 6.1: A bar under buckling load and the undeformed segment with stress resultants according to Engesser's approach

Engesser starts with the undeformed state of a segment of the bar. As the lateral displacement and the shear angle are small in this state, the stress resultants are given as

$$N = -P \tag{6.1}$$

$$Q = Pv' \tag{6.2}$$

$$M = -Pv \tag{6.3}$$

In the Euler theory as shear is not considered, the only constitutive relation is

$$M = EI\kappa \tag{6.4}$$

in which EI is the flexural rigidity of the bar and κ is the curvature of the bar and is defined as $\kappa = v''$. Using Eqs. (6.3) and (6.4) the differential equation is obtained

$$EIv'' + Pv = 0 \quad \rightarrow \quad v'' + \frac{P}{EI}v = 0 \tag{6.5}$$

Considering the boundary conditions of the simply supported column $v(0) = v(l) = 0$ and having $\beta L = \pi$, we have the solution of the above equation is given as

$$v = A\sin \ \beta x \tag{6.6}$$

By taking the first and second derivatives from Eq. (6.6) we have

$$v' = A\beta\cos \ \beta x \tag{6.7}$$

$$v'' = -A\beta^2\sin \ \beta x \tag{6.8}$$

Substituting Eqs. (6.7) and (6.8), Eq. (6.5) will become

$$-\frac{\pi^2}{L^2} + \frac{P}{EI} = 0 \tag{6.9}$$

Therefore, the buckling load is obtained as

$$P = \frac{\pi^2 EI}{L^2} \tag{6.10}$$

which is equal to the Euler‘s buckling load.

To include the shear effect, Engesser provided a second constitutive relation as

$$Q = GA_s\psi \tag{6.11}$$

in which GA_s is the shear rigidity of the bar.

In addition, he redefined the curvature as below

$$\kappa = v'' - \psi' \tag{6.12}$$

Considering Eqs. (6.11) and (6.12) we have

$$\psi' = \frac{Q'}{GA_s} \tag{6.13}$$

Therefore, Eq. (6.4) will become

$$M = EI\left(v'' - \frac{Q'}{GA_s}\right) \tag{6.14}$$

By using Eq. (6.2), Eq. (6.14) can be written as

$$M = EI\left(1 - \frac{P}{GA_s}\right)v'' \tag{6.15}$$

Having Eqs. (6.3) and (6.15), the differential equation is obtained as

$$v'' + \frac{P / EI}{1 - P / \mathrm{GA}_s} v = 0 \tag{6.16}$$

With the same boundary conditions as before, the Engesser buckling load is given as

$$P = \frac{\dfrac{\pi^2}{L^2} EI}{1 + \dfrac{\pi^2 EI}{\mathrm{GA}_s\, L^2}} \tag{6.17}$$

Defining $P_b = \dfrac{\pi^2 EI}{l^2}$ the Euler buckling load and $P_s = GA_s$ the shear buckling load, Eq. (6.17) becomes

$$P = \frac{P_s P_b}{P_s + P_b} \tag{6.18}$$

6.2.3. Haringx' approach

Unlike the Engesser's approach, this method is based on the deformed shape of the element. A segment of the bar in its deformed position along with the stress resultants are shown in Figure 6.2.

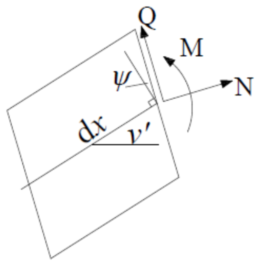

Figure 6.2: Deformed segment of a bar with stress resultants according to Haringx' approach

The stress resultants in this method are given as

$$N = -P \tag{6.19}$$

$$Q = P(v' - \psi) \tag{6.20}$$

$$M = -Pv \tag{6.21}$$

In Haringx' theory, Eq. (6.11) can still be used to include the shear effect.

From Eqs. (6.11) and (6.20), one can obtain

$$\psi = \frac{P}{P + GA_s} v' \tag{6.22}$$

The same assumption is adopted for the curvature (Eq. (6.12)). As a result, Eq. (6.4) will become

$$M = EI\left(1 - \frac{P}{P + GA_s}\right)v'' \tag{6.23}$$

Having Eqs. (6.21) and (6.23) the differential equation can be obtained as

$$v'' + \frac{P}{EI}\left(1 + \frac{P}{\mathrm{GA}_s}\right)v = 0 \tag{6.24}$$

With the same boundary conditions as before, the Haringx' buckling load is given as

$$P_{cr} = \frac{1}{2}\ \text{-}P_s + \sqrt{P_s^2 + 4P_sP_b} \tag{6.25}$$

From Eqs. (6.18) and (6.25) one can conclude that, for very large shear rigidity cases, the critical load will approach P_b in both methods. In the case of very large flexural rigidity (i.e. shear-weak), Engesser's solution yields $P_{cr} = P_s$. However, for this extreme case Haringx' theory obtains a significantly larger value of $P_{cr} = \sqrt{P_bP_s}$ (Blaauwendraad 2010). In other words, the buckling load never exceeds the values of P_b or P_s in Engesser's theory whereas it can be greater than P_s for the beams with very small shear rigidities in Haringx' theory.

6.2.4. Current study

In order to show the agreement of the current hybrid finite element model with the Engesser's solution, the buckling load is obtained for two special cases of pure bending and pure shear in the following section. These two loads are the upper limits of the buckling load for very large shear rigidity cases and very large flexural rigidity cases, respectively.

By putting the hybrid functional (Eq. (5.45)) equal to zero, the Rayleigh factor can be obtained as

$$\lambda N^p = \frac{\int_L \left[2Mv'' - \left(\frac{M^2}{J_{yy}} + \frac{V^2}{\Lambda_{yy}} \right) \right] \mathrm{d}x}{\int_L v'^2 \mathrm{d}x} \tag{6.26}$$

Considering the fact that the first variation of the hybrid formulation vanishes:

$$\delta \Pi_{III} = \int_L \left[\delta M \left(v'' - \frac{M}{J_{yy}} + \frac{V'}{\Lambda_{yy}} \right) - \delta v' \left(M' + \lambda N^p v' \right) \right] \mathrm{d}x - \delta M \left. \frac{V}{\Lambda_{yy}} \right|_L - \delta v' M \Big|_L = 0 \tag{6.27}$$

One can obtain

$$\left(v'' - \frac{M}{J_{yy}} + \frac{V'}{\Lambda_{yy}} \right) = 0 \tag{6.28}$$

In order to calculate the buckling load from Eq. (6.26) in the special case of a simply supported beam, we refer to the differential equation of a buckled column.

The differential equation of a buckled column can be written as the following (Timoshenko and Gere 1961)

$$v'' + \frac{P}{GA} v'' - \frac{P}{EI} v = 0 \tag{6.29}$$

A general solution of the above differential equation can be written as

$$v = A \sin \ \beta x \tag{6.30}$$

Substitution of the solution in Eq. (6.29) yields

$$\beta^2 - \frac{P}{GA} \beta^2 - \frac{P}{EI} = 0 \tag{6.31}$$

6.2.4.1. Pure bending

In the special case of pure bending where the shear rigidity is very large, by setting $\Lambda_{yy}^{-1} = 0$, Eq. (6.28) will be reduced to

$$v'' = \frac{M}{J_{yy}} \tag{6.32}$$

Substituting Eq. (6.32) in Eq. (6.26) it will become

$$\lambda N^p = \frac{\int_L \left[2v''^2 J_{yy} - \left(\frac{v''^2 J_{yy}^{\ 2}}{J_{yy}} + 0 \right) \right] \mathrm{d}x}{\int_L v'^2 \mathrm{d}x} = \frac{\int_L J_{yy} v''^2 \mathrm{d}x}{\int_L v'^2 \mathrm{d}x} \tag{6.33}$$

From Eq. (6.30) we have

$$v' = A\beta \cos \ \beta x \tag{6.34}$$

$$v'' = -A\beta^2 \sin \ \beta x \tag{6.35}$$

By substituting Eqs. (6.34) and (6.35) in Eq. (6.33), it becomes

$$\lambda N^p = \frac{\int_L J_{yy} \left(-A\left(\frac{\pi}{L}\right)^2 \sin\left(\frac{\pi}{L}x\right) \right)^2 \mathrm{d}x}{\int_L \left(A\frac{\pi}{L} \cos\left(\frac{\pi}{L}x\right) \right)^2 \mathrm{d}x} = J_{yy} \left(\frac{\pi}{L}\right)^2 \frac{\int_L \sin^2\left(\frac{\pi}{L}x\right) \mathrm{d}x}{\int_L \cos^2\left(\frac{\pi}{L}x\right) \mathrm{d}x} \tag{6.36}$$

By taking the integrals, the buckling load is obtained as

$$\lambda N^p = J_{yy} \left(\frac{\pi}{L}\right)^2 \frac{\frac{1}{2}L - \frac{1}{4\left(\frac{\pi}{L}\right)} \sin\left(2\frac{\pi}{L}L\right)}{\frac{1}{2}L + \frac{1}{4\left(\frac{\pi}{L}\right)} \sin\left(2\frac{\pi}{L}L\right)} = \frac{J_{yy}\pi^2}{L^2} \tag{6.37}$$

which is equal to the Euler buckling load.

6.2.4.2. Pure shear

In the special case of pure shear where the flexural rigidity is very large, by setting ${J_{yy}}^{-1} = 0$, Eq. (6.28) will be reduced to

$$v'' = -\frac{V'}{\Lambda_{yy}} \tag{6.38}$$

In this case, the differential equation is $(1 - nP / GA)v'' = 0$, where n is the shape factor.

Substituting Eq. (6.38) in Eq. (6.26), one can obtain the buckling load as

$$\lambda N^{p} = \frac{\int_{L}\left(2Mv'' - \frac{V^{2}}{\Lambda_{yy}}\right)\mathrm{d}x}{\int_{L} v'^{2}\mathrm{d}x} = \Lambda_{yy} \tag{6.39}$$

where Λ_{yy} can be shown to be equal to GA/n.

It can be observed that, in the case of small shear rigidity, critical buckling load has the upper limit of GA/n as in the Engesser's theory. Therefore, it has been proven that the current hybrid finite element solution is able to capture the buckling behaviour of shear-weak columns.

The applicability and accuracy of the model is verified in the following section through numerical example for a full range of shear flexibilities.

6.2.5. Numerical verification

In this section, the buckling behaviour of an axially-loaded column is studied. The results obtained from the current hybrid finite element method are presented and compared with the results calculated by Engesser and Haringx solutions in order to show the agreement of the current model with Engesser's solution.

The column studied in this example is simply-supported, and the dimensions of the cross section are shown in Figure 6.3. The analysis is performed for various buckling lengths. The column is subjected to an axial load P which is applied at the centroid *C* of the cross-section.

The column is made of isotropic material, and the material properties of the element are

$$E = 144MPa, \quad G = 4.14MPa, \quad \upsilon = 0.3$$

The flexural buckling happens around the weak axis of the column which is the y axis.

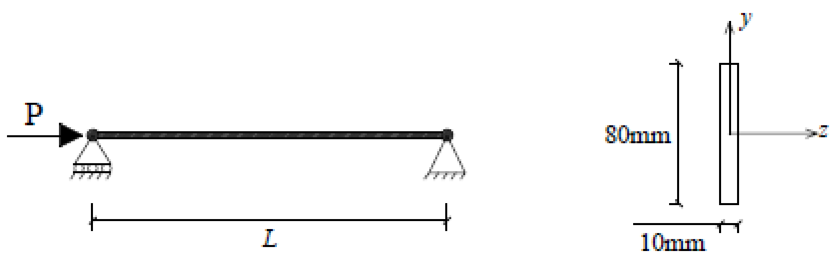

Figure 6.3: Simply Supported column and its Cross-section

6.2.5.1. Results and discussions

In Figure 6.4, the critical buckling loads obtained by the current hybrid method are presented and compared with the buckling loads calculated by Engesser and Haringx solutions. The results are shown for the full range of P_b/P_s in terms of dimensionless ratios of P_{cr}/P_s and P_{cr}/P_b. In the right-hand part of the figure (i.e. shear-rigid cases) the values of P_{cr}/P_b and in the left-hand side (i.e. shear-weak cases) P_{cr}/P_s will be discussed. The dotted lines in Figure 6.4 show the values of P_{cr}/P_s for shear-rigid cases and P_{cr}/P_b for shear-weak cases which are not of interest in here.

It can be concluded from Figure 6.4 that when $P_b \ll P_s$, the results obtained by the current hybrid finite element method are in acceptable agreement with the results of both Engesser and Haringx theories. Results from all the methods approach the upper limit of Euler buckling load in this case.

As shear rigidity decreases, the difference between Engesser and Haringx results increases significantly. As discussed previously, at this extreme case Engesser's solution yields $P_{cr} = P_s$ whereas Haringx' theory obtains a significantly larger value of $P_{cr} = \sqrt{P_b P_s}$. One can see that in this case the results of the current finite element analysis are very close to the results of Engesser theory. The small difference in the Engesser's figure and the current study figure is due to the round-off errors and they will match in the limit case.

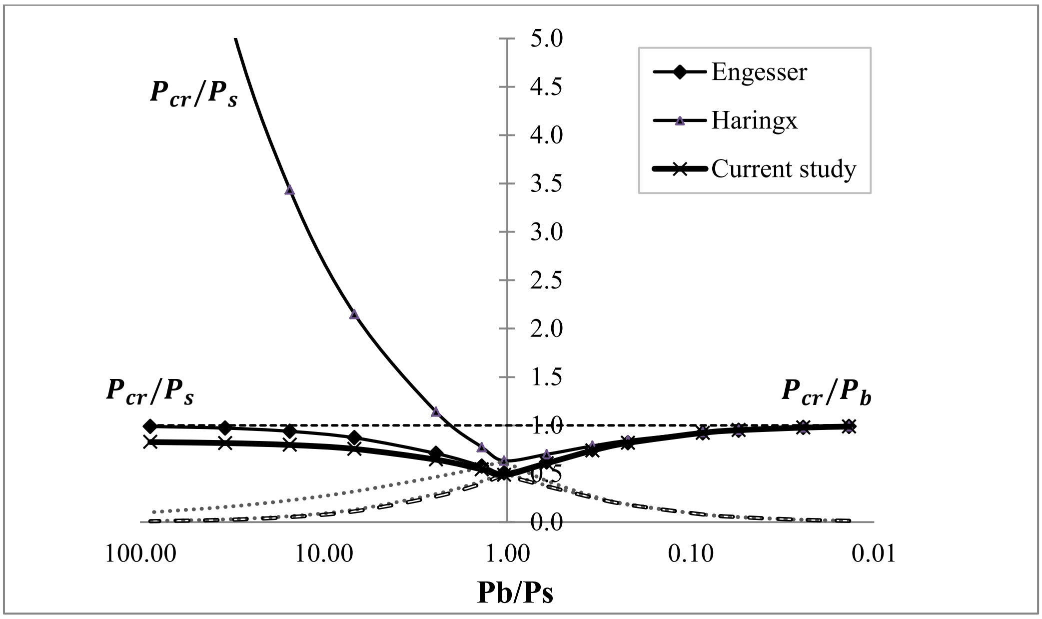

Figure 6.4: Comparison with Engesser and Haringx formulations

6.3. The effects of shear deformation in short composite laminate columns

In this section, the importance of shear deformation effects in short composite laminate columns and the capability of the current hybrid method for catching these effects are discussed. The flexural buckling load of an axially-loaded laminate composite column is obtained for two different lengths to see the effect of shear deformation explicitly.

The element is assumed to be made of graphite-epoxy (AS4/3501) with the following material properties:

$$E_1 = 144MPa, \quad E_2 = 9.65MPa$$
$$G_{12} = 4.14MPa$$
$$\upsilon_{12} = 0.3$$

The subscript 1 corresponds to the direction parallel to fibre orientation and subscripts 2 and 3 are related to the directions perpendicular to it.

The cross-section is assumed to be a doubly symmetric I section. The dimensions and the boundary conditions of the column are illustrated in Figure 6.5.

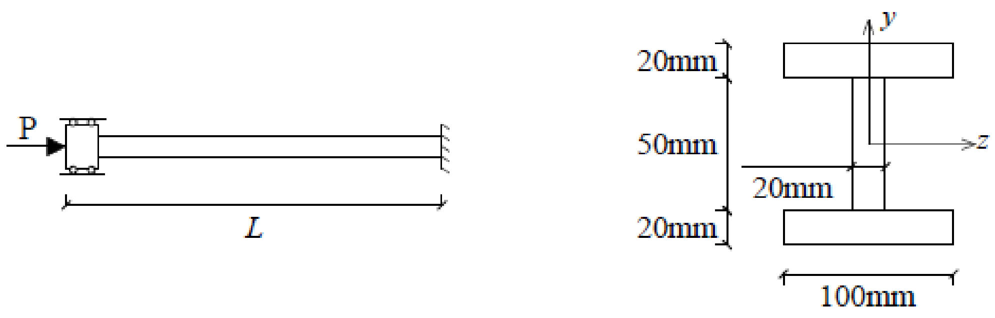

Figure 6.5: Fixed-fixed Short column with Symmetric Cross-section

The web and flanges are laminated with layers of equal thickness t=2.5*mm* and the fibre orientation is along the column axis. The column is subjected to an axial load P which is applied at the centroid *C* of the cross-section. The flexural buckling happens around the weak axis of the column which is the y axis.

To see the effects of shear deformation, the analyses are done with and without the shear deformation for two different lengths of column: L=1200*mm* and L=700*mm*.

6.3.1. Checking the column for local buckling

It should be noted that in short columns, local buckling may occur at a lower load than the global buckling. Therefore, in this example the column needs to be checked for local buckling as well. It means that the cross sectional dimensions and length of the column should be chosen in a way such that the local buckling load of web and flanges are more than the global buckling load of the column.

In the following, based on the paper presented by Kollár (2003), the assumptions, methodologies and formulations for local buckling analysis of laminate composite thin-walled members are briefly discussed.

The local buckling analyses can be performed based on the following assumptions:

1. The wall segments are considered as orthotropic plates,
2. The shared edges between two or more plates remain straight

Considering the mentioned assumptions, there are two main approaches for determining the local buckling load:

1. The exact solution, in which all the wall segments are assumed to buckle simultaneously. In this approach the continuity conditions at the plate intersections are satisfied (Bulson 1955).
2. The approximate solution, in which the wall segments are considered as individual plates which are elastically restrained by the adjacent walls (Bleich 1952). In this approach, elastic restraints due to the adjacent walls in addition to the buckling load of the plate whose edges are restrained should be determined.

In here, the explicit expression developed by Kollár (2003) which is based on the second approach is adopted for calculating the local buckling load.

Firstly, each segment of the member is assumed to be simply-supported (Figure 6.6), and the critical buckling load $\left(N_{x\ cr}\right)^{ss}$ for each segment is calculated (Bleich 1952).

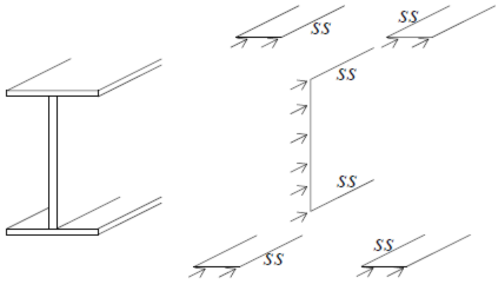

Figure 6.6: Modelling of local buckling of axially loaded member

If the web was simply supported at both edges and the flanges were simply supported at one edge and free at the other edge, the buckling loads of flanges would be calculated by Eq. (6.40) (Barbero 1999) and the buckling load of web would be calculated by Eq. (6.41) (Lekhnitskii 1968).

$$\left(N_{x\ cr}\right)_f^{ss} = \frac{12D_{66}}{L_y^{\ 2}} + \frac{\pi^2 D_{11}}{L_x^{\ 2}} \tag{6.40}$$

$$\left(N_{x\ cr}\right)_w^{ss} = \frac{\pi^2}{L_y^{\ 2}}\left(2\sqrt{D_{11}D_{22}} + 2\left[D_{12} + 2D_{66}\right]\right) \tag{6.41}$$

in which

L_y : The plate width

L_x : The plate length

$D_{ij}\left(i,j=1,2,6\right)$: The elements of the bending stiffness matrix and for the column studied in this example with the mentioned lay-up. We have

$$D_{11}=\frac{E_1h^3}{12R},\quad D_{22}=\frac{E_2h^3}{12R},\quad D_{12}=\nu_{12}D_{22},\quad D_{66}=\frac{G_{12}h^3}{12R}\quad where\quad R=1-\nu_{12}{}^2\frac{E_2}{E_1}$$

By considering $L_x \gg L_y$ and $L_y=\frac{b_f}{2}$ for the flanges and $L_y=b_w$ for the web, Eqs. (6.40) and (6.41) will reduce to

$$\left(N_{x\ cr}\right)_f^{ss}=\frac{12\left(D_{66}\right)_f}{\left(b_f/2\right)^2} \tag{6.42}$$

$$\left(N_{x\ cr}\right)_w^{ss}=\frac{\pi^2}{b_w{}^2}\left(2\sqrt{\left(D_{11}\right)_w\left(D_{22}\right)_w}+2\left[\left(D_{12}\right)_w+2\left(D_{66}\right)_w\right]\right) \tag{6.43}$$

Next step is calculating the axial strain for each segment (Eq. (6.44)).

$$\varepsilon_{x\ cr}=\left(N_{x\ cr}\right)^{ss}a_{11} \tag{6.44}$$

where $a_{11}=\frac{1}{E_1h}$ is the tensile compliance of the segment.

The segment with the lowest critical axial strain is the one that will buckle first. It means that if $\left(N_{x\ cr}\right)_f^{ss}\left(a_{11}\right)_f<\left(N_{x\ cr}\right)_w^{ss}\left(a_{11}\right)_w$ the flange buckles first and if $\left(N_{x\ cr}\right)_w^{ss}\left(a_{11}\right)_w<\left(N_{x\ cr}\right)_f^{ss}\left(a_{11}\right)_f$ the web buckles first.

After determining the most susceptible segment, we calculate its buckling load. In this stage, the segment is considered as a plate rotationally restrained by the adjacent segments.

The restraining effect varies depending on the segments configurations. Since the column in this example has an I-shaped cross-section, two cases are discussed: the first one is a restraining wall with both edges attached to the adjacent segments; and the second one is a restraining wall with only one edge attached to the adjacent segment. The first case happens when the flange buckles first and the web restrains the rotation of the flange (Figure 6.7b), and the second case occurs when the web buckles first and the flanges restrain the rotation of web (Figure 6.7b).

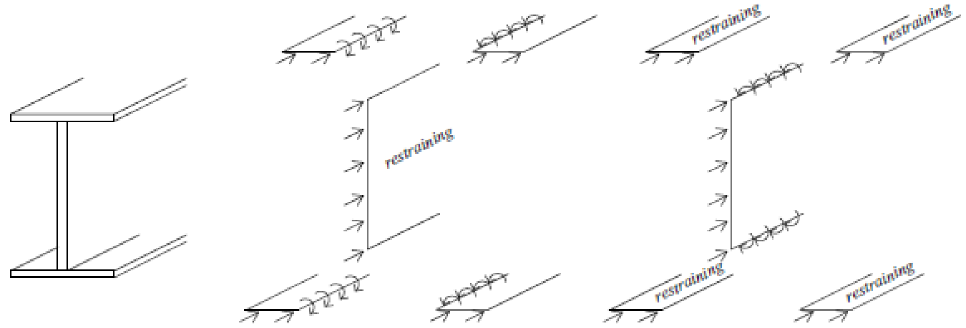

(a) (b)

Figure 6.7: (a) The web restraining the rotation of the flanges **(b)** The flanges restraining the rotation of the web

In the first case, by assuming the cylindrical deformed shape (Bleich 1952), the rotational spring constant is given as

$$k = \frac{c\left(D_{22}\right)_{rs}}{L_{rs}} \tag{6.45}$$

where constant $c = 2$ is adopted for this case, and D_{22} is the bending stiffness matrix element. Subscript rs is for the restraining segment.

In the second case, the effect of restraining segment is taken into account by the torsional stiffness which is given as

$$GI_t = 4\left(D_{66}\right)_{rs} L_{rs} \tag{6.46}$$

When we have an axial load, Eqs. (6.45) and (6.46) will be modified by an amplification factor r as follows

$$k = \frac{c\left(D_{22}\right)_{rs}}{L_{rs}} \frac{1}{r} \tag{6.47}$$

$$GI_t = 4\left(D_{66}\right)_{rs} L_{rs} \frac{1}{r} \tag{6.48}$$

in which r is defined as

$$r = \frac{1}{1 - \dfrac{\left(N_{x\ cr}\right)_{bu}^{ss} \left(a_{11}\right)_{bu}}{\left(N_{x\ cr}\right)_{rs}^{ss} \left(a_{11}\right)_{rs}}} \tag{6.49}$$

Subscript bu refers to the segment that buckles.

When the flange buckles first, its buckling load is calculated from the expression developed by Kollaor (2002b):

$$\begin{aligned} \left(N_{x\ cr}\right)_f &= \sqrt{\left(D_{11}\right)_f \left(D_{22}\right)_f}\, \frac{\left(K\left(\eta 15.1\sqrt{1-\nu} + \left(1-\eta\right)6\left(1-\nu\right)\right) + 7\dfrac{\left(1-K\right)}{\sqrt{1+4.12\zeta}}\right)}{L_y{}^2} && when\ K \le 1 \\ \left(N_{x\ cr}\right)_f &= \sqrt{\left(D_{11}\right)_f \left(D_{22}\right)_f}\, \frac{\left(\eta 15.1\sqrt{1-\nu} + \left(K-\eta\right)6\left(1-\nu\right)\right)}{L_y{}^2} && when\ 1 < K \end{aligned} \tag{6.50}$$

in which $K = \dfrac{\left(2D_{66} + D_{12}\right)}{\sqrt{D_{11}D_{22}}}$, $\eta = \dfrac{1}{\sqrt{1+\left(7.22-3.55\nu\right)}}$, $\nu = \dfrac{D_{12}}{2D_{66}+D_{12}}$, $L_y = \dfrac{b_f}{2}$ and $\zeta = \dfrac{D_{22}}{kL_y}$. Based on Eq. (6.47), the rotational spring constant is given as

$$k = \frac{1}{2}\frac{c\left(D_{22}\right)_w}{b_w}\left(1 - \frac{\left(N_{x\ cr}\right)_f^{ss}\left(a_{11}\right)_f}{\left(N_{x\ cr}\right)_w^{ss}\left(a_{11}\right)_w}\right) \tag{6.51}$$

where $c = 2$, and factor $1/2$ is applied because the web is restraining two half flanges.

If the web buckles first, its buckling load is calculated from the expression developed by Kollaor (2002a):

$$\left(N_{x\ cr}\right)_w = \frac{\pi^2\left(2\sqrt{1+4.139\xi}\sqrt{\left(D_{11}\right)_w\left(D_{22}\right)_w} + \left(2+0.62\xi^2\right)\left(\left(D_{12}\right)_w + 2\left(D_{66}\right)_w\right)\right)}{L_y^{\ 2}} \tag{6.52}$$

in which $\xi = \dfrac{1}{1+0.61\zeta'^{1.2}}$, $\zeta' = \dfrac{D_{22}L_y}{GI_t}$ and $L_y = b_w$. Based on Eq. (6.48), the rotational torsional stiffness is given as

$$GI_t = 4\left(D_{66}\right)_f b_f\left(1 - \frac{\left(N_{x\ cr}\right)_w^{ss}\left(a_{11}\right)_w}{\left(N_{x\ cr}\right)_f^{ss}\left(a_{11}\right)_f}\right) \tag{6.53}$$

For the column studied in this example, the flanges will buckle locally before the web ($\left(N_{x\ cr}\right)_f^{ss}\left(a_{11}\right)_f < \left(N_{x\ cr}\right)_w^{ss}\left(a_{11}\right)_w$). Using Eq. (6.50) the value of the local buckling load of flanges is calculated as 43724.2 *N*. This value is greater than the global buckling loads shown in Table 6.1. Therefore, the local buckling will not occur before the global flexural buckling of the column.

6.3.2. Results and discussion

In Table 6.1 the critical buckling load obtained from the shear-flexible analysis and the one that does not include the shear deformation ($\Lambda_{yy}^{-1} = 0$) along with the percentage difference between these two analyses are presented for each column.

Table 6.1: Buckling Loads of Columns (in Newtons)

Length(mm)	With shear	No shear	Difference (%)
1200	13802.3	14540.3	5.1
700	36732.1	42700.3	16.3

The following conclusions can be made from the analysis results:

1. By comparing the values of predicted buckling loads of each column obtained by shear deformable and non-shear deformable analyses one can verify the capability of the current model in capturing the effect of shear deformation.
2. From Table 6.1, it can be observed that by decreasing the column length the difference between the buckling loads calculated by two analyses (with and without shear deformation) increases from 5.1% to 16.3%. It shows that in short columns, shear deformations can have a significant effect on the value of the critical buckling load.
3. In some cases, ignoring the effects of shear deformations leads to an overestimation of the critical buckling load, which is not desirable.

6.4. Flexural buckling in sandwich columns

6.4.1. Literature review

A sandwich cross-section is composed of two thin and stiff faces separated by a lightweight core. The core, which is often a homogenous foam, provides the light weight of the member with sandwich cross-section. On the other hand, the tensile property and flexural rigidity of the element are mainly provided by the faces due to their material properties and distance from each other. Therefore, the bending and in-plane loads are carried by the faces and the shear is carried by the core in sandwich cross-sections.

Sandwich elements are used increasingly in many structural fields because of their high bending strength and low weight. Due to the geometric configuration and the stiffness ratios between the different components of sandwich cross-sections, buckling is one of the main reasons of failure in these composite materials (Douville and Le Grognec 2013).

There are many analytical solutions as well as experimental studies in the literature for buckling analysis of sandwich elements. The study of buckling behaviour of sandwich columns dates back to the works of Hoff and Mautner (1945). Hoff and Mautner (1948) then performed an experimental study for the buckling behaviour of sandwich columns.

The basics of sandwich element construction and design approaches are presented by Allen (1969) and Zenkert (1995). An analytical solution for buckling analysis of sandwich elements with thick skins and weak cores was developed by Drysdale *et al.* (1979).

Sandwich columns subjected to end compression loads were tested by Fleck and Sridhar (2002). They developed simple analytical models for the axial strength to compare with the experimental results. Attard and Hunt (2008) derived buckling equations for a sandwich column assuming Timoshenko beam displacement approximation. Their equations were in agreement with the equation of Allen (1969). Douville and Le Grognec (2013) studied the buckling behaviour of sandwich beam-columns under various types of loading. They developed an exact analytical solution for the critical buckling load considering the faces as Euler-Bernoulli beams and the core as a 2D continuous solid.

In this section, using the current finite element hybrid method, the flexural buckling analysis of an axially-loaded column with a sandwich cross-section is studied and the obtained values for the critical buckling load are compared with the results calculated by the developed solutions existing in the literature. It will be proven that the current shear deformable hybrid model is capable of efficiently capturing the behaviour of these types of elements.

The column studied in this example is simply-supported, and the dimensions of the cross section are shown in Figure 6.8. The column is subjected to an axial load P which is applied at the centroid *C* of the cross-section. The flexural buckling happens around the weak axis of the column which is the y axis.

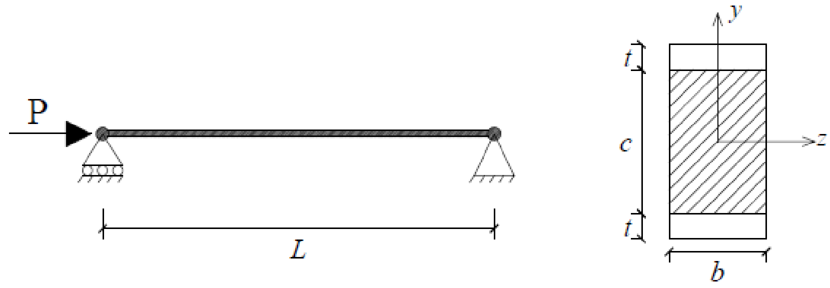

Figure 6.8: Simply Supported Column with Sandwich Cross-section

The material properties of the core and faces and the cross sectional dimensions are as follows

$$E_f = 30000MPa \quad , \quad G_f = 10000MPa$$
$$E_c = 75MPa \quad , \quad G_c = 30MPa$$
$$b = 10mm \quad , \quad c = 20mm \quad , \quad t = 1mm$$

The analyses are done for various lengths of the column varying from 500*mm* to 40*mm*.

Based on the discussion at the beginning of this section, we can assume that the stiff skins in the sandwich columns are mainly responsible for bending stiffness of the member. Therefore in here, the critical buckling load P_{cr} is calculated by adding up the load obtained from shear deformable analysis of the core P_c and the non-shear deformable analysis of faces $P_{E,f}$ (Euler buckling load). As mentioned before, the non-shear deformable analysis is performed by setting $\Lambda_{yy}^{-1} = 0$ in this study.

To verify the accuracy of the current hybrid model, the obtained buckling load is compared with the results from the analytical solution of Allen (1969), the formula developed by Blaauwendraad (2010) and the hyperelastic formulation of Attard and Hunt (2008). In the following a brief description of each method is presented.

The formula of Allen (1969) which is quoted widely in the literature is given as

$$\frac{P_{cr}}{G_c A_m} = \frac{P_f}{G_c A_m} + \frac{\dfrac{P_{Euler}}{G_c A_m} - \dfrac{P_f}{G_c A_m}}{1 + \dfrac{P_{Euler}}{G_c A_m} - \dfrac{P_f}{G_c A_m}} \tag{6.54}$$

in which

$A_m = A_c \dfrac{(c+t)^2}{c^2}$: The effective core area,

$A_c = cb$: The core area,

$P_f = \dfrac{\pi^2 E_f I_f}{L^2}$: The Euler buckling load of the faces,

$P_{Euler} = \dfrac{\pi^2 \left(E_c I_c + E_f I_f\right)}{L^2}$: The Euler buckling load of the whole sandwich section.

The formulation developed by Attard and Hunt (2008) includes both the axial deformation prior to buckling and the transverse shear deformations of both the core and faces. It can be written as

$$\frac{P_{cr}}{G_c A_m} = \frac{\dfrac{P_{Euler}}{G_c A_m}\left(1 + \dfrac{P_f}{G_c A_m}\right)}{1 + \dfrac{P_f}{G_c A_m}} \tag{6.55}$$

The formula suggested by Blaauwendraad (2010) for buckling analysis of sandwich columns is given as

$$P_{cr} = P_f + \frac{P_o P_s}{P_o + P_s} \tag{6.56}$$

in which

$P_s = A_s G_c$: The buckling load on the basis of the core shear rigidity where $A_s = \frac{be^2}{c}$,

e: Distances between centrelines of the faces,

$P_o = \frac{\pi^2 EI_o}{L^2}$: The Euler buckling load of the sandwich element excluding the contribution of the faces P_f ,

$P_f = \frac{\pi^2 E_f I_f}{L^2}$: The Euler buckling load of the faces.

6.4.2. Results and discussion

In Table 6.2 the predicted buckling loads obtained by current hybrid finite element method for various column lengths are presented and compared with the results calculated by the formulas mentioned in the previous section.

Table 6.2: Buckling Loads of Columns (in Newtons)

L (mm)	500	250	100	50	40
Allen (1969)	2.63E+03	1.05E+04	6.58E+04	2.63E+05	4.10E+05
Blaauwendraad (2010)	4.49E+03	1.45E+04	7.13E+04	2.68E+05	4.15E+05
Attard and Hunt (2008)	2.63E+03	1.05E+04	6.54E+04	2.61E+05	4.08E+05
Current model	2.63E+03	1.05E+04	6.58E+04	2.63E+05	4.15E+05

The following conclusions can be made from the analysis results:

1. Based on Table 6.2, one can observe that the results obtained by the current shear-deformable hybrid finite element method are in a very good agreement with the results from other methods.
2. It is of interest to note that in the current model for a very short column the critical buckling load can be obtained by simply adding the Euler buckling load of the faces $P_{E,f}$ and shear buckling load of the core $P_{S,c} = G_c A_c$. It is due to the fact that, compared to the long columns, in short columns the Euler buckling load of the core $P_{E,c}$ is very large compared to the shear buckling load $P_{S,c}$. Therefore, it is not the dominant buckling load for the core. To make the point more clear, two columns with different lengths are analysed here and the results are presented in Table 6.3.

Table 6.3: Buckling Loads of Columns (in Newtons)

L (mm)	500	40
$P_{S,c}$	5.00E+03	5.00E+03
$P_{E,c}$	1.97E+01	3.08E+03
$P_{E,f}$	2.61E+03	4.09E+05
$P_{cr,Short} = P_{S,c} + P_{E,f}$	7.61E+03	4.14E+05
$P_{cr} = P_c + P_{E,f}$	2.63E+03	4.10E+05
Difference	189.2%	0.76%

The first and second rows of Table 6.3 show the shear buckling load and Euler buckling load of the core respectively, and in the third row, the Euler buckling load of the faces is given. Then the calculated critical buckling loads for short column ($P_{cr,Short} = P_{S,c} + P_{E,f}$) are shown in the fourth row. In the last row the critical buckling loads of sandwich section for all types of columns are calculated ($P_{cr} = P_c + P_{E,f}$).

As we can see in the last row of Table 6.3, for the long column, i.e. L=500*mm*, the difference between P_{cr} and $P_{cr,Short}$ is considerable and cannot be ignored whereas for the shorter column it is negligible.

6.5. Flexural buckling in built-up columns

6.5.1. Literature review

Built-up columns are widely used in steel structures and bridges. These types of columns are mainly composed of two or more parallel longitudinal elements that are connected to each other by a number of transverse members at the points along their length. Since the moment of inertia of the built-up column increases as the distance between the centroids of the main elements increases, these columns have large bending rigidity. However, the shear stiffness in built-up columns is less than solid columns with the same bending rigidity, which can potentially reduce their buckling resistance.

The buckling behaviour of built-up columns has been comprehensively studied in the last decades. A theoretical method was proposed by Wang (1985) for determining the torsional-flexural buckling load of battened thin-walled open sections. It was proven that the buckling behaviour of these elements is dependent on the number and spacing of the battens. Geng-Shu and Shao-Fan (1989) established an interactive buckling theory for built-up beam-columns by modelling the element as a member with a sandwich cross-section. A method of analysis for built-up columns was presented by Gjelsvik (1990). His method is an extension of the classical Engesser method for columns and the Timoshenko theory for beams. Paul (1995) presented a generalized theory for the buckling analysis of built-up columns which is a modification over the method of Gjelsvik (1990). Chen and Li (2013) developed an analytical solution for the buckling analysis of simply supported battened columns subjected to axial load based on the classical energy method.

Experimental results of the buckling behaviour of laced and battened columns are reported in the literature as well. For example, Hosseini Hashemi and Jafari (2009) performed a series of tests for batten columns subjected to pure axial compression and determined the critical load. Bonab *et al.* (2013) conducted a number of tests on columns composed of two U-section profiles to study the elastic buckling of laced columns.

In this section, the buckling behaviour of a laced built-up column is studied. As discussed in previous sections, in the current hybrid finite element method the non-collinear elements can be connected very easily. Unlike the complementary energy based methods, in this method there is no need to satisfy the inter-element equilibrium. Therefore, the assemblage procedure is as simple as in the displacement based method. This is one of the advantages of this method over force-based finite element methods. To show this capability, a laced built-up column is analysed in this section, and the obtained buckling load is compared with the Euler buckling load of the column.

The built-up column studied here consists of two I-shaped elements spaced by a lacing system connecting them, and the column is axially loaded. The configuration of the laced column dimensions of the I-sections and laces and the boundary conditions are illustrated in Figure 6.9.

The material properties of the elements are

$$E = 205MPa,\ G = 82MPa, \upsilon = 0.3$$

Each element in the structure is modelled separately; that makes the total of 48 elements.

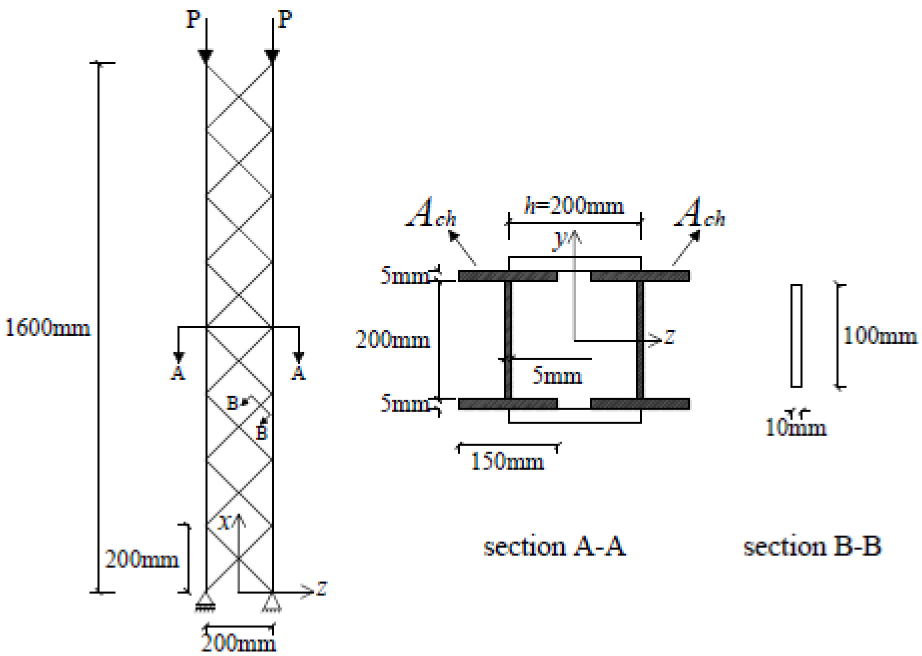

Figure 6.9: Laced Built-up Column and its Cross-section

The first mode of buckling is the overall bending of the column around the y axis and therefore, the critical flexural buckling load excluding shear deformation effects is comparable with the equivalent Euler buckling load of the column.

The Euler buckling load of the built-up column is given as (Kalochairetis and Gantes 2011)

$$P_E = \frac{\pi^2 EI_{col}}{(kL)^2} \tag{6.57}$$

in which

$EI_{col} = 0.5h^2 EA_{\mathrm{ch}}$: The effective bending rigidity of the built-up column

$\mathrm{k} = 2$: The effective length factor

In addition, in order to show the capability and accuracy of the hybrid model in capturing the buckling behaviour of each segment of the structure, one of the buckling modes that involves buckling of one of the segments is depicted and the corresponding buckling mode is presented in Figure 6.10.

6.5.2. Results and discussion

The predicted buckling loads by the current hybrid model in shear deformable and non-shear deformable analyses along with the Euler buckling load for the built-up column calculated by Eq. (6.57) are shown in Table 6.4.

Table 6.4: Buckling Loads of Columns (in Newtons)

Current study with shear	Current study without shear	P_E Kalochairetis and Gantes (2011)
10974.5	11036.8	10991.5

Additionally, the fifth buckling mode of the column can be observed in Figure 6.10, which has a buckling load of 801.0 *kN*.

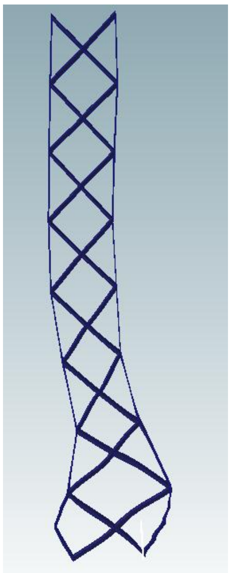

Figure 6.10: Fifth buckling mode of the built-up column

The following conclusions can be made from the analysis results:

1. As one can observe in Table 6.4, predicted buckling load by the current hybrid model (the non-shear deformable) is in a very good agreement with the Euler buckling load.
2. The current hybrid method can easily and efficiently predict all of the buckling modes and loads of the built-up column with a large number of elements. It is due to the fact that in this method the inter-element equilibrium does not need to be satisfied which makes the assemblage procedure very easier.

6.6. Summary and Conclusions

In section (6.2), the buckling load values of an axially-loaded column are obtained and compared with the results from Engesser and Haringx theories. It was proven that the predicted values of buckling load by the current hybrid method in the case of large shear rigidity are in agreement with both solutions, and is equal to the Euler buckling load. For the case of very large flexural rigidity (i.e. shear-weak), the current hybrid solution is in a very good agreement with the Engesser solution.

One of the very important advantages of the developed shear deformable hybrid finite element method is including shear deformation effects without modifying the kinematic assumptions. In section (6.3), a short column with fibre-reinforced laminate composite cross-section was studied and the effect of shear deformations in the flexural buckling load of the column is presented. It was shown that the current hybrid method is capable of effectively capturing these effects.

In section (6.4), it was proven that the current method is able to efficiently predict the flexural buckling load of the sandwich columns.

Since one of the advantages of the current hybrid method over the force-based method is the straightforward connecting of the non-collinear elements without the need to satisfy the inter-element equilibrium, a laced built-up column subjected to the axial load was analysed in section (6.5), and the agreement of the buckling load predicted by this model with the Euler buckling load of the column was illustrated.

Chapter 7: Shear Deformable Hybrid Finite-element Formulation for Lateral-Torsional Buckling Analysis of Thin-walled Composite Beams

7.1. Introduction

In this chapter, the lateral-torsional buckling behaviour of fibre-reinforced laminated composite thin-walled beams is studied.

The chapter starts with a comprehensive literature review of the theories and previous research works relevant to the lateral-torsional buckling of thin-walled fibre reinforced composite elements. Next, the kinematic relations for the beams are developed based on the kinematics of general open thin-walled elements. Then, the constitutive relations of thin-walled beam with laminate composite cross-section subjected to loads that induce bending moment about its strong axis are obtained. Using the developed kinematic relations and the constitutive equations, equations for stress and stress resultants are obtained in section (7.6). In section (7.7) the hybrid formulation is developed from the potential energy functional by relaxing the strain-displacement equations as auxiliary conditions through the Lagrange Multipliers method. The discretised form of the hybrid functional for buckling analysis is obtained after the interpolations of stress resultants and lateral displacements in section (7.8). The numerical verifications are presented in section (7.9) to validate the efficiency and accuracy of the developed hybrid finite element model in lateral-torsional buckling analysis of thin-walled beams with fibre reinforced laminate composite cross-sections. Beams with various boundary conditions are studied and the effect of fibre orientation and beam slenderness on the lateral-torsional buckling moment is presented. In addition, the effect of shear deformations on the lateral-torsional buckling analysis of beams is illustrated through a numerical example.

7.2. Literature review

In this section, a comprehensive literature review of the previous studies and research works about the lateral-torsional buckling of thin-walled composite beams is presented.

By extending the theories for bending and twisting of thin-walled beams with open cross-sections made from isotropic materials, Bauld and Tzeng (1984) presented a Vlasov-type theory for thin-walled beams with open cross-sections made from mid-plane symmetric fibre-reinforced laminates.

An analytical study of the transverse shear strain effect on the lateral buckling of thin-walled open-section fibrous composite beams was developed by Sherbourne and Kabir (1995). Pandey *et al.* (1995a) obtained the beam stiffness coefficients of thin-walled composite open-section members based on a Vlasov-type linear hypothesis. They presented an analytical study of optimal fibre direction for improving the lateral buckling strength of these elements.

Roberts (2002) presented theoretical studies of the influence of shear deformation on the flexural, torsional, and lateral buckling of pultruded FRP I-profiles.

Sapkas and Kollar (2002) studied the lateral-torsional buckling analysis of thin-walled open-section orthotropic composite beams. They derived an explicit expression for the buckling load of composite beams which considers both the transverse shear and the restrained warping induced shear deformations.

Machado (2010) derived analytical solutions for the lateral stability analysis of cross-ply laminated thin-walled beams subjected to combined axial and bending loads. The closed-form analytic expressions include both the transvers shear and the restrained warping induced shear deformations and are valid for simply supported bisymmetric beams.

The lateral- torsional buckling of beams with composite materials has been the subject of many experimental studies as well. Mottram (1992) performed an experimental study of lateral-torsional buckling of simply-supported beams subjected to a central point load and illustrated the agreement of the test results with the classical solution for the lateral buckling load. Brooks and Thrvey (1995) and Turvey (1996) described a series of lateral buckling tests on pultruded GRP I-section cantilever beams. The comparisons of the theoretical buckling loads determined from approximate formula and numerical finite element eigenvalue analysis with the test results were presented in their study. Roberts and Masri (2003) based on a full section and coupon tests, described the experimental determination of the flexural and torsional properties of a pultruded FRP profile. In addition, they developed closed-form solutions for the influence of shear deformation on global flexural, torsional, and lateral buckling of pultruded FRP profiles.

On the other hand, the finite element method has been extensively used for the lateral-torsional buckling analysis of thin-walled composite members. Lin *et al.* (1996) presented a finite element model to study the buckling behaviour of thin-walled glass FRP members. Lee *et al.* (2002) and Lee and Kim (2002) developed a general analytical model based on the classical lamination theory which is applicable to the lateral buckling of thin-walled open-section composite beams subjected to various types of loadings. They developed a displacement-based one-dimensional finite element model based on Vlasov‘s thin-walled beam theory to obtain critical loads for thin-walled composite beams with various boundary conditions. Lee (2006) studied lateral buckling of thin-walled composite beams with mono-symmetric cross-sections. By using a systematic variational formulation based on the classical lamination theory, a geometrically nonlinear model was given in his model, and a displacement-based one-dimensional finite element model was developed to formulate the problem.

Kim *et al.* (2007) proposed a numerical method to evaluate exactly the element stiffness matrix for lateral buckling analysis of thin-walled composite beams subjected to end moments. In their study, the bifurcation type buckling theory of thin-walled composite beams subjected to pure bending is developed based on the energy functional. In addition, they derived analytical solutions for lateral buckling moments of unidirectional and cross-ply laminated composite beams with various boundary conditions as a special case. Back and Will (2008) developed a shear-flexible finite element model for buckling analysis of thin-walled composite I-beams. The governing equations in their model are derived based on the principle of minimum total potential energy. In addition, they obtained the geometric stiffness for the buckling analysis of axially loaded thin-walled composite beams. Kim and Lee (2013) performed shear-deformable lateral buckling analysis of laminate composite mono-symmetric I-sections.

In their method, the displacement fields were defined using the first-order shear deformable beam theory, and the second order torque terms were introduced from the geometric nonlinearity.

In this study, a hybrid finite element formulation for lateral-torsional buckling analysis of thin-walled open-sections members made of fibre-reinforced composite materials is developed. In this method, shear deformations are included in the formulations by using the strain energy of the equilibrating shear stress field without modifying the basic kinematic assumptions of the beam theory (the advantage of this method over the displacement-based methods). In addition, non-collinear elements can be connected easily in this method without the need to satisfy the inter-element equilibrium (the advantage of this method over the force-based methods).

7.3. Problem statement

When an unbraced beam with sufficient slenderness undergoes loads which induce bending moment around its strong axis, it may fail by a combined lateral displacement and twisting of cross-section before yielding of its material. This phenomenon is known as lateral-torsional buckling (Figure 7.1).

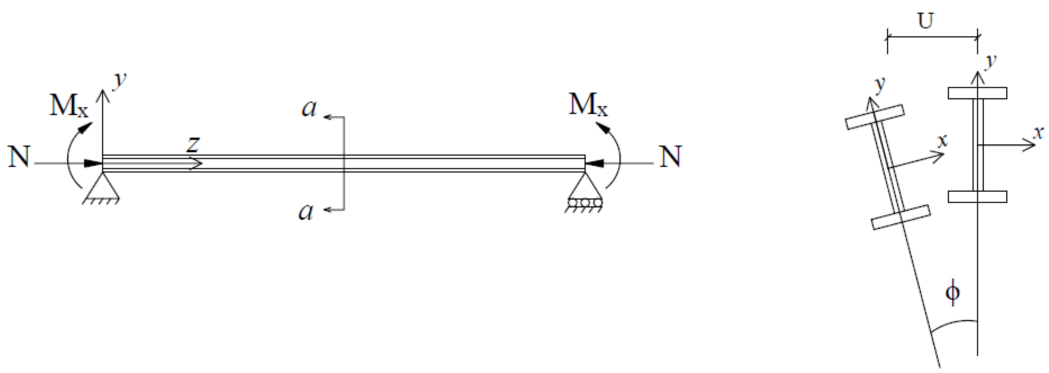

Figure 7.1: A beam subjected to bending moment around the major axis

At the pre-buckling state, the applied loads do not cause any shear forces and associated bending moment along the minor axis, St. Venant torsion, bimoments and twisting moments due to warping ($V_x{}^p = M_y{}^p = T_{sv}{}^p = B^p = T_\omega{}^p = 0$).

Throughout the lateral-torsional buckling, the vertical deflection, moments about the major axis and associated shear force acting along the minor axis all vanish ($V = M_x = V_y = 0$). In addition, the increment in axial force is equal to zero $(N = 0)$ in agreement with the inextensional buckling assumption (Trahair 1993b).

7.4. Kinematics

In order to develop the theoretical model, the following assumptions are adopted in this study:

7. The thin-walled member is assumed to be prismatic and straight.
8. Cross-sections remain rigid in plane during deformation in accordance with the first assumption of Thin-walled Beam Theory of Vlasov.
9. Strains are small.
10. Material is linearly elastic and obeys Hooke's law.
11. Inextensional buckling assumption is adopted, which means that the shortening of the beam during the buckling behaviour is ignored.
12. Pre-buckling deformation effects are neglected.

Two sets of mutually interrelated coordinate systems are required in this study. The first one is an Orthogonal Cartesian Coordinate System (x, y, z) in which the z axis is parallel to the longitudinal axis of the beam and x and y axes lie in the plane of the cross-section and are parallel to the weak and strong axes of the cross-section, respectively (Figure 7.2). The second coordinate system is an orthogonal local coordinate system (n,s,z) for the plate segment of the beam wherein the s axis is at a tangent to the mid-surface of a plate element and is oriented along the contour line of the cross-section and the n axis is normal to the mid-surface of the plate. The two coordinate systems are related through θ which is the angle between the s axis at point A and the x axis as shown in Figure 7.2.

In agreement with the first Vlasov assumption, cross sections remain rigid under deformation. Therefore, as mentioned in chapter 2, the horizontal and the vertical components of displacement $u(s,z)$ and $v(s,z)$ of an arbitrary point $A\left(x(s),y(s)\right)$ on the mid-surface of the cross-section can be expressed in terms of the horizontal $U(z)$ and vertical $V(z)$ displacement components of a pole $P\left(a_x,a_y\right)$, and the angle of twist of the beam cross-section, $\phi(z)$.

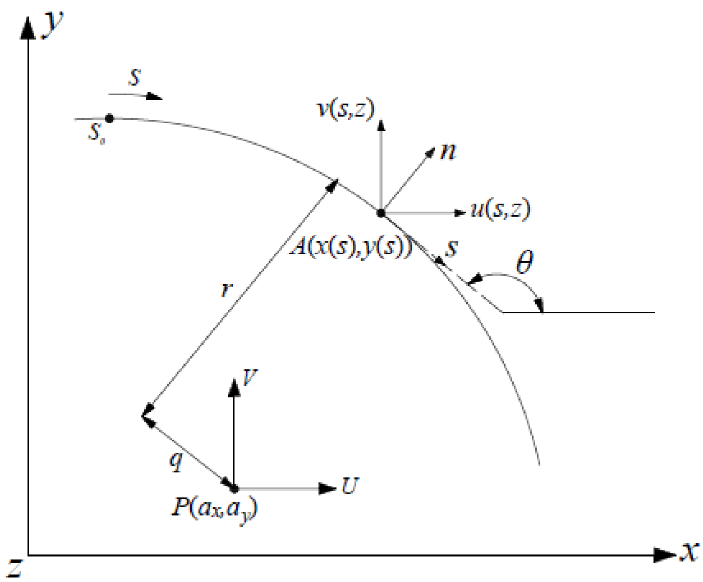

Figure 7.2: Coordinate systems in thin-walled section

It should be noted that coordinate s is defined as a sectorial coordinate and is measured from a sectorial origin S_0 located on the mid-surface of the cross-section (Figure 7.2). As a result, the arbitrary point *P* can be identified to have coordinates $x(s)$ and $y(s)$, and the definition of the displacement components can be written as follows:

$$u(s,z) = U(z) - \left[y(s) - a_y \right] \phi(z) \tag{7.1}$$

$$v(s,z) = V(z) + \left[x(s) - a_x \right] \phi(z) \tag{7.2}$$

Since this study considers beams with mono-symmetric cross-section we can assume that $a_x = 0$.

The axial component of displacement of point *A* is obtained from the second assumption of Vlasov, i.e. the shear strain λ_{zt} in the middle plane of the plate element is zero for each plate element (Bauld and Tzeng 1984) (Section 2.2).

$$w(s,z) = W(z) - x(s)U'(z) - y(s)V'(z) - \omega(s)\phi'(z) \tag{7.3}$$

where ω is a section property called sectorial area by Vlasov and is defined as $\omega = \int r \mathrm{d}s$. All primes denote differentiation with respect to longitudinal coordinate *z*.

As mentioned in section (5.3), during lateral-torsional buckling, the beam does not deflect in the vertical direction, i.e. $V(z) = 0$. In addition, in agreement with the inextensional buckling assumption, the shortening of the beam is assumed to be negligible during buckling, i.e. $W(z) = 0$. Therefore, Eq. (7.3) will reduce to

$$w(s,z) = -x(s)U'(z) - \omega(s)\phi'(z) \tag{7.4}$$

Consequently, the longitudinal normal strain induced by the lateral-torsional buckling deformations can be expressed as

$$\varepsilon_z = -x(s)U''(z) - \phi''(z)\omega(s) \tag{7.5}$$

where x and y are measured from the weighted centroid (or neutral axis) of the cross-section.

On the other hand, the shear strains of the cross-section are assumed to be equal to zero based on the second assumption of the Vlasov theory.

$$\gamma_{zx} = 0 \tag{7.6}$$

7.5. Constitutive relation

Consider a laminate composed of n orthotropic layers in which the fibre orientation of each layer with respect to the global coordination is determined by angle Φ_k about the z axis. Assuming that perfect inter-laminar bond exists between the layers, the stress-strain relationship for the k^{th} layer is given as:

$$\boldsymbol{\sigma}^{(k)} = \bar{\mathbf{Q}}^{(k)}\boldsymbol{\varepsilon} \Rightarrow \begin{Bmatrix} \sigma_z^{(k)} \\ \sigma_x^{(k)} \\ \tau_{zx}^{(k)} \end{Bmatrix} = \begin{bmatrix} \bar{Q}_{11}^{(k)} & \bar{Q}_{12}^{(k)} & \bar{Q}_{16}^{(k)} \\ \bar{Q}_{12}^{(k)} & \bar{Q}_{22}^{(k)} & \bar{Q}_{26}^{(k)} \\ \bar{Q}_{16}^{(k)} & \bar{Q}_{26}^{(k)} & \bar{Q}_{66}^{(k)} \end{bmatrix} \begin{bmatrix} \varepsilon_z \\ \varepsilon_x \\ \gamma_{zx} \end{bmatrix} \tag{7.7}$$

In here, subscripts 1 to 6 are consistent with the convention adopted for laminated composites (Wang 1997).

In Eq. (7.7)

$$\bar{Q}_{11}^{(k)} = Q_{11}^{(k)}\cos^4\Phi_k + 2\left(Q_{12}^{(k)} + 2Q_{66}^{(k)}\right)\sin^2\Phi_k\cos^2\Phi_k + Q_{22}^{(k)}\sin^4\Phi_k \tag{7.8}$$

$$\bar{Q}_{12}^{(k)} = \left(Q_{11}^{(k)} + Q_{22}^{(k)} - 4Q_{66}^{(k)}\right)\sin^2\Phi_k\cos^2\Phi_k + Q_{12}^{(k)}\left(\sin^4\Phi_k + \cos^4\Phi_k\right) \tag{7.9}$$

$$\bar{Q}_{22}^{(k)} = Q_{11}^{(k)}\sin^4\Phi_k + 2\left(Q_{12}^{(k)} + 2Q_{66}^{(k)}\right)\sin^2\Phi_k\cos^2\Phi_k + Q_{22}^{(k)}\cos^4\Phi_k \tag{7.10}$$

$$\bar{Q}_{26}^{(k)} = \left(Q_{11}^{(k)} - Q_{22}^{(k)} - 2Q_{66}^{(k)}\right)\sin^3\Phi_k\cos\Phi_k + \left(Q_{12}^{(k)} - Q_{22}^{(k)} + 2Q_{66}^{(k)}\right)\sin\Phi_k\cos^3\Phi_k \tag{7.11}$$

$$\bar{Q}_{16}^{(k)} = \left(Q_{11}^{(k)} - Q_{12}^{(k)} - 2Q_{66}^{(k)}\right)\sin\Phi_k\cos^3\Phi_k + \left(Q_{12}^{(k)} - Q_{22}^{(k)} + 2Q_{66}^{(k)}\right)\sin^3\Phi_k\cos\Phi_k \tag{7.12}$$

$$\bar{Q}_{66}^{(k)} = \left(Q_{11}^{(k)} + Q_{22}^{(k)} - 2Q_{12}^{(k)} - 2Q_{66}^{(k)}\right)\sin^2\Phi_k\cos^2\Phi_k + Q_{66}^{(k)}\left(\sin^4\Phi_k + \cos^4\Phi_k\right) \tag{7.13}$$

where

$$Q_{11}^{(k)} = \frac{E_1^{(k)}}{1 - \upsilon_{12}^{(k)}\upsilon_{21}^{(k)}} \tag{7.14}$$

$$Q_{12}^{(k)} = \frac{\upsilon_{12}^{(k)}E_1^{(k)}}{1 - \upsilon_{12}^{(k)}\upsilon_{21}^{(k)}} \tag{7.15}$$

$$Q_{22}^{(k)} = \frac{E_2^{(k)}}{1 - \upsilon_{12}^{(k)}\upsilon_{21}^{(k)}} \tag{7.16}$$

$$Q_{66}^{(k)} = G_{12}^{(k)} \tag{7.17}$$

where $E_1^{(k)}$ and $E_2^{(k)}$ are Young's moduli of the k^{th} layer in the local $\bar{z}_k$ and $\bar{y}_k$ directions, respectively, $G_{12}^{(k)}$ is the shear modulus in $\bar{z}_k\bar{y}_k$ plane of the k^{th} layer, $\upsilon_{12}^{(k)}$ is the Poisson's ratio defined as the ratio of the transverse strain in the $\bar{y}_k$ direction to the axial strain in $\overline{z}_k$ direction due to the normal stress in $\overline{z}_k$ direction, and $\upsilon_{21}^{(k)}$ is the Poisson's ratio defined as the ratio of the transverse strain in the $\overline{z}_k$ direction to the axial strain in $\overline{y}_k$ direction due to the normal stress in $\overline{y}_k$ direction (Omidvar and Ghorbanpoor 1996, Reddy 2003). In this study laminate configuration is limited to symmetric angle-ply stacking sequence with respect to mid-plane.

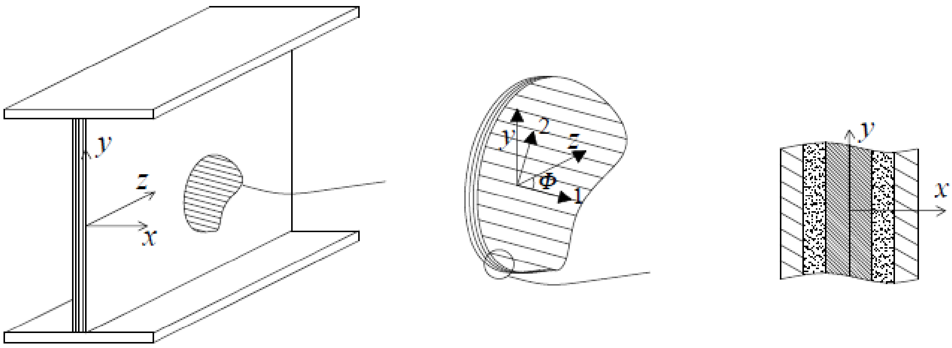

Figure 7.3: Thin-walled beam Composed of Fibre-reinforced Laminates

As one can see in Figure 7.3, the y direction is assumed to be perpendicular to the element thickness so in the web the coordinate system rotates 90 degrees around the x axis. Adopting the assumption of free stress in contour direction $\sigma_x = 0$, Eq. (7.7) will be reduced to

$$\begin{Bmatrix} \sigma_z{}^{(k)} \\ \tau_{zx}{}^{(k)} \end{Bmatrix} = \begin{bmatrix} \overline{Q}_{11}^{(k)*} & \overline{Q}_{16}^{(k)*} \\ \overline{Q}_{16}^{(k)*} & \overline{Q}_{66}^{(k)*} \end{bmatrix} \begin{bmatrix} \varepsilon_z \\ \gamma_{zx} \end{bmatrix} \tag{7.18}$$

in which

$$\overline{Q}_{11}^{(k)*} = \overline{Q}_{11}^{(k)} - \frac{\overline{Q}_{12}^{(k)2}}{\overline{Q}_{22}^{(k)}} \tag{7.19}$$

$$\overline{Q}_{16}^{(k)*} = \overline{Q}_{16}^{(k)} - \frac{\overline{Q}_{12}^{(k)}\overline{Q}_{26}^{(k)}}{\overline{Q}_{22}^{(k)}} \tag{7.20}$$

$$\bar{Q}_{66}^{(k)*} = \bar{Q}_{66}^{(k)} - \frac{\bar{Q}_{26}^{(k)2}}{\bar{Q}_{22}^{(k)}} \tag{7.21}$$

7.6. Stresses and stress resultants

In this section, the stress expressions $\sigma_z^{(k)}$ and $\tau_{zx}^{(k)}$ are obtained in terms of the stress resultants existing throughout the lateral-torsional buckling (M_y, B, V_x, T_ω). Firstly, the relations between stresses and displacements (W, U, V, ϕ) are obtained and then by using the stress resultants-displacements equations, the expressions of stresses in terms of stress resultants are developed.

Based on the developed constitutive relations in section (7.5), the normal stress can be expressed in terms of strains as below:

$$\sigma_z = \bar{Q}_{11}^{(k)*} \varepsilon_z \tag{7.22}$$

By substituting the matrix form of the expression of the longitudinal strains developed in the previous section (Eq. (7.5)) in Eq. (7.22), the longitudinal stress is obtained as

$$\sigma_z = \bar{Q}_{11}^{(k)*} \begin{bmatrix} 1 & -x & -y & -\omega \end{bmatrix} \begin{bmatrix} W' \\ U'' \\ V'' \\ \phi'' \end{bmatrix} \tag{7.23}$$

The shear stress $\tau_{zx}^{(k)}$ which is due to the shear force can be obtained as follows:

The shear force F_s is obtained from the longitudinal equilibrium of the free-body diagram of a piece cut from the beam (Figure 7.4).

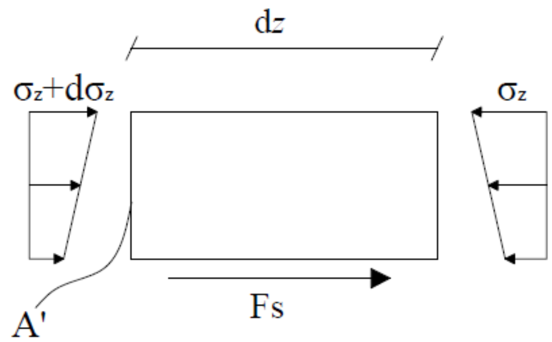

Figure 7.4: Free-body Diagram of a Piece Cut from the beam

$$\mathrm{d}F_s + \int_{A'} (\sigma_z + \mathrm{d}\sigma_z)\mathrm{d}A - \int_{A'} \sigma_z \mathrm{d}A = 0 \tag{7.24}$$

in which A' is the cross-sectional area of the piece cut from the segment $\mathrm{d}z$. Substituting Eq. (7.24) in relation $\tau_{zx} = F_s/(\mathrm{t.d}z)$, the shear stress is calculated

$$\tau_{zx} = \int_{A'} \frac{-\mathrm{d}\sigma_z}{\mathrm{t.d}z}\mathrm{d}A = -\int_{A'} \frac{\sigma_z'}{t}\mathrm{d}A \tag{7.25}$$

in which t is the thickness of the segment. The longitudinal stress obtained in Eq. (7.23) is substituted into the above expressions and the shear stress expression in terms of displacements is obtained.

$$\tau_{zx} = -\frac{1}{t}\int_{A'} \bar{Q}_{11}^{(k)*} \begin{bmatrix} 1 & -x & -y & -\omega \end{bmatrix} \begin{bmatrix} W'' \\ U''' \\ V''' \\ \phi''' \end{bmatrix} \mathrm{d}A = -\frac{1}{t}\begin{bmatrix} \bar{A} & -\bar{S}_y & -\bar{S}_x & -\bar{S}_\omega \end{bmatrix} \begin{bmatrix} W'' \\ U''' \\ V''' \\ \phi''' \end{bmatrix} \tag{7.26}$$

in which $\bar{A} = \int_{A'} \bar{Q}_{11}^{(k)*} \mathrm{d}A$, $\bar{S}_y = \int_{A'} \bar{Q}_{11}^{(k)*} x \mathrm{d}A$, $\bar{S}_x = \int_{A'} \bar{Q}_{11}^{(k)*} y \mathrm{d}A$, $\bar{S}_\omega = \int_{A'} \bar{Q}_{11}^{(k)*} \omega \mathrm{d}A$ is defined.

After obtaining the stress-displacement relationship, the expressions of stresses in terms of stress resultants will be developed.

The stress resultants in terms of stresses are given as

$$N = \int_A \sigma_z \mathrm{d}A \tag{7.27}$$

$$M_x = \int_A \sigma_z \mathrm{y} \mathrm{d}A \tag{7.28}$$

$$M_y = -\int_A \sigma_z x \mathrm{d}A \tag{7.29}$$

$$V_x = \int_A x \frac{\partial \sigma_z}{\partial z} \mathrm{d}A = -\frac{\partial M_y}{\partial z} \tag{7.30}$$

$$V_y = \int_A y \frac{\partial \sigma_z}{\partial z} \mathrm{d}A = \frac{\partial M_x}{\partial z} \tag{7.31}$$

$$B = \int_A \sigma_z \omega \mathrm{d}A \tag{7.32}$$

$$T_\omega = \int_A \omega \frac{\partial \sigma_z}{\partial z} \mathrm{d}A = \frac{\partial B}{\partial z} \tag{7.33}$$

Therefore, using the stress-displacement relationships one can obtain the stress resultant functions in terms of the displacement derivatives.

$$N = \int_A \bar{Q}_{11}^{(k)*} \varepsilon_z \mathrm{d}A = AW' - S_y U'' - S_x V'' - S_\omega \phi'' \tag{7.34}$$

$$M_y = -\int_A \bar{Q}_{11}^{(k)*} \varepsilon_z x \mathrm{d}A = -S_y W' + J_{yy} U'' + J_{xy} V'' + J_{x\omega} \phi'' \tag{7.35}$$

$$M_x = \int_A \bar{Q}_{11}^{(k)*} \varepsilon_z y \mathrm{d}A = S_x W' - J_{xy} U'' - J_{xx} V'' - J_{y\omega} \phi'' \tag{7.36}$$

$$B = \int_A \bar{Q}_{11}^{(k)*} \varepsilon_z \omega \mathrm{d}A = S_\omega W' - J_{\omega x} U'' - J_{\omega y} V'' - J_{\omega\omega} \phi'' \tag{7.37}$$

Eqs. (7.34) to (7.37) are arranged in a matrix form and the resulting system of equations is inverted to develop the expressions for the vector of displacement derivatives in terms of stress resultants.

$$\begin{bmatrix} W' \\ U'' \\ V'' \\ \phi'' \end{bmatrix} = \mathbf{D}^{-1} \begin{bmatrix} N \\ M_y \\ -M_x \\ -B \end{bmatrix} \tag{7.38}$$

in which $\mathbf{D} = \begin{bmatrix} A & -S_y & -S_x & -S_\omega \\ -S_y & J_{yy} & J_{xy} & J_{\omega x} \\ -S_x & J_{xy} & J_{xx} & J_{\omega y} \\ -S_\omega & J_{\omega x} & J_{\omega y} & J_{\omega\omega} \end{bmatrix}$ is given and $A = \int_A \bar{Q}_{11}^{(k)*} \mathrm{d}A$, $S_x = \int_A \bar{Q}_{11}^{(k)*} y \mathrm{d}A$,

$S_y = \int_A \bar{Q}_{11}^{(k)*} x \mathrm{d}A$, $S_\omega = \int_A \bar{Q}_{11}^{(k)*} \omega \mathrm{d}A$, $J_{xx} = \int_A \bar{Q}_{11}^{(k)*} y^2 \mathrm{d}A$, $J_{yy} = \int_A \bar{Q}_{11}^{(k)*} x^2 \mathrm{d}A$, $J_{\omega\omega} = \int_A \bar{Q}_{11}^{(k)*} \omega^2 \mathrm{d}A$,

$J_{xy} = \int_A \bar{Q}_{11}^{(k)*} xy \mathrm{d}A$, $J_{x\omega} = \int_A \bar{Q}_{11}^{(k)*} x\omega \mathrm{d}A$, $J_{y\omega} = \int_A \bar{Q}_{11}^{(k)*} y\omega \mathrm{d}A$ are defined.

Substituting Eq. (7.23) in Eq. (7.38), the expression for stress σ_z in terms of stress resultant function is obtained as

$$\sigma_z = \bar{Q}_{11}^{(k)*} \begin{bmatrix} 1 & -x & -y & -\omega \end{bmatrix} \mathbf{D}^{-1} \begin{bmatrix} N \\ M_y \\ -M_x \\ -B \end{bmatrix} \tag{7.39}$$

Using Eqs. (7.30), (7.31) and (7.33) the shear stress resultants can be obtained in terms of the displacement derivatives as,

$$V_x = S_y W'' - J_{yy} U''' - J_{xy} V''' - J_{x\omega} \phi''' \tag{7.40}$$

$$V_y = S_x W'' - J_{xy} U''' - J_{xx} V''' - J_{y\omega} \phi''' \tag{7.41}$$

$$T_\omega = S_\omega W'' - J_{\omega x} U''' - J_{\omega y} V''' - J_{\omega\omega} \phi''' \tag{7.42}$$

Eqs. (7.40) to (7.42) are written in matrix form and then inverted to develop the displacement vector derivatives in terms of stress resultants:

$$\begin{bmatrix} W'' \\ U''' \\ V''' \\ \phi''' \end{bmatrix} = -\mathbf{D}^{-1} \begin{bmatrix} 0 \\ V_y \\ V_x \\ T_\omega \end{bmatrix} \tag{7.43}$$

Substituting Eq. (7.43) in Eq. (7.26), the shear stress is expressed in terms of shear stress resultant.

$$\tau_{zx} = \frac{1}{t} \begin{bmatrix} \overline{A} & -\overline{S}_y & -\overline{S}_x & -\overline{S}_\omega \end{bmatrix} \mathbf{D}^{-1} \begin{bmatrix} 0 \\ V_x \\ V_y \\ T_\omega \end{bmatrix} \tag{7.44}$$

As explained in section 5.3, throughout buckling the increment of axial force, moments about the major axis and associated shear force acting along the minor axis all vanish ($N = M_x = V_y = 0$). Therefore, the expressions for stresses (Eqs. (7.39) and (7.44)) reduce to

$$\sigma_z^{(k)} = \overline{Q}_{11}^{(k)*} \begin{bmatrix} 1 & -x & -y & -\omega \end{bmatrix} \mathbf{D}^{-1} \begin{bmatrix} 0 \\ M_y \\ 0 \\ -B \end{bmatrix} \tag{7.45}$$

$$\tau_{zx} = \frac{1}{t} \begin{bmatrix} \overline{A} & -\overline{S}_y & -\overline{S}_x & -\overline{S}_\omega \end{bmatrix} \mathbf{D}^{-1} \begin{bmatrix} 0 \\ V_x \\ 0 \\ T_\omega \end{bmatrix} \tag{7.46}$$

On the other hand, the stress component due to St. Venant torsion is

$$\tau_{sv} = \frac{2rT_{sv}}{J_d} \tag{7.47}$$

where J_d is the torsional constant.

7.7. Variational formulation

As comprehensively described in chapter 4, the current hybrid formulation is developed from the potential energy functional by relaxing the strain-displacement equations as auxiliary conditions through the Lagrange Multipliers method.

The total potential energy of the buckled configuration of a system is expressed as the sum of strain energy U and work done by external forces W ,

$$\Pi = U + W \tag{7.48}$$

The strain energy U can be expressed as below

$$U = \frac{1}{2}\int_{V_0} \left(\sigma_z \varepsilon_z + \tau_{zx}\gamma_{zx} + \tau_{sv}\gamma_{sv}\right) \mathrm{d}V \tag{7.49}$$

where V_0 = Volume of the beam.

The work done by external forces W can be written as

$$W = -\frac{1}{2}\int_{V_0} \sigma_z{}^p \left(u'(s,z)^2 + v'(s,z)^2\right) \mathrm{d}V \tag{7.50}$$

Substituting Eqs. (7.1) and (7.2) in Eq. (7.50) we have

$$W = -\frac{1}{2}\int_{V_0} \sigma_z{}^p \left(\left(U' - \left(y - a_y\right)\phi'\right)^2 + \left(x\phi'\right)^2\right) \mathrm{d}V \tag{7.51}$$

Using stress resultant-stress equations (Eqs. (7.27) and (7.28)) Eq. (7.51) will become

$$W = -\frac{1}{2}\int_L \left(N^p U'^2 + N^p a_y{}^2 \phi'^2 - 2M_x^p a_y \phi'^2 - 2M_x^p U'\phi' + 2N^p a_y U'\phi'\right) \mathrm{d}z - \frac{1}{2}\int_L W_{Wagner} \phi'^2 \mathrm{d}z \tag{7.52}$$

where L is the Length of the beam and N^p and M_x^p are the initial axial compressive load and bending moment, respectively. In addition, W_{Wagner} is Wagner stress resultant which is given as $W_{Wagner} = \int_A \sigma_z^p \left(y^2 + x^2\right) dA$ (Trahair 1993b). By using Eq. (7.45) in pre-buckling state, one can obtain

$$W_{Wagner} = \bar{Q}_{11}^{(k)*} \begin{bmatrix} I_p & -I_{py} & -I_{px} & -I_{p\omega} \end{bmatrix} \mathbf{D}^{-1} \begin{bmatrix} N^p \\ 0 \\ -M_x^p \\ 0 \end{bmatrix} \tag{7.53}$$

in which the sectional properties $I_p = \int_A \bar{Q}_{11}^{(k)*} \left(x^2 + y^2\right) \mathrm{d}A$, $I_{py} = \int_A \bar{Q}_{11}^{(k)*} x \left(x^2 + y^2\right) \mathrm{d}A$, $I_{px} = \int_A \bar{Q}_{11}^{(k)*} y \left(x^2 + y^2\right) \mathrm{d}A$, $I_{p\omega} = \int_A \bar{Q}_{11}^{(k)*} \omega \left(x^2 + y^2\right) \mathrm{d}A$ are defined. By defining constants r_{N0}^2 and β_{Nx} as

$$r_{N0}^2 = \begin{bmatrix} I_p & -I_{py} & -I_{px} & -I_{p\omega} \end{bmatrix} \mathbf{D}^{-1} \begin{bmatrix} 1 \\ 0 \\ 0 \\ 0 \end{bmatrix} \tag{7.54}$$

and

$$\beta_{Nx} = \begin{bmatrix} I_p & -I_{py} & -I_{px} & -I_{p\omega} \end{bmatrix} \mathbf{D}^{-1} \begin{bmatrix} 0 \\ 0 \\ -1 \\ 0 \end{bmatrix} - 2a_y \tag{7.55}$$

The Wagner stress resultant for mono-symmetric cross-sections in terms of stress resultant (at pre-buckling state) can be expressed as

$$W_{Wagner} = N^p r_{N0}^2 + M_x^p \left(\beta_{Nx} + 2a_y\right) \tag{7.56}$$

Therefore, the work done by the external forces (Eq. (7.52)) can be written as

$$W = -\frac{1}{2}\int_L \left(U'^2 N^p + 2U'\phi'\left(-M_x{}^p + N^p a_y\right) + \phi'^2\left(r_{N0}^2 + a_y{}^2\right)N^p + \phi'^2 \beta_{Nx} M_x{}^p\right)\mathrm{d}z \tag{7.57}$$

In here, the axillary conditions are the conditions of compatibility (the strain-displacement equations), which can be written as follows:

$$\varepsilon_z + x(s)U''(z) + \phi''(z)\omega(s) = 0 \tag{7.58}$$

$$\gamma_{zx} = 0 \tag{7.59}$$

These conditions are introduced to the total potential energy expression through the Lagrange Multipliers method.

$$\Pi_{II} = U + W - \int_{V_0} \beta_1(\varepsilon_z + xU'' + \omega\phi'')\mathrm{d}V - \int_{V_0} \beta_2(\gamma_{zx})\mathrm{d}V - \int_{V_0} \beta_3(\gamma_{sv} - \frac{\tau_{sv}}{Q_{66}^{(k)}})\mathrm{d}V \tag{7.60}$$

in which β_1 , β_2 and β_3 are the Lagrange Multipliers.

From the variations of the functional Π_{II} with respect to the strains one obtains

$$\frac{\partial U_d}{\partial \varepsilon_x} - \beta_1 = 0 \tag{7.61}$$

$$\frac{\partial U_d}{\partial \gamma_{zy}} - \beta_2 = 0 \tag{7.62}$$

$$\frac{\partial U_d}{\partial \gamma_{sv}} - \beta_3 = 0 \tag{7.63}$$

where U_d is the internal strain energy density and is defined as $U = \int_{V_0} U_d \mathrm{d}V$. Eqs. (7.61) to (7.63) show that β_1 , β_2 and β_3 are the energy conjugates of the strains ε_x, γ_{zx} and γ_{sv}, respectively. Therefore, they can be replaced with stresses σ_x , τ_{zx} and τ_{sv} in Eq. (7.60), i.e.

$$\Pi_{II} = U + W - \int_{V_0} \sigma_z(\varepsilon_z + xU'' + \omega\phi'')\mathrm{d}V - \int_{V_0} \tau_{zx}(\gamma_{zx})\mathrm{d}V - \int_{V_0} \tau_{sv}(\gamma_{sv} - \frac{\tau_{sv}}{Q_{66}^{(k)}})\mathrm{d}V \tag{7.64}$$

By substituting Eqs. (7.49) and (7.57) in Eq. (7.64) it will become

$$\begin{aligned}\Pi_{II} = &-\frac{1}{2}\int_{V_0}\left(\sigma_z\varepsilon_z + \tau_{zx}\gamma_{zx} + \tau_{sv}\gamma_{sv}\right)\mathrm{d}V - \int_{V_0}\sigma_z(xU'' + \omega\phi'')\mathrm{d}V + \int_{V_0}\tau_{sv}(\frac{\tau_{sv}}{Q_{66}^{(k)}})\mathrm{d}V \\ &-\frac{1}{2}\int_L\left(U'^2N^p + 2U'\phi'\left(-M_x{}^p + N^p a_y\right) + \phi'^2\left(r_{N0}^2 + a_y{}^2\right)N^p + \phi'^2\beta_{Nx}M_x{}^p\right)\mathrm{d}z\end{aligned} \tag{7.65}$$

Substituting the inverse of the constitutive relations for composite laminates and using Eqs. (7.29) and (7.32), the hybrid functional Π_{III} can be expressed as

$$\begin{aligned}\Pi_{III} = &-\frac{1}{2}\int_{V_0}\left(\begin{bmatrix}\sigma_z{}^{(k)} & \tau_{zx}{}^{(k)}\end{bmatrix}\begin{bmatrix}\bar{Q}_{11}^{(k)*} & \bar{Q}_{16}^{(k)*} \\ \bar{Q}_{16}^{(k)*} & \bar{Q}_{66}^{(k)*}\end{bmatrix}^{-1}\begin{bmatrix}\sigma_z{}^{(k)} \\ \tau_{zx}{}^{(k)}\end{bmatrix} + \tau_{sv}\gamma_{sv}\right)\mathrm{d}V \\ &-\int_L\left(M_yU'' + B\phi''\right)\mathrm{d}z + \int_L T_{sv}\phi'\mathrm{d}z \\ &-\frac{1}{2}\int_L\left(U'^2N^p + 2U'\phi'\left(-M_x{}^p + N^p a_y\right) + \phi'^2\left(r_{N0}^2 + a_y{}^2\right)N^p + \phi'^2\beta_{Nx}M_x{}^p\right)\mathrm{d}z\end{aligned} \tag{7.66}$$

By using Eqs. (7.45), (7.46) and (7.47), the final form of hybrid formulation, Π_{III}, in the buckled state is obtained

$$\Pi_{III} = -\frac{1}{2}\left(\int_L\left(\begin{bmatrix} M_y & B \end{bmatrix}\mathbf{D}_b^{-1}\begin{bmatrix} M_y \\ B \end{bmatrix} + \begin{bmatrix} M_y & B \end{bmatrix}\boldsymbol{\psi}_b^{-1}\begin{bmatrix} V_x \\ T_\omega \end{bmatrix} + \begin{bmatrix} V_x & T_\omega \end{bmatrix}\boldsymbol{\chi}_b^{-1}\begin{bmatrix} V_x \\ T_\omega \end{bmatrix}\right)\mathrm{d}z\right)$$
$$-\frac{1}{2}\int_L \frac{T_{sv}^{\ 2}}{Q_{66}^{(k)} J_d}\mathrm{d}z - \int_L \left(M_y U'' + B\phi''\right)\mathrm{d}z + \int_L T_{sv}\phi'\mathrm{d}z \tag{7.67}$$
$$-\frac{1}{2}\int_L\left(U'^2 N^p + 2U'\phi'\left(-M_x^{\ p} + N^p a_y\right) + \phi'^2\left(r_{N0}^2 + a_y^{\ 2}\right)N^p + \phi'^2\beta_{Nx}M_x^{\ p}\right)\mathrm{d}z$$

in which $\mathbf{D}_b^{-1} = \left(\int_A \frac{\bar{Q}_{66}^{(k)*}\bar{Q}_{11}^{(k)*}}{\bar{Q}_{11}^{(k)*}\bar{Q}_{66}^{(k)*} - \bar{Q}_{16}^{(k)*2}}\mathrm{d}A\right)\begin{bmatrix} 0 & 1 & 0 & 0 \\ 0 & 0 & 0 & -1 \end{bmatrix}\mathbf{D}^{-1}\begin{bmatrix} 0 & 0 \\ 1 & 0 \\ 0 & 0 \\ 0 & -1 \end{bmatrix}$,

$$\boldsymbol{\chi}_b^{-1} = \begin{bmatrix} 0 & 1 & 0 & 0 \\ 0 & 0 & 0 & 1 \end{bmatrix}\mathbf{D}^{-1}\int_A \frac{1}{t^2}\frac{\bar{Q}_{11}^{(k)*}}{\bar{Q}_{11}^{(k)*}\bar{Q}_{66}^{(k)*} - \bar{Q}_{16}^{(k)*2}}\begin{bmatrix} \bar{A}^2 & -\bar{A}\bar{S}_y & -\bar{A}\bar{S}_x & -\bar{A}\bar{S}_\omega \\ -\bar{A}\bar{S}_y & \bar{S}_y^{\ 2} & \bar{S}_y\bar{S}_x & \bar{S}_y\bar{S}_\omega \\ -\bar{A}\bar{S}_x & \bar{S}_y\bar{S}_x & \bar{S}_x^{\ 2} & \bar{S}_x\bar{S}_\omega \\ -\bar{A}\bar{S}_\omega & \bar{S}_y\bar{S}_\omega & \bar{S}_x\bar{S}_\omega & \bar{S}_\omega^{\ 2} \end{bmatrix}\mathrm{dA}\mathbf{D}^{-1}\begin{bmatrix} 0 & 0 \\ 1 & 0 \\ 0 & 0 \\ 0 & 1 \end{bmatrix}$$

and

$$\boldsymbol{\psi}_b^{-1} = \begin{bmatrix} 0 & 1 & 0 & 0 \\ 0 & 0 & 0 & -1 \end{bmatrix}\mathbf{D}^{-1}\int_A \frac{1}{t}\frac{-2\bar{Q}_{16}^{(k)*}\bar{Q}_{11}^{(k)*}}{\bar{Q}_{11}^{(k)*}\bar{Q}_{66}^{(k)*} - \bar{Q}_{16}^{(k)*2}}\begin{bmatrix} \bar{A} & -\bar{S}_y & -\bar{S}_x & -\bar{S}_\omega \\ -x\bar{A} & x\bar{S}_y & x\bar{S}_x & x\bar{S}_\omega \\ -y\bar{A} & y\bar{S}_y & y\bar{S}_x & y\bar{S}_\omega \\ -\omega\bar{A} & \omega\bar{S}_y & \omega\bar{S}_x & \omega\bar{S}_\omega \end{bmatrix}\mathrm{dA}\mathbf{D}^{-1}\begin{bmatrix} 0 & 0 \\ 1 & 0 \\ 0 & 0 \\ 0 & 1 \end{bmatrix}$$

are defined.

7.8. Finite element formulation

7.8.1. Interpolation of the stress resultants and displacement fields

In this section the assumed interpolation for the variables in the hybrid functional (stress resultants M_y, B and T_{sv}, the lateral displacement U and angle of twist ϕ) are introduced.

For an element i with a span of L, the internal stress resultants are assumed as linear bending moment and bimoment and constant St. Venant torsion, i.e.

$$M_y(z) = \mathbf{L}(z)^T \mathbf{M}_{yi} \tag{7.68}$$

$$B(z) = \mathbf{L}(z)^T \mathbf{B}_i \tag{7.69}$$

$$T_{sv}(z) = T_{svi} \tag{7.70}$$

in which $\mathbf{L}(z)^{\mathrm{T}} = \langle (1-z/L) \quad z/L \rangle$ and $\mathbf{M}_{yi}{}^{\mathbf{T}} = \langle M_{yi}(0) \quad M_{yi}(L) \rangle$ and $B_i^{\mathbf{T}} = \langle B_i(0) \quad B_i(L) \rangle$.

A set of the interpolation function based on cubic polynomials is assumed for lateral displacement and angle of twist, i.e.

$$u_i = \mathbf{N}(z)^{\mathbf{T}} \mathbf{u}_i \tag{7.71}$$

$$\phi_i = \mathbf{N}(z)^{\mathbf{T}} \boldsymbol{\varphi}_i \tag{7.72}$$

where

$\mathbf{N}(z)^{\mathrm{T}} = \langle (1-3z^2/L^2+2z^3/L^3) \quad (z-2z^2/L+z^3/L^2) \quad (3z^2/L^2-2z^3/L^3) \quad (-z^2/L+z^3/L^2) \rangle$, $\mathbf{u}_i{}^{\mathbf{T}} = \langle u_i(0) \quad u_i'(0) \quad u_i(L) \quad u_i'(L) \rangle$ and $\boldsymbol{\varphi}_i{}^{\mathbf{T}} = \langle \phi_i(0) \quad \phi_i'(0) \quad \phi_i(L) \quad \phi_i'(L) \rangle$ are defined.

7.8.2. Discretised form of the hybrid functional for buckling analysis

By substituting Eqs. (7.68) to (7.72) in Eq. (7.67), the discretised form of hybrid functional for buckling analysis can be written as

$$
\Pi_{II}=\int_L\left(\begin{array}{l}
-\frac{1}{2}\left\langle \mathbf{M}_{yi}{}^{\mathbf{T}} \quad \mathbf{B}_i{}^{\mathbf{T}}\right\rangle\begin{bmatrix}\mathbf{L} & 0\\ 0 & \mathbf{L}\end{bmatrix}\mathbf{D}_b{}^{-1}\begin{bmatrix}\mathbf{L}^{\mathbf{T}} & 0\\ 0 & \mathbf{L}^{\mathbf{T}}\end{bmatrix}\begin{Bmatrix}\mathbf{M}_{yi}{}^{\mathbf{T}}\\ \mathbf{B}_i{}^{\mathbf{T}}\end{Bmatrix}\\
-\left\langle \mathbf{M}_{yi}{}^{\mathbf{T}} \quad \mathbf{B}_i{}^{\mathbf{T}}\right\rangle\begin{bmatrix}\mathbf{L} & 0\\ 0 & \mathbf{L}\end{bmatrix}\boldsymbol{\psi}_b^{-1}\begin{bmatrix}\mathbf{L}'^{\mathbf{T}} & 0\\ 0 & \mathbf{L}'^{\mathbf{T}}\end{bmatrix}\begin{Bmatrix}\mathbf{M}_{yi}{}^{\mathbf{T}}\\ \mathbf{B}_i{}^{\mathbf{T}}\end{Bmatrix}\\
-\frac{1}{2}\left\langle \mathbf{M}_{yi}{}^{\mathbf{T}} \quad \mathbf{B}_i{}^{\mathbf{T}}\right\rangle\begin{bmatrix}\mathbf{L}' & 0\\ 0 & \mathbf{L}'\end{bmatrix}\boldsymbol{\chi}_b^{-1}\begin{bmatrix}\mathbf{L}'^{\mathbf{T}} & 0\\ 0 & \mathbf{L}'^{\mathbf{T}}\end{bmatrix}\begin{Bmatrix}\mathbf{M}_{yi}{}^{\mathbf{T}}\\ \mathbf{B}_i{}^{\mathbf{T}}\end{Bmatrix}-\frac{1}{2}\frac{T_{sv}{}^2}{\bar{Q}_{66}^{(k)*}J_d}\\
-\frac{1}{2}\lambda N^p\mathbf{u}_i^{\mathbf{T}}\mathbf{N}'\mathbf{N}'^{\mathbf{T}}\mathbf{u}_i+\lambda\left(M_x{}^p-a_yN^p\right)\mathbf{u}_i^{\mathbf{T}}\mathbf{N}'\mathbf{N}'^{\mathbf{T}}\boldsymbol{\varphi}_i\\
-\frac{1}{2}\lambda\left(r_{N0}^2+a_y{}^2\right)N^p\boldsymbol{\varphi}_i^{\mathbf{T}}\mathbf{N}'\mathbf{N}'^{\mathbf{T}}\boldsymbol{\varphi}_i-\frac{1}{2}\lambda\beta_{Nx}M_x{}^p\boldsymbol{\varphi}_i^{\mathbf{T}}\mathbf{N}'\mathbf{N}'^{\mathbf{T}}\boldsymbol{\varphi}_i\\
-\mathbf{M}_{yi}{}^{\mathbf{T}}\mathbf{L}\mathbf{N}''^{\mathbf{T}}\mathbf{u}_i-\mathbf{B}_i{}^{\mathbf{T}}\mathbf{L}\mathbf{N}''^{\mathbf{T}}\boldsymbol{\varphi}_i+T_{sv}\mathbf{N}'^{\mathbf{T}}\boldsymbol{\varphi}_i
\end{array}\right)\mathrm{d}z \tag{7.73}
$$

The developed functional depends on unknowns $\mathbf{M}_{yi}$ and $\mathbf{B}_i$. By applying the partial stationary condition with respect to the unknowns ($\partial\Pi_{\mathrm{III}}/\partial\mathbf{M}_{yi}=0$, $\partial\Pi_{\mathrm{III}}/\partial\mathbf{B}_i=0$ and $\partial\Pi_{\mathrm{III}}/\partial T_{svi}=0$), one obtains

$$
\begin{Bmatrix}\mathbf{M}_{yi}\\ \mathbf{B}_i\\ T_{svi}\end{Bmatrix}=\mathbf{H}_b\mathbf{G}_b\begin{Bmatrix}\mathbf{u}_i\\ \boldsymbol{\varphi}_i\end{Bmatrix} \tag{7.74}
$$

where

$$
\mathbf{H}_b=\left\{\begin{array}{l}
\int_L\begin{bmatrix}\mathbf{L} & \mathbf{0} & \mathbf{0}\\ \mathbf{0} & \mathbf{L} & \mathbf{0}\\ 0 & 0 & 1\end{bmatrix}\begin{bmatrix}\mathbf{D}_b{}^{-1} & \mathbf{0}\\ \mathbf{0} & \dfrac{1}{\bar{Q}_{66}^{(k)*}J_d}\end{bmatrix}\begin{bmatrix}\mathbf{L}^{\mathbf{T}} & \mathbf{0} & \mathbf{0}\\ \mathbf{0} & \mathbf{L}^{\mathbf{T}} & \mathbf{0}\\ 0 & 0 & 1\end{bmatrix}+\begin{bmatrix}\mathbf{L} & \mathbf{0}\\ \mathbf{0} & \mathbf{L}\\ 0 & 0\end{bmatrix}\psi_b^{-1}\begin{bmatrix}\mathbf{L}'^{\mathbf{T}} & \mathbf{0} & 0\\ \mathbf{0} & \mathbf{L}'^{\mathbf{T}} & 0\end{bmatrix}\\
+\begin{bmatrix}\mathbf{L}' & \mathbf{0}\\ \mathbf{0} & \mathbf{L}'\\ 0 & 0\end{bmatrix}\boldsymbol{\chi}_b^{-1}\begin{bmatrix}\mathbf{L}'^{\mathbf{T}} & \mathbf{0} & 0\\ \mathbf{0} & \mathbf{L}'^{\mathbf{T}} & 0\end{bmatrix}\mathrm{d}z
\end{array}\right\}^{-1} \tag{7.75}
$$

and

$$\mathbf{G}_b = \begin{bmatrix} \int_L \mathbf{L}\mathbf{N}''^{\mathbf{T}} \mathrm{d}z & 0 \\ 0 & \int_L \mathbf{L}\mathbf{N}''^{\mathbf{T}} \mathrm{d}z \\ 0 & \int_L \mathbf{N}'^{\mathbf{T}} \mathrm{d}z \end{bmatrix} \tag{7.76}$$

It should be noted that the stationary condition with respect to the stress resultant parameters can be written at the element level. This is due to the relaxation of inter-element equilibrium as a result of which the nodal stress resultant parameters are not coupled between the elements. By using Eq. (7.74), Eq. (7.73) can be written as

$$\begin{aligned} \Pi_{III} &= \sum_{i=1}^{N} \int_L \left(-\frac{1}{2} \left\langle \mathbf{u}_i^{\mathbf{T}} \quad \boldsymbol{\varphi}_i^{\mathbf{T}} \right\rangle \mathbf{G}_b^{\,T} \mathbf{H}_b \mathbf{G}_b \begin{Bmatrix} \mathbf{u}_i \\ \boldsymbol{\varphi}_i \end{Bmatrix} \right) \mathrm{d}z \\ &-\frac{1}{2} \lambda \sum_{i=1}^{N} \int_L \left\langle \mathbf{u}_i^{\mathbf{T}} \quad \boldsymbol{\varphi}_i^{\mathbf{T}} \right\rangle \begin{bmatrix} N^p \mathbf{N}'\mathbf{N}'^{\mathbf{T}} & \left(-M_x^{\ p} + a_y N^p\right) \mathbf{N}'\mathbf{N}'^{\mathbf{T}} \\ \left(-M_x^{\ p} + a_y N^p\right) \mathbf{N}'\mathbf{N}'^{\mathbf{T}} & \left(\left(r_{N0}^2 + a_y^{\ 2}\right) N^p + \beta_{Nx} M_x^{\ p}\right) \mathbf{N}'\mathbf{N}'^{\mathbf{T}} \end{bmatrix} \begin{Bmatrix} \mathbf{u}_i \\ \boldsymbol{\varphi}_i \end{Bmatrix} \mathrm{d}z \end{aligned} \tag{7.77}$$

From the stationary condition with respect to $\mathbf{u}_i$ and $\boldsymbol{\varphi}_i$, i.e. $\partial\Pi_{\mathrm{III}}/\partial\mathbf{u}_i = 0$, $\partial\Pi_{\mathrm{III}}/\partial\boldsymbol{\varphi}_i = 0$ the discretised equilibrium equations of the system can be obtained as

$$\sum_{i=1}^{N} \left[\mathbf{K}_{bi} - \lambda \mathbf{K}_{gi} \right] \begin{Bmatrix} \mathbf{u}_i \\ \boldsymbol{\varphi}_i \end{Bmatrix} = 0 \tag{7.78}$$

in which $\mathbf{K}_{bi}$ is the element stiffness matrix for buckling analysis and $\mathbf{K}_{gi}$ is the element geometric stiffness matrix.

7.9. Numerical examples

7.9.1. A simply-supported doubly-symmetric I-beam subjected to uniform bending moment

In this example, a simply-supported thin-walled composite beam with doubly-symmetric I-section subjected to a uniform bending moment is studied. In addition, the buckling analysis of beam ignoring the shear deformation effects is performed in this example to illustrate the importance of shear deformations in the predicted values of critical buckling load.

The element is assumed to be made of graphite-epoxy (AS4/3501) with the following material properties:

$$E_1 = 144MPa, \quad E_2 = 9.65MPa$$
$$G_{12} = G_{13} = 4.14MPa$$
$$\upsilon_{12} = 0.3$$

The subscript 1 corresponds to the direction parallel to fibre orientation and subscripts 2 and 3 are related to the directions perpendicular to it.

The boundary condition, loading and cross-sectional dimensions of the beam are illustrated in Figure 7.5.

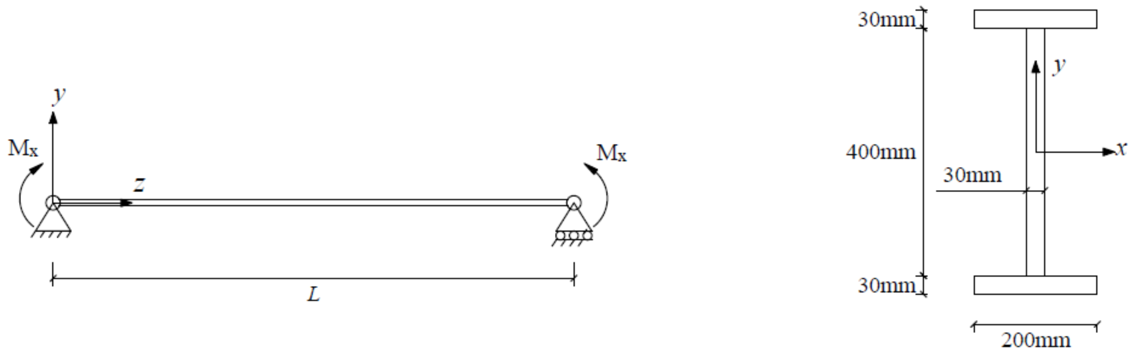

Figure 7.5: The simply-supported beam with the Cross-sectional dimensions

The web and flanges are laminated symmetrically with respect to the mid-plane and consist of 4 layers with equal thickness of 7.5 mm. The buckling analysis is performed for various beam spans from 2 m to 6 m and three different stacking sequences.

The values of the buckling moments obtained by the current model for two different lay-ups are compared with the shell model. The shell element used in the current study is a 4-node element with 6 degrees of freedom for each node.

Based on Discrete Kirchhoff Quadrilateral (DKQ) according to Batoz and Tahar (1982), the plate bending component of the element is formulated. In this method, the element is developed based on the Kirchhoff's classical theory for thin plates in which the shear deformation effects across the thickness of the plate element are assumed to be negligible. The degrees of freedom of DKQ include the vertical displacement (w_{sh}) of nodes in addition to two bending rotations ($\theta_{x,sh}$) and ($\theta_{y,sh}$).

Based on the model proposed by Ibrahimbegovic *et al.* (1990), the membrane component of the element is produced. In this model, the rotation around the out-of-plane axis, $\theta_{z,sh}$ (i.e. drilling degrees of freedom) is employed. Therefore, the degrees of freedom associated with the membrane component of the element consist of two displacements in two directions along the plate, u_{sh} and v_{sh}, and drilling rotation $\theta_{z,sh}$. Therefore, there are 6 degrees of freedom in total for the shell element. (Figure 7.6)

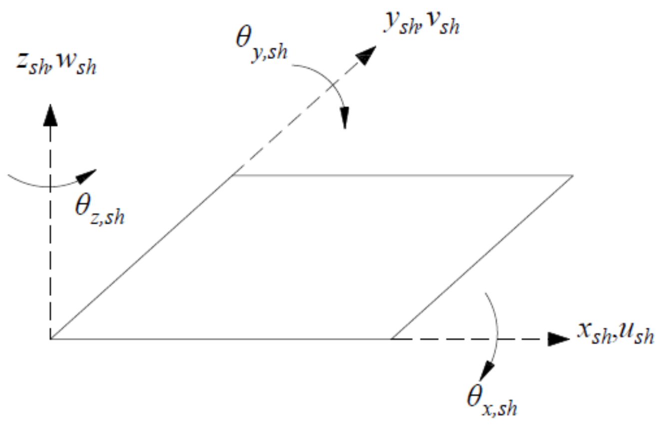

Figure 7.6: Shell element degrees of freedom

7.9.1.1. Results and discussions

The beam is modelled efficiently by using six elements. The predicted buckling moments by the hybrid method (both shear deformable and non-shear deformable) are presented and compared with the results obtained by the shell model in Figure 7.7 and Figure 7.8.

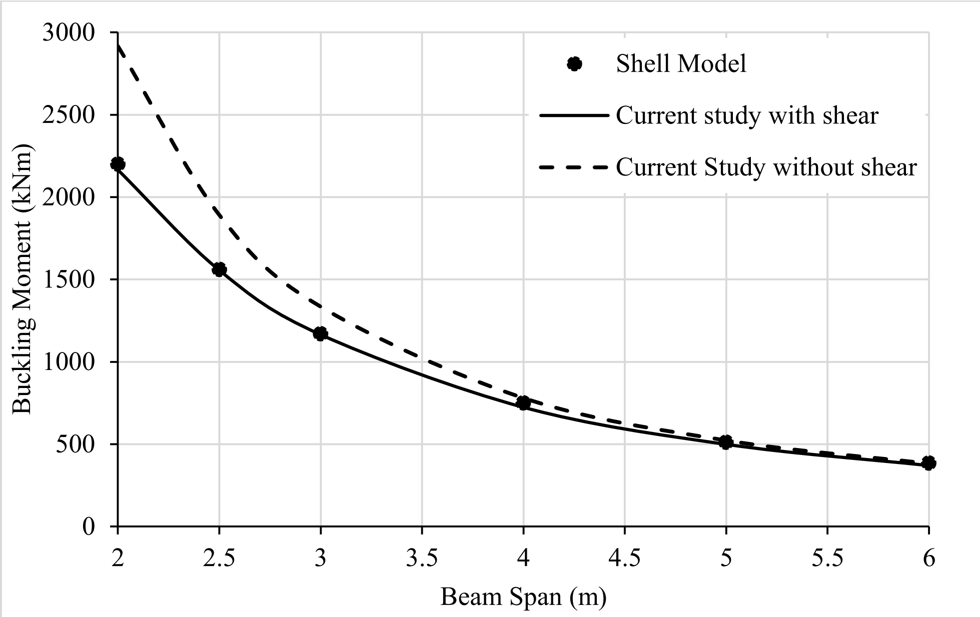

Figure 7.7: The buckling moment (kNm) for [0,0,0,0] stacking sequence

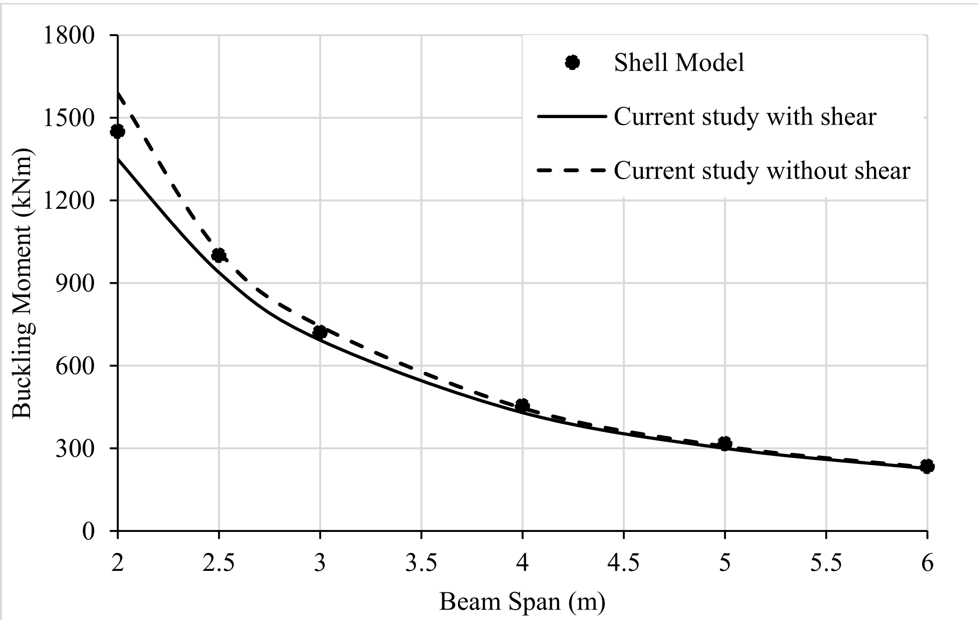

Figure 7.8: The buckling moment (kNm) for [0,90,90,0] stacking sequence

The following conclusions can be made from the analysis results:

1. From Figure 7.7 and Figure 7.8 we can observe that the predicted buckling moment by shear-deformable hybrid finite element model is in a good agreement with the results obtained by the shell model.
2. In addition, the noticeable difference between the buckling moments obtained from the analyses with and without the shear deformations shows the importance of considering the effect of shear deformations in the buckling analysis of a composite thin-walled member. This effect becomes more considerable by decreasing the length of the beam.
3. As the length of the beam increases the critical buckling moment decreases. It confirms the direct relation of the value of the buckling moment to the beam slenderness.

7.9.2. A simply-supported mono-symmetric I-beam subjected to uniform bending moment

In this example, the capability of the current hybrid finite element method in capturing the buckling behaviour of laminate composite cross-sections with mono-symmetric cross-sections is illustrated.

The element is assumed to be made of glass-epoxy with the following material properties:

$$E_1 = 53.78MPa, \quad E_2 = 17.93MPa$$
$$G_{12} = G_{13} = 8.96MPa$$
$$\upsilon_{12} = 0.25$$

The subscript 1 corresponds to the direction parallel to fibre orientation and subscripts 2 and 3 are related to the directions perpendicular to it.

The beam has an I-shape mono-symmetric cross-section and is subjected to a uniform bending moment. The beam length, boundary conditions and the cross-sectional dimensions are illustrated in Figure 7.9.

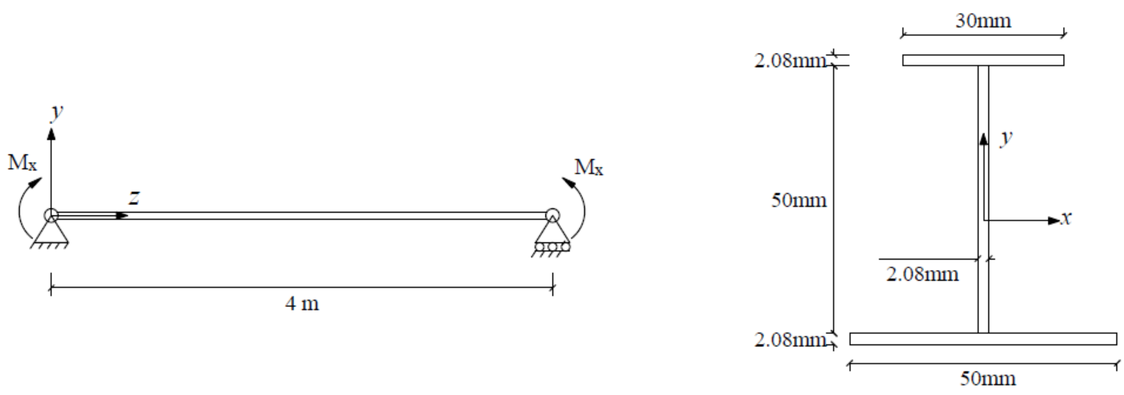

Figure 7.9: The simply-supported beam with the Cross-sectional dimensions

The web and flanges are laminated symmetrically with respect to the mid-plane and consist of 16 layers with equal thickness. The buckling analysis is performed for various lay-ups in the web and flanges.

The values of the buckling moments obtained by the current model are compared with the numerical method developed by Kim *et al.* (2007).

7.9.2.1. Results and discussions

The beam is modelled in here by using nine elements. The predicted buckling loads from the hybrid method are presented and compared with the results from Kim *et al.* (2007) along with the differences percentage in Table 7.1. In the numerical method of Kim et al. (2007) which is developed based on the energy functional, the element stiffness matrix for lateral buckling analysis of thin-walled composite I- and channel-section beams subjected to end moments is evaluated exactly.

Table 7.1: Buckling moments of beam (N.m)

Lay-up	Current study	(Kim *et al.* 2007)	Differences (%)
$\left[0^o\right]_{16}$	47.282	46.737	1.2
$\left[15^o/\text{-}15^o\right]_{4s}$	47.715	49.337	3.3
$\left[45^o/\text{-}45^o\right]_{4s}$	46.564	45.421	2.5
$\left[75^o/\text{-}75^o\right]_{4s}$	30.189	31.655	4.6
$\left[0^o/90^o\right]_{4s}$	39.463	38.437	2.7
$\left[0^o/-45^o/90^o/45^o\right]_{2s}$	40.866	42.508	3.9

It can be observed from Table 7.1 that the values of buckling moment obtained by the current hybrid method are in a good agreement with the values from Kim *et al.* (2007). Therefore, the accuracy and efficiency of the hybrid finite element method for lateral buckling behaviour of thin-walled fibre-reinforced laminate composite beams with mono-symmetric cross-sections are verified.

7.9.3. A cantilever beam with mono-symmetric I beam subjected to end bending moment

In this example, a cantilever thin-walled composite beam with mono-symmetric cross-section subjected to an end bending moment and various stacking sequences is studied. (Figure 7.10)

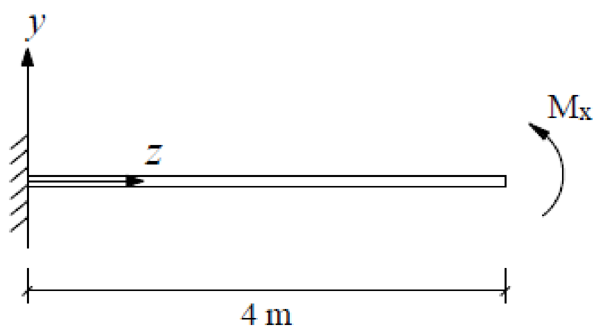

Figure 7.10: The cantilever beam under the bending moment

The material properties of the element and the beam length and cross-sectional dimensions are the same as the ones given in section 7.9.2.

The web and flanges are laminated symmetrically with respect to the mid-plane and consist of 16 layers with equal thickness. The buckling analysis is performed for various lay-ups in the web and flanges. The values of the buckling moments obtained by the current model are compared with the ABAQUS FEA shell element model.

7.9.3.1. Results and discussions

The beam is modelled in here by using nine elements. The predicted buckling loads from the hybrid method are presented and compared with the results from the ABAQUS FEA shell element model in Table 7.2.

Table 7.2: Buckling moments of beam (N.m)

Lay-up	Current study	ABAQUS
$\left[0^o\right]_{16}$	25.497	24.673
$\left[15^o / \text{-}15^o\right]_{4s}$	25.464	25.877
$\left[30^o / \text{-}30^o\right]_{4s}$	24.148	26.068
$\left[45^o / \text{-}45^o\right]_{4s}$	21.103	23.24
$\left[60^o / \text{-}60^o\right]_{4s}$	17.979	19.632
$\left[75^o / \text{-}75^o\right]_{4s}$	15.967	16.388
$\left[0^o / 90^o\right]_{4s}$	21.161	20.555
$\left[0^o / -45^o / 90^o / 45^o\right]_{2s}$	21.712	22.054

From Table 7.2, one can conclude that the values of buckling moment obtained by the current hybrid method are in an acceptable agreement with the values from ABAQUS shell element model.

7.9.4. A simply-supported doubly-symmetric I-section subjected to uniform bending moment (effect of beam length)

A simply-supported thin-walled laminate composite I-beam with various stacking sequences is studied in this example in order to verify the capability of the current hybrid model in capturing the behaviour of composite elements with different lay-ups. In addition, the effect of beam length on the lateral buckling load of thin-walled composite beams is shown in this example.

The element is assumed to be made of graphite-epoxy (AS4/3501) with the following material properties:

$$E_1 = 144MPa, \quad E_2 = 9.65MPa$$
$$G_{12} = G_{13} = 4.14MPa$$
$$\upsilon_{12} = 0.3$$

The subscript 1 corresponds to the direction parallel to fibre orientation and subscripts 2 and 3 are related to the directions perpendicular to it.

The beam length, boundary and loading conditions and the cross-sectional dimensions of the beam are illustrated in Figure 7.11.

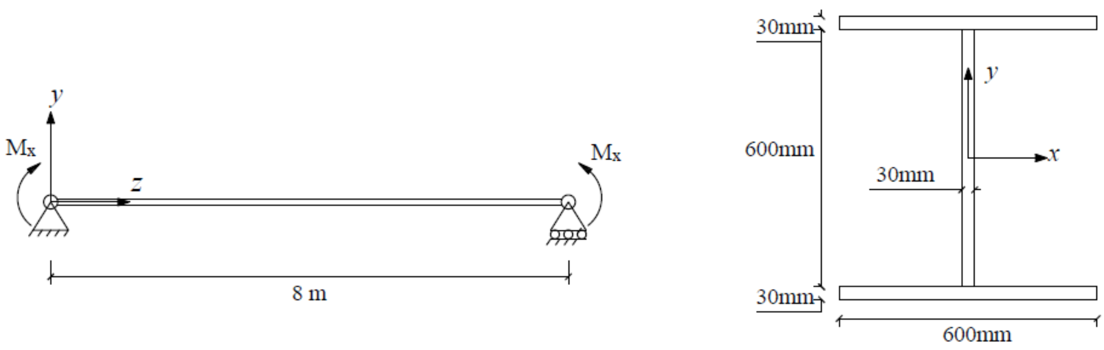

Figure 7.11: The simply-supported beam with the Cross-sectional dimensions

The web and flanges are laminated symmetrically with respect to the mid-plane and consist of 4 layers with equal thickness of 7.5 mm. The stacking sequences for the FRP laminate composite studied in this example are $[0,0,0,0]$ and $[0,90,90,0]$.

The values of the buckling moments obtained by the current model are compared with the results obtained by the shear-deformable linear buckling analysis developed by Machado and Cortínez (2005). In addition, by performing the lateral buckling analysis for various beam spans from 6 m to 12 m the effect of beam length on the lateral buckling load of thin-walled composite beams is shown.

7.9.4.1. Results and discussions

The beam is modelled efficiently by using six elements. The predicted buckling moments by the current hybrid method for the beam span equal to 8 m for the lay-ups $[0,0,0,0]$ and $[0,90,90,0]$ are presented and compared with the results obtained by the shear-deformable linear buckling analysis of Machado and Cortínez (2005) in Table 7.3.

Table 7.3: Buckling moments of beam (MN.m)

Lay-up	Current study	Machado and Cortínez (2005)	Differences (%)
$[0,0,0,0]$	6.6	6.9	4.3
$[0,90,90,0]$	3.9	3.8	2.6

Additionally, in order to show the effect of beam length on the lateral-torsional buckling of a thin-walled composite beam the values of buckling moments versus the beam span for stacking sequences $\left[0,0,0,0\right]$ and $\left[0,90,90,0\right]$ are presented in Figure 7.12 and Figure 7.13, respectively.

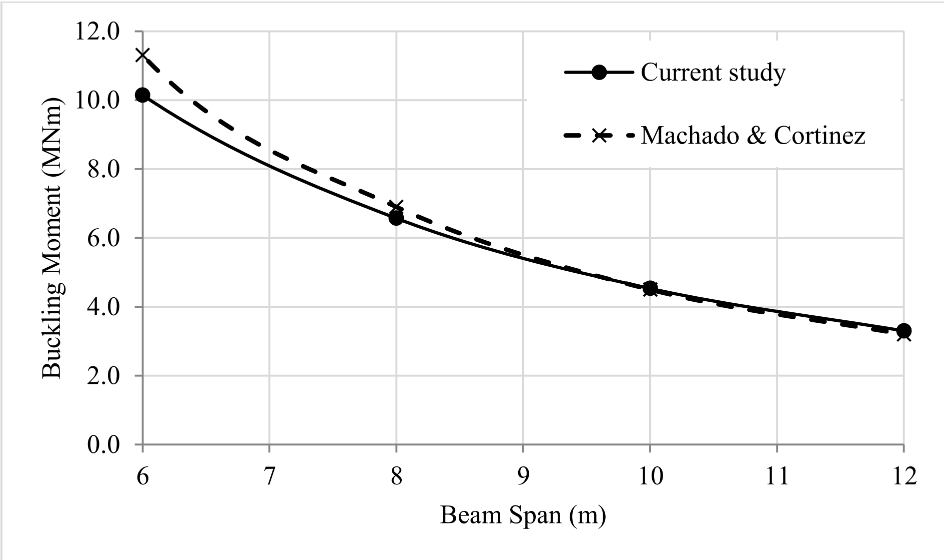

Figure 7.12: The buckling moment (MNm) for [0,0,0,0] stacking sequence

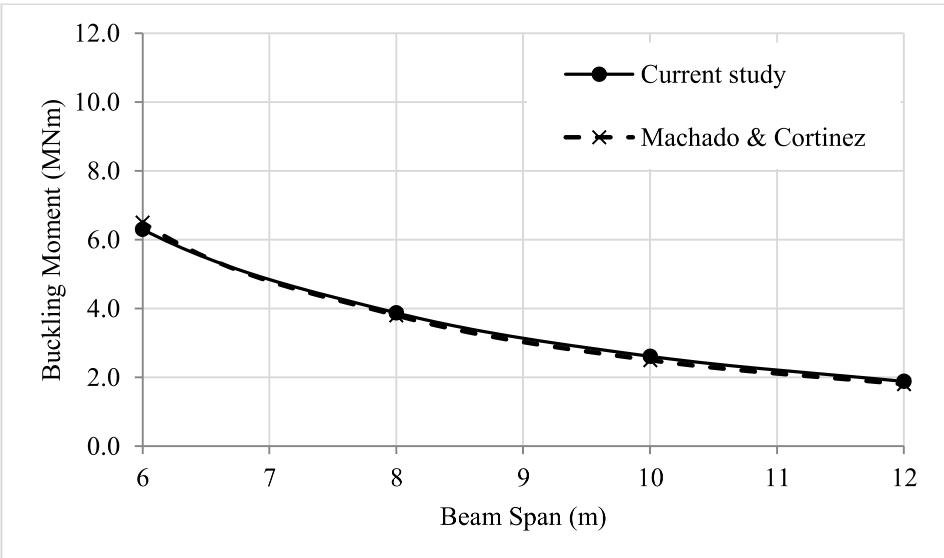

Figure 7.13: The buckling moment (MNm) for [0,90,90,0] stacking sequence

The following conclusions can be made from the analysis results:

1. From Table 7.3 we can observe that the predicted buckling moment from the shear-deformable hybrid finite element model is in an excellent agreement with the results obtained by Machado and Cortínez (2005) model.
2. From Figure 7.12 and Figure 7.13, we can see that as the length of the beam increases the critical lateral-torsional buckling moment decreases. It shows the direct effect of the beam slenderness on the value of the buckling moment of the beam.

7.9.5. A channel-section with various boundary conditions subjected to end moment

In this example, the validity of the current hybrid method for the lateral-torsional buckling of a thin-walled laminate composite beam with channel cross-section is verified. The buckling analysis is performed for various stacking sequences of laminate composite. The element is assumed to be made of glass-epoxy with the following material properties:

$$E_1 = 53.78MPa, \quad E_2 = 17.93MPa$$
$$G_{12} = G_{13} = 8.96MPa$$
$$\upsilon_{12} = 0.25$$

The subscript 1 corresponds to the direction parallel to fibre orientation and subscripts 2 and 3 are related to the directions perpendicular to it. The beam cross-sectional dimensions are illustrated in Figure 7.14.

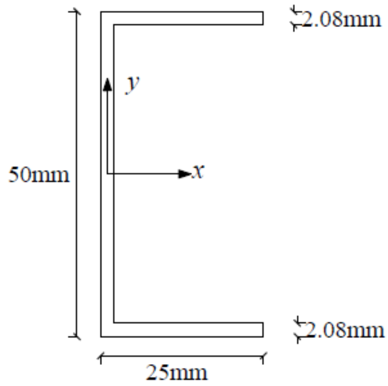

Figure 7.14: Cross-sectional dimensions of the channel-section

The web and flanges are laminated symmetrically with respect to the mid-plane and consist of 16 layers with equal thickness of 0.13 mm.

The analyses are done for two different boundary conditions: simply supported (S-S) and clamped-free (C-F) boundary conditions. The length of the column is assumed to be equal to 4 m for both S-S and C-F boundary conditions.

The values of the buckling moments obtained by the current model are compared with the numerical method developed by Kim *et al.* (2007) in which the element stiffness matrix for lateral buckling analysis of a thin-walled composite is evaluated exactly.

7.9.4.1. Results and discussions

The beam is modelled by using eight elements. The predicted buckling moments by the current hybrid method for various stacking sequences of laminate composite are compared with the results obtained by the numerical method developed by Kim *et al.* (2007). The results for simply-supported and clamped-free boundary conditions are shown in Table 7.4 and Table 7.5 , respectively.

Table 7.4: Buckling moments of beam (N.m) for S-S boundary condition

Lay-up	Current study	(Kim *et al.* 2007)
$\left[0^o\right]_{16}$	36.61	36.05
$\left[15^o / \text{-}15^o\right]_{4s}$	35.60	37.15
$\left[30^o / \text{-}30^o\right]_{4s}$	32.71	36.35
$\left[45^o / \text{-}45^o\right]_{4s}$	28.22	31.95
$\left[60^o / \text{-}60^o\right]_{4s}$	24.05	26.75
$\left[75^o / \text{-}75^o\right]_{4s}$	21.46	22.25
$\left[0^o / 90^o\right]_{4s}$	20.62	20.35

Table 7.5: Buckling moments of beam (N.m) for C-F boundary condition

Lay-up	Current study	(Kim *et al.* 2007)
$\left[0^o\right]_{16}$	17.90	17.56
$\left[15^o / \text{-}15^o\right]_{4s}$	17.56	18.19
$\left[30^o / \text{-}30^o\right]_{4s}$	16.27	17.99
$\left[45^o / \text{-}45^o\right]_{4s}$	14.07	15.88
$\left[60^o / \text{-}60^o\right]_{4s}$	11.99	13.27
$\left[75^o / \text{-}75^o\right]_{4s}$	10.66	11.08
$\left[0^o / 90^o\right]_{4s}$	10.26	10.15

From Table 7.4 and Table 7.5 we can observe that the predicted buckling moment by the current shear-deformable hybrid finite element model is in an acceptable agreement with the results obtained by Kim *et al.* (2007) model for both simply-supported and clamped-free conditions.

7.10. Summary and Conclusions

A shear-deformable hybrid finite element formulation has been developed for the lateral-torsional buckling analysis of beams with fibre-reinforced laminate composite cross-sections subjected to loads which induce bending moment around their strong axes. The hybrid functional has been obtained from the potential energy functional by relaxing the strain-displacement equations as auxiliary conditions through the Lagrange Multipliers method. The shear deformation effects are taken into account by using the strain energy of the equilibrating shear stress field without modifying the basic kinematic assumptions of the beam theory.

Numerical comparisons against other finite element methods and shell element models have been presented to show the validity, accuracy and efficiency of the current method in capturing the lateral-torsional buckling behaviour of beams with fibre reinforced laminate composite cross-sections. It has been illustrated that the lateral-torsional buckling moments obtained by the current method for the composite beams with various boundary conditions are in a very good agreement with the results calculated by the other methods in the literature. The validity of the hybrid method for mono-symmetric cross-sections in addition to the doubly-symmetric cross-sections is shown and the effects of fibre orientation and slenderness of the beam on the value of lateral-torsional buckling moment are studied. In addition, the effect of shear deformations on the lateral-torsional buckling behaviour of thin-walled composite beams and the capability of the current hybrid finite element method in capturing these effects are discussed.

Chapter 8: Conclusion and Recommendations

8.1. Summary and conclusion

In this thesis, a shear-deformable hybrid finite element formulation is developed for the buckling analysis of thin-walled composite beams and columns.

An introduction to the theory of thin-walled beams and a literature review of the most common methods in the analysis and design of these members were presented in chapter 2. Fibre-reinforced composite laminates were introduced in Chapter 3, followed by a discussion about their advantages and disadvantages, and a review of the existing methods in literature for their analysis. The importance of shear deformation effects in the behaviour of composite laminates is discussed in this chapter.

In Chapter 4, different methods in the analysis of thin-walled composite members were discussed, including closed-form solutions and numerical methods. It was argued that the closed-form solutions are only applicable to a limited range of structural geometry and boundary conditions, which stressed the necessity of reliable numerical methods. Finite element method was then described as the most commonly used numerical technique in the field, and the different families of finite element method, namely displacement-based and stress-based methods were introduced. The hybrid finite element method is then introduced as a solution to overcome the disadvantages of each of the primal finite element types.

Chapter 5 was dedicated to developing a hybrid formulation for the flexural buckling analysis of thin-walled composite columns, based on the Hellinger-Reissner energy functional. The constitutive relations of composite laminates were used, and the shear deformation effects were considered by the summation of the energy field resulting from shear to the total energy of the system. The displacement components and stress resultants were then interpolated to obtain a finite element formulation, the accuracy of which was verified through a number of comparisons with test results and numerical methods in the literature.

Chapter 6 explored the applicability of the developed hybrid element for the analysis of short columns, sandwich columns, and laced built-up columns, with examples to certify the accuracy and efficiency of the method.

The hybrid formulation for lateral-torsional analysis of composite thin-walled beams was developed in Chapter 7 by considering the kinematics of thin-walled beams. The formulation was formed by using the constitutive relations of the composite laminates, and by relaxing the strain-displacement equations through Lagrange Multipliers. A number of examples were then presented to demonstrate the accuracy and the efficiency of the method.

It was observed that the developed method is capable of capturing the buckling load of thin-walled beams and columns accurately. It should be noted that the shear deformation effects were considered in this method without modifying the Vlasov kinematic assumptions. It is the main advantage of the developed hybrid method over the displacement-based method. In addition, the resulting matrix equations in the current method are defined only in terms of the nodal displacement values as unknowns, even though the multi-field Hellinger-Reissner functional is used in the formulation. Consequently, the assemblage procedure is as straightforward as in a displacement-based finite element. Finally, unlike in stress-based methods, the inter-element force equilibrium does not need to be satisfied a-priori in the hybrid method.

8.2. Recommendations for further research

The areas of further research include the following:

The buckling analysis of composite thin-walled members has been studied in this thesis. However, the hybrid finite element formulation has the potential to be extended for the geometrically nonlinear analyses in order to be able to capture the pre-buckling deformation effects as well.

Introducing time-dependant creep behaviour into the analysis for FRP laminated composite elements is another field for future research.

Predicting the local buckling behaviour of thin-walled members made of composite materials was not in the scope of this study. To capture this phenomenon, developing a 2D shell element is required. Therefore, applying the current hybrid method to develop such an element to capture the local buckling effects can be the other recommendation for future research.

References

Alemdar, B.N. and White, D.W. (2005), "Displacement, Flexibility, and Mixed Beam-Column Finite Element Formulations for Distributed Plasticity Analysis", *Journal of Structural Engineering (New York, N.Y.)*, **131** (12), 1811-9.

Allen, H.G. (1969), *Analysis and design of structural sandwich panels*, Pergamon,Oxford.

Alsafadie, R., Hjiaj, M. and Battini, J.M. (2010), "Corotational mixed finite element formulation for thin-walled beams with generic cross-section", *Computer Methods in Applied Mechanics and Engineering*, **199** (49-52), 3197-212.

Attard, M.M. (1986), "Lateral Buckling Analysis of Beams by the FEM", *Comput. Struct.*, **23** (1), 217-31.

Attard, M.M. and Hunt, G.W. (2008), "Sandwich column buckling – A hyperelastic formulation", *International Journal of Solids and Structures*, **45** (21), 5540-55.

Back, S.Y. and Will, K.M. (2008), "Shear-flexible thin-walled element for composite I-beams", *Engineering Structures*, **30** (5), 1447-58.

Barbero, E. and Raftoyiannis, I. 1990, 'Buckling analysis of pultruded composite columns', *American Society of Mechanical Engineers, Aerospace Division (Publication) AD*, vol. 20, pp. 47-52.

Barbero, E. and Tomblin, J. (1993), "Euler buckling of thin-walled composite columns", *Thin-Walled Structures*, **17** (4), 237-58.

Barbero, E.J. (1999), *Introduction to composite materials design*, Philadelphia.

Barsoum, R.S. and Gallagher, R.H. (1970), "Finite element analysis of torsional and torsional-flexural stability problems (Structure of flexural members, analyzing torsional and lateral stability by finite element method and matrix formulation)", *International Journal for Numerical Methods in Engineering* **2**(1), 335-52.

Batoz, J.L. and Tahar, M.B. (1982), "Evaluation of a new quadrilateral thin plate bending element", *INT J NUMER METHODS ENG*, **V 18** (N 11), 1655-77.

Bauld, N.R. and Tzeng, L.-S. (1984), "A Vlasov theory for fiber-reinforced beams with thin-walled open cross sections", *International Journal of Solids and Structures*, **20** (3), 277-97.

Blaauwendraad, J. (2010), "Shear in Structural Stability: On the Engesser–Haringx Discord", *Journal of Applied Mechanics*, **77** (3), 031005-.

Bleich, F. (1952), "Buckling of metal structures".

Bonab, A.P., Hashemi, B.H. and Hosseini, M. (2013), "Experimental evaluation of the elastic buckling and compressive capacity of laced columns", *Journal of Constructional Steel Research*, **86** (1), 66-73.

Bradford, M.A. (1985), "Distortional buckling of monosymmetric I-beams", *Journal of Constructional Steel Research*, **5** (2), 123-36.

Bradford, M.A. (1994), "Buckling of post-tensioned composite beams", *Structural Engineering and Mechanics*, **2** (1), 113-23.

Bradford, M.A. (2000), "Strength of compact steel beams with partial restraint", *Journal of Constructional Steel Research*, **53** (2), 183-200.

Bradford, M.A. and Ronagh, H.R. (1997), "Generalized elastic buckling of restrained I-beams by FEM", *Journal of Structural Engineering*, **123** (12), 1631-7.

Bradford, M.A. and Trahair, N.S. (1981), "Distortional buckling of I-beams", *ASCE J Struct Div*, **107** (2), 355-70.

Bradford, M.A. and Waters, S.W. (1988), "Distortional instability of fabricated monosymmetric I-beams", *Computers and Structures*, **29** (4), 715-24.

Brooks, R.J. and Thrvey, G.J. (1995), "Lateral buckling of pultruded GRP I-section cantilevers", *Composite Structures*, **32** (1), 203-15.

Bulson, P.S. (1955), "Local instability problems of light alloy struts", *Aluminium Development Association*.

Chajes, A. and Winter, G. (1965), "Torsional Buckling of Thin-Walled Members", *Journal of Structural Division, ASCE*, **91** (ST4), 103-25.

Chen, J.K. and Li, L.Y. (2013), "Elastic axially compressed buckling of battened columns", *International Journal of Mechanical Sciences*, **77** (1-7.

Chen, S. and Wang, X. (2012), "Finite element analysis of distortional lateral buckling of continuous composite beams with transverse web stiffeners", *Advances in Structural Engineering*, **15** (9), 1607-16.

Cortínez, V.H. and Piovan, M.T. (2006), "Stability of composite thin-walled beams with shear deformability", *Computers & Structures*, **84** (15–16), 978-90.

Davalos, J.F. and Qiao, P. (1997), "Analytical and Experimental Study of Lateral and Distortional Buckling of FRP Wide-Flange Beams", *Journal of Composites for Construction*, **1** (4), 150-9.

Douville, M.-A. and Le Grognec, P. (2013), "Exact analytical solutions for the local and global buckling of sandwich beam-columns under various loadings", *International Journal of Solids and Structures*, **50** (16), 2597-609.

Drysdale, R.G., Betancourt-Angel, F. and Haddad, G.B. (1979), "Thick skin sandwich beam columns with weak cores", *ASCE J Struct Div*, **105** (12), 2601-19.

Engesser, F. (1891), "Die Knickfestigheit gerader Stabe ", *Zentralblatt der Bauverwaltung* **11** (483-6.

Erkmen, R.E. (2014), "Shear deformable hybrid finite-element formulation for buckling analysis of thin-walled members", *Finite Elements in Analysis and Design*, **82** (1), 32-45.

Erkmen, R.E. and Attard, M.M. (2011), "Lateral-torsional buckling analysis of thin-walled beams including shear and pre-buckling deformation effects", *International Journal of Mechanical Sciences*, **53** (10), 918-25.

Erkmen, R.E. and Mohareb, M. (2008), "Buckling analysis of thin-walled open members—A complementary energy variational principle", *Thin-Walled Structures*, **46** (6), 602-17.

Erkmen, R.E., Mohareb, M. and Bradford, M.A. (2009), "Complementary energy based on formulation for torsional buckling of columns", *Journal of Engineering Mechanics*, **135** (12), 1420-6.

Fleck, N.A. and Sridhar, I. (2002), "End compression of sandwich columns", *Composites Part A: Applied Science and Manufacturing*, **33** (3), 353-9.

Geng-Shu, T. and Shao-Fan, C. (1989), "An interactive buckling theory for built-up beam-columns and its application to centrally compressed built-up members", *Journal of Constructional Steel Research*, **14** (3), 221-41.

Gjelsvik, A. (1990), "Buckling of built-up columns with or without stay plates", *Journal of Engineering Mechanics*, **116** (5), 1142-59.

Hancock, G.J., Bradford, M.A. and Trahair, N.S. (1980), "Web distortion and flexural-torsional buckling", *ASCE J Struct Div*, **106** (7), 1557-71.

Hancock, G.J., Kwon, Y.B. and Stefan Bernard, E. (1994), "Strength design curves for thin-walled sections undergoing distortional buckling", *Journal of Constructional Steel Research*, **31** (2-3), 169-86.

Haringx, J.A. (1948-1949), "On highly compressible helical springs and rubber rods, and their application for vibration-free mountings, I - III .", **3** (1), 1-97.

Hassan, N.K. and Mosallam, A.S. (2004), "Buckling and Ultimate Failure of Thin-Walled Pultruded Composite Columns", *Polymers & Polymer Composites*, **12** (6), 469-81.

Hoff, N.J. and Mautner, S.E. (1945), "Buckling of sandwich type panels.", *Journal of the Aeronautical Sciences*, **12** (3), 285-97.

Hoff, N.J. and Mautner, S.E. (1948), "Bending and buckling of sandwich beams", *Journal of the Aeronautical Sciences*, 707–20.

Hosseini Hashemi, B. and Jafari, M.A. (2009), "Experimental evaluation of elastic critical load in batten columns", *Journal of Constructional Steel Research*, **65** (1), 125-31.

Ibrahimbegovic, A., Taylor, R.L. and Wilson, E.L. (1990), "Robust quadrilateral membrane finite element with drilling degrees of freedom", *International Journal for Numerical Methods in Engineering*, **30** (3), 445-57.

Jönsson, J. (1999), "Distortional theory of thin-walled beams", *Thin-Walled Structures*, **33** (4), 269-303.

Kalochairetis, K.E. and Gantes, C.J. (2011), "Numerical and analytical investigation of collapse loads of laced built-up columns", *Computers & Structures*, **89** (11), 1166-76.

Kim, N.-I. and Lee, J. (2013), "Lateral buckling of shear deformable laminated composite I-beams using the finite element method", *International Journal of Mechanical Sciences*, **68** (1), 246-57.

Kim, N.-i. and Lee, J. (2014), "Efficient laminated composite beam element subjected to variable axial force for coupled stability analysis", *Acta Mechanica*, **225** (7), 2021-41.

Kim, N.-I., Shin, D.K. and Kim, M.-Y. (2007), "Exact lateral buckling analysis for thin-walled composite beam under end moment", *Engineering Structures*, **29** (8), 1739-51.

Kim, N.-I., Shin, D.K. and Kim, M.-Y. (2008), "Flexural–torsional buckling loads for spatially coupled stability analysis of thin-walled composite columns", *Advances in Engineering Software*, **39** (12), 949-61.

Kollaor, L.P. (2002a), "Discussion of ‗Local buckling of composite FRP shapes by discrete plate analysis' by P. Qiao, J. F. Davalos, and J.Wang", *Journal of Structural Engineering*, **128** (8), 1091–3.

Kollaor, L.P. (2002b), "Buckling of Unidirectionally Loaded Composite Plates with One Free and One Rotationally Restrained Unloaded Edge", *Journal of Structural Engineering*, **128** (9), 1202-11.

Kollár, L.P. (2001), "Flexural–torsional buckling of open section composite columns with shear deformation", *International Journal of Solids and Structures*, **38** (42), 7525-41.

Kollár, L.P. (2003), "Local buckling of fiber reinforced plastic composite structural members with open and closed cross sections", *Journal of Structural Engineering*, **129** (11), 1503-13.

Krajcinovic, D. (1969), "A consistent discrete elements technique for thinwalled assemblages (Matrix formulation for discrete element method applied to linear static and eigenvalue problems of thin walled segments, using homogeneous differential equations)", *International Journal of Solids and Structures*, **5** (1), 639-62.

Lee, J. (2005), "Flexural analysis of thin-walled composite beams using shear-deformable beam theory", *Composite Structures*, **70** (2), 212-22.

Lee, J. (2006), "Lateral buckling of I-section composite beams with monosymmetric section", *Engineering Structures*, **28** (1), 1997-2009.

Lee, J. and Kim, S.-E. (2001), "Flexural–torsional buckling of thin-walled I-section composites", *Computers & Structures*, **79** (10), 987-95.

Lee, J. and Kim, S.E. (2002), "Lateral buckling analysis of thin-walled laminated channel-section beams", *Composite Structures (UK)*, **56** (4), 391-9.

Lee, J., Kim, S.E. and Hong, K. (2002), "Lateral buckling of I-section composite beams", *Engineering Structures*, **24** (7), 955-64.

Lee, S.W. and Rhiu, J.J. (1986), "A new efficient approach to the formulation of mixed finite element models for structural analysis", *International Journal for Numerical methods in Engineering* **23** (1), 1629-41.

Lekhnitskii, S.G. (1968), "Anisotropic plates", *Gordon and Breach Science Publishers*.

Libove, C. (1988), "Stresses and rate of twist in single-cell thin-walled beams with anisotropic walls", *AIAA Journal*, **26** (1107-18.

Lim, N.H., Park, N.H., Kang, Y.J. and Sung, I.H. (2003), "Elastic buckling of I-beams under linear moment gradient", *International Journal of Solids and Structures*, **40** (21), 5635-47.

Lin, Z.M., Polyzois, D. and Shah, A. (1996), "Stability of thin-walled pultruded structural members by the finite element method", *Thin-Walled Structures (UK)*, **24** (1), 1-18.

Machado, S.P. (2010), "Interaction of combined loads on the lateral stability of thin-walled composite beams", *Engineering Structures*, **32** (11), 3516-27.

Machado, S.P. and Cortínez, V.H. (2005), "Lateral buckling of thin-walled composite bisymmetric beams with prebuckling and shear deformation", *Engineering Structures*, **27** (8), 1185-96.

Maddur, S.S. and Chaturvedi, S.K. (2000), "Laminated composite open profile sections: Non-uniform torsion of I-sections", *Composite Structures*, **50** (2), 159-69.

Michell, A. 1899, 'Elastic stability of long beams under transverse forces', *Philos Mag*, vol. 48, pp. 298-309.

Mottram, J. (1992), "Lateral–torsional buckling of a pultruded I-beam.", *Composite*, **23** (2), 81-92.

Murakami, H. and Yamakawa, J. (1996), "On approximate solutions for the deformation of plane anisotropic beams", *Composites Part B: Engineering*, **27B** (5), 493-504.

Nethercot, D.A. and Trahair, N.S. (1976), "Lateral buckling approximations for elastic beams", *Structural Engineer*, **54** (6), 197-204.

Nguyen, X.-H., Kim, N.-I. and Lee, J. (2015), "Optimum design of thin-walled composite beams for flexural–torsional buckling problem", *Composite Structures*, **132** (1), 1065-74.

Nukala, P.K.V.V. and White, D.W. (2004), "Variationally consistent state determination algorithms for nonlinear mixed beam finite elements", *Computer Methods in Applied Mechanics and Engineering*, **193** (33-35), 3647-66.

Omidvar, B. (1998), "Shear Coefficient in Orthotropic Thin-Walled Composite Beams", *Journal of Composites for Construction*, **2** (1), 46-56.

Omidvar, B. and Ghorbanpoor, A. (1996), "Nonlinear FE solution for thin-walled open-section composite beams", *Journal of Structural Engineering*, **122** (11), 1369-77.

Pandey, M.D., Kabir, M.Z. and Sherbourne, A.N. (1995a), "Flexural-torsional stability of thin-walled composite I-section beams", *Composites Engineering*, **5** (3), 321-42.

Pandey, M.D., Kabir, M.Z. and Sherbourne, A.N. (1995b), "Flexural-torsional stability of thin-walled composite I-section beams", *Composites Engineering (UK)*, **5** (3), 321-42.

Paul, M. (1995), "Theoretical and experimental study on buckling of built-up columns", *Journal of Engineering Mechanics*, **121** (10), 1098-105.

Petrangeli, M. and Ciampi, V. (1997), "Equilibrium based iterative solutions for the non-linear beam problem", *International Journal for Numerical methods in Engineering* **40** (3), 423-37.

Pian, T.H.H. 1964, *Derivation of element stiffness matrices by assumed stress distributions (Derivation of element stiffness matrices based on principle of minimum complementary energy)*.

Pian, T.H.H. (1978), "A historical note about ‗hybrid elements'", *INTERNATIONAL JOURNAL FOR NUMERICAL METHODS IN ENGINEERING*, **12** (5), 891-2.

Pian, T.H.H. 1985, *Recent advances in hybrid/mixed finite elements*, vol. NASA-CR-175574; NAS 1.26:175574; Pagination 8P.

Pian, T.H.H. (1994), "Thirty-Year history of hybrid stress finite element methods", *in: P.K.K. Lee and L.G. Tham (eds.), Y.K. Cheung Symposium,*.

Pian, T.H.H. (1995), "State-of-the-art development of hybrid/mixed finite element method", *Finite Elements in Analysis and Design*, **21** (1-2), 5-20.

Pian, T.H.H. and Tong, P. 1968, *A variational principle and the convergence of a finite-element method based on assumed stress distribution Interim scientific report*, vol. ASRL-TR-144-1; AFOSR-68-0384; AD-667813; Pagination 23P.

Piovan, M.T. and Cortínez, V.H. (2007), "Mechanics of shear deformable thin-walled beams made of composite materials", *Thin-Walled Structures*, **45** (1), 37-62.

Prandtl L, K. 1899, 'Doctoral dissertation', Universitat Munchen.

Qiao, P., Zou, G. and Davalos, J.F. (2003), "Flexural–torsional buckling of fiber-reinforced plastic composite cantilever I-beams", *Composite Structures*, **60** (2), 205-17.

Qin, Z. and Librescu, L. (2002), "On a shear-deformable theory of anisotropic thin-walled beams: further contribution and validations", *Composite Structures*, **56** (4), 345-58.

Reddy, J.N. 2003, 'Mechanics of laminated composite plates and shells: Theory and analysis, 2nd ed.', CRC Press.

Rehfield, L. and Atilgan, A. 1989, 'On the buckling of thin-walled laminated composite open-section beams', *Structural Dynamics and Materials Conference, AIAA*, ed. P.o.t.A.A.A.A.A. Structures, Washington D.C.

Reissner, H. (1904), "Uber die Stabilitat der Biegung.", *Sitzungsber Berl Math Ges Beil Arch Math Phys*, **III** (53-6).

Roberts, T. (2002), "Influence of shear deformation on buckling of pultruded fiber reinforced plastic profiles.", *Journal of Composites for Construction*, **6** (4), 241-8.

Roberts, T.M. and Jhita, P.S. (1983), "Lateral, local and distortional buckling of I-beams", *Thin-Walled Structures*, **1** (4), 289-308.

Roberts, T.M. and Masri, H. (2003), "Section Properties and Buckling Behavior of Pultruded FRP Profiles", *Journal of Reinforced Plastics and Composites*, **22** (14), 1305-17.

Rusch, A. and Lindner, J. (2001), "Remarks to the Direct Strength Method", *Thin-Walled Structures*, **39** (9), 807-20.

Santos, H.A.F.A., Pimenta, P.M. and Moitinho De Almeida, J.P. (2010), "Hybrid and multi-field variational principles for geometrically exact three-dimensional beams", *International Journal of Non-Linear Mechanics*, **45** (8), 809-20.

Sapkas, A. and Kollar, L.P. (2002), "Lateral-torsional buckling of composite beams", *International Journal of Solids and Structures*, **39** (11), 2939-63.

Schafer, B.W. (2008), "Review: The Direct Strength Method of cold-formed steel member design", *Journal of Constructional Steel Research*, **64** (7–8), 766-78.

Schafer, B.W. and Pekoz, T. 1998, 'Direct Strength Prediction of Cold-Formed Steel Members using Numerical Elastic Buckling Solutions', *14th International Specialty Conference on Cold-Formed Steel Structures*, St. Louis, Missouri, pp. 69-76.

Sherbourne, A.N. and Kabir, M.Z. (1995), "Shear Strain Effects in Lateral Stability of Thin-walled Fibrous Composite Beams", *Journal of Engineering Mechanics*, **121** (5), 640-7.

Spacone, E., Ciampi, V. and Filippou, F.C. (1996), "Mixed formulation of nonlinear beam finite element", *Computers & Structures*, **58** (1), 71-83.

Tang, L.M., Chen, W.J. and Liu, Y.X. 1981, 'String net function approximation and quasi-conforming element technique (for finite element problems)', Apr 1981.

Taylor, R.L., Filippou, F.C., Saritas, A. and Auricchio, F. (2003), "A mixed finite element method for beam and frame problems", *Computational Mechanics*, **31** (1-2 SPEC.), 192-203.

Timoshenko, S.P. and Gere, J.M. (1961), *Theory of elastic stability*, 2nd edn, McGraw-Hil, New York.

Trahair, N.S. (1993a), *Flexural-Torsional Buckling of Structures*, CRC Press, Boca Raton, FL, USA.

Trahair, N.S. (1993b), *Flexural-Torsional Buckling of Structures*, FL,USA.

Turvey, G. (1996), "Effects of load position on the lateral buckling response of pultruded GRP cantilevers--comparisons between theory and experiment", *Composite Structures (UK)*, **35** (1), 33-47.

Vlasov, V.Z. (1961), *Thin-walled elastic beams*, 2nd edn, Israel Program for Scientific Translations, Jerusalem, Israel.

Vo, T.P. and Lee, J. (2010), "Geometrically nonlinear analysis of thin-walled open-section composite beams", *Computers & Structures*, **88** (5), 347-56.

von Karman, T., Sechler, E.E. and Donnell, L.H. (1932), "The Strength of Thin Plates in Compression", *ASME*, **54** (5), 53-70.

Vrcelj, Z. and Bradford, M.A. (2009), "Inelastic restrained distortional buckling of continuous composite T-beams", *Journal of Constructional Steel Research*, **65** (4), 850-9.

Wackerfuß, J. and Gruttmann, F. (2009), "A mixed hybrid finite beam element with an interface to arbitrary three-dimensional material models", *Computer Methods in Applied Mechanics and Engineering*, **198** (27-29), 2053-66.

Wagner, H. (1936), "Torsion and buckling of open sections", *Translated technical memorandum no. 807, NACA—National Advisory Committee for Aeronautics;*.

Wang, S.-J. (1985), "Torsional-flexural buckling of open thin-walled columns with battens", *Thin-Walled Structures*, **3** (4), 323-44.

Wang, S. (1997), "Free vibration analysis of skew fibre-reinforced composite laminates based on first-order shear deformation plate theory", *Computers & Structures*, **63** (3), 525-38.

Washizu, K. (1982), *Variational methods in elasticity and plasticity /3rd edition/ (Book)*.

Wong, E. and Driver, R.G. (2010), "Critical evaluation of equivalent moment factor procedures for laterally unsupported beams", *Engineering Journal*, **47** (1), 1-20.

Yang, Y.B. and McGuire, W. (1986), "Stiffness Matrix for Geometric Nonlinear Analysis", *Journal of Structural Engineering, ASCE*, **112** (ST4), 853-77.

Zenkert, D. (1995), "An introduction to sandwich construction", *London: Engineering Materials Advisory Services*.

Zhou, W.B., Li, S.J. and Yan, W.J. (2016), "Practical formulas towards distortional buckling failure analysis for steel–concrete composite beams", *Structural Design of Tall and Special Buildings*, **25** (18), 1055-72.

Ziegler, H. (1982), "Arguments for and against Engesser's buckling formulas", *Ingenieur-Archiv*, **52** (1-2), 105-13.